A Novel Silicate Ceramic-Magnetite Nanocomposite for Biomedical Application

Amirsalar Khandan

Submitted to the
Institute of Graduate Studies and Research
in partial fulfillment of the requirements for the degree of

Doctor of Philosophy
in
Mechanical Engineering

Eastern Mediterranean University
July 2017
Gazimağusa, North Cyprus

Approval of the Institute of Graduate Studies and Research

Prof. Dr. Mustafa Tümer
Director

I certify that this thesis satisfies the requirements as a thesis for the degree of Doctor of Philosophy in Mechanical Engineering.

Assoc. Prof. Dr. Hasan Hacişevki
Chair, Department of Mechanical Engineering

We certify that we have read this thesis and that in our opinion it is fully adequate in scope and quality as a thesis for the degree of Doctor of Philosophy in Mechanical Engineering.

Assist. Prof. Dr. Neriman Ozada
Supervisor

Examining Committee

1. Prof. Dr. Mohammad Mohammadi Aghdam
2. Prof. Dr. Murat Bengisu
3. Assoc. Prof. Dr. Hasan Hacişevki
4. Assoc. Prof. Dr. Qasim Zeeshan
5. Asst. Prof. Dr. Neriman Ozada

ABSTRACT

Some of the most common human bone diseases like trauma, bone cracks and tumour, have been able to provide the necessary key information required for designing scaffolds used for replacing a diseased bone. Many of the scaffolds' properties are mainly associated with the microstructure of material's microstructure and range of porosity, as well as the dimension of its pores and interconnectivity. Recently, bredigite ($Ca_7MgSi_4O_{16}$), a Mg-containing ceramic, has been reported to have an inherent apatite-forming ability and chemical stability for bone tissue engineering application. Moreover, bone reconstruction significantly accelerated by employing thermal and electrical currents in the defect area. Magnetite is a bioresorbable material that has been widely employed within the biomaterials domain; also, it has been used in cancer therapy techniques such as hyperthermia treatment behavior under the temperature change and AC magnetic field. The combination of (0 wt. %, 10 wt. %, 20 wt. % and 30 wt.%) magnetite with bredigite bioceramic resulted in the fabrication of nanocomposite material. Three-dimensional printing (3DP), as a common rapid prototyping technique, can fabricate complex scaffolds structures for bone replacement as well as partake in electrical stimulation. The aim of this study is to evaluate the thermal, electrical, mechanical, biological and magnetic behavior of the bredigite-magnetite scaffold nanocomposite for possible application in bone tissue engineering. The scaffolds was successfully developed with the optimum nanocomposite magnetite content and it was observed that the porosity was increased from 63.1% to 75.9%. The properties of the bredigite-magnetite nanocomposites are: bending strength (148 MPa), fracture toughness (2.69 MPa $m^{1/2}$) and Young's modulus (29 GPa) i.e. for a sample containing 30 wt.%

magnetite. The compressive strength of the sample increased from 1.8 MPa to 3.6 MPa. From the results, it is observed that the higher electrical conductivity (160 µS/m) belongs to the sample with higher percentage of magnetite nanoparticles (MNPs), while the sample without MNPs powder shows the lowest amount of electrical conductivity (35 µS/m). Samples with 30 wt.% magnetite show an increase in temperature of about 25°C within 60 second, while 10 wt.% magnetite sample show an increase of 15°C in an AC magnetic field. Furthermore, the results revealed that the surface morphology and particles interface, have meaningful effects on the bioactivity and biodegradation rate. Therefore, by increasing the magnetite nanoparticles amount and Si ions, the bone-like apatite and degradation rate of the scaffold nanocomposite was enlarged considerably. The findings of this research showed that the nanocomposites with magnetite nanoparticles, have a proper electromagnetic inducements characteristics and are credible candidates for hyperthermia treatment.

Keywords: Scaffold, Nanocomposite, Hyperthermia treatment, Bone tissue engineering

ÖZ

Travma, kemik çatlakları ve tümör gibi yaygın kemik hastalıkları ve bozuklukları, doku kaybı olan kemiğin yerini doldurmak için kullanılacak yapay doku malzemesinin tasarımında gerekli temel bilgileri sağlayabilmiştir. Yapay dokunun özellikleri, içerdiği malzemenin gözenek ve mikro yapısına, gözeneklerinin ve bağlantı özelliklerinin boyutuna bağlıdır. Son zamanlarda, Magnezyum (Mg) içeren bir seramik olan Bredigite ($Ca_7MgSi_4O_{16}$) in, doku mühendisliği uygulaması için doğal bir yapı oluşturma özelliği ve kimyasal stabilitesi olduğu rapor edilmiştir. Ayrıca, kemiğin kusurlu olan bölgesinde, termal uygulama ve elektriksel akımlar kullanılarak kemik rekonstrüksiyonunun belirgin bir şekilde hızlandığı da bildirilmiştir. Manyetit, biyomalzemeler alanında yaygın şekilde kullanılan biyolojik olarak emilebilir bir malzemedir ve hipertermi gibi kanser terapisi ve tedavisinde kullanılmaktadır. Bu doktora calışmasında, Bredigit ile Manyetit`in kombinasyonu ile nanokompozit malzeme imal edilmiştir. Yapay donukun imalatı için, üç boyutlu baskı (3DP), prototipleme tekniği olarak kullanılmıştır.Bu çalışmanın amacı, Bredigite-Manyetit yapay doku nanokompozitinin, termal, elektriksel, mekanik, biyolojik ve manyetik özelliklerini incelemek ve doku mühendisliği alanında kullanımının uygunluğunu değerlendirmektir. Bu çalışmanın özgünlüğü, geliştirilen Bredigite-Manyetit yapay doku nanokompozitinin, hipertermi tedavisinin uygulanması sırasında gösterdiği etki ve sıcaklık değişimi ile manyetik alandaki davranışının incelenmesidir. Yapılan bu çalışma sonuçlarına göre, nanokompozit yapay doku`nun gözenekli yapısı, % 63.1'den %75.9'a çıkmış ve Manyetit içeriğine bağlı olarak başarıyla geliştirilmiştir. Bu çalışmada kullanılan Bredigite-Manyetit nanokompozit`in özellikleri de sırayla; 148MPa bükülme mukavemeti, 2.69

MPa $m^{1/2}$ kırılma tokluğu ve 29 GPa Young modülü ile % 30 oranında Manyetit içeriğidir. Bunalara ek olarak, yapılan test sonuçlarına göre, Manyetit içermeyen malzemenin sıkışma mukavemeti 1.8 MPa olarak bulunurken, Bredigite-Manyetit nanokompozit`in sıkışma mukavemeti iki kat daha fazla ve 3.6 MPa olarak bulunmuştur. Elektrik alanında yapılan testler ve elde edilen sonuçlara göre, yüksek elektriksel iletkenlik (160 μS /m), Manyetit nanoparçacıklarının (MNP) yüksek yüzdesine sahip olan numuneye aitken, MNPs içermeyen numuneler en düşük elektriksel iletkenlik (35 μS/m) göstermiştir. %30 ağırlıklı Manyetit içeren numuneler 60 saniyede yaklaşık 25°C sıcaklık artışı gösterirken, %10 ağırlıklı Manyetit içeren numuneler, manyetik alanda 15°C'lik bir sıcaklık artışı göstermiştir. Elde edilen sonuçlar, yüzey morfolojisinin ve parçacık arayüzünün, biyoaktivite ve biyolojik bozunma oranı üzerinde olumlu etkileri olduğunu ortaya koymuştur. Ayrıca, ağırlıkça % 30 oranında Manyetit nanoparçacık içeren numuneler doğal bir apatit oluşum özelliğine de sahip olduklarını göstermiştir. Bu nedenle, Manyetit nanopartikül ile Si iyonlarını arttırarak, yapay doku nanokompozitinin kemik benzeri apatit oluşturduğu ve parçalanma oranının önemli derecede arttığı da tespit edilmiştir. Bu araştırmanın bulguları, Manyetit nanoparçacıkları içeren nanokompozitlerin uygun elektromanyetik indüksiyon özelliklerine sahip olduğunu ve hipertermi tedavisinde kullanılmalarının güvenilir olduğunu göstermiştir.

Anahtar Kelimeler: Yapay Doku, Nanokompozit, Hipertermi tedavisi, Kemik dokusu mühendisliği

To my kind mother, my supportive Father, and my helpful supervisor

"Asst. Prof. Dr. Neriman Özada"

To my beautiful country

ACKNOWLEDEGMENT

I would like to thank my supervisor Asst. Prof. Dr. Neriman Özada, not only for all her brilliant scientific oversight in my Ph.D program but also for the excellent and kind manner in which she would resolve all my issues. She has inspired me to continue my study toward Ph.D and how handle my problems with her supports, and how an independent academic researcher becomes.

Also, my family receive my greatest love for all their support and dedication. They have a source of inspiration for me throughout many years.

I would like to acknowledge the members of my graduate committee for their advice, recommendations, comments, and guidance, most especially Assoc. Prof. Dr. Qasim Zeeshan and Assoc. Prof. Dr. Hasan Hacışevki for all their advice and encouragement.

My thanks go to my friends who helped and encouraged me during the period of my studies and thesis.

TABLE OF CONTENTS

LIST OF TABLES

LIST OF FIGURES

LIST OF ABBREVIATIONS

AANN	Aggregated Artificial Neural Network
AAOS	American Academy of Orthopedic Surgeons
ACM	Advanced Composites
AM	Additive Manufacturing
ANOVA	One-Way Analysis Of Variance
BMD	Bone Mineral Density
CaPs	Calcium Phosphates
CAD/CAM	Computer Aided Design and Computer Aided Manufacturing
CCT	Clinical Computer Tomography
Co-Cr	Cobalt-Chrome
CMCs	Ceramic Matrix Composites
DA	Dimensional Accuracy
DOE	Design of Experiments
EDX	Energy Dispersive Spectroscopy
ECM	Extracellular Matrix
FDM	Fused Deposition Modelling
GEP	Gene Expression Programming
HA	Hydroxyapatite
ICP-AES	Inductive Coupled Plasma Atomic Emission Spectroscopy
MNPs-Fe_3O_4	Magnetite Nanoparticles
MMCs	Metal Matrix Composites
PCL	Polycaprolactone
PMCs	Polymer Matrix Composites

PSO	Particle Swarm Optimization
PBS	Phosphate-Buffered Saline
RP	Rapid Prototyping
SAR	Specific Absorption Rate
SBF	Simulated Body Fluid
SD	Standard Deviation
SEM	Scanning Electron Microscopy
SFF	Solid Free Form Fabrication
STL	Stereolithography
TCP	Tricalcium Phosphate
TEM	Transmission Electron Microscopy
XRD	X-Ray Diffraction
μCT	Micro-Computed Tomography
3DP	Three Dimensional printing

Chapter 1

INTRODUCTION

1.1 Bone Disease and Disorders

Treatment of bone disease, bone trauma, arthritis, osteoporosis, and osteonecrosis may cost more than hundreds billion dollar each year around the world [1-2]. It has been shown that more than 10 million people are affected with osteoporosis in USA. Also more than 30 million people are faced with bone disorder like health disease around the world. According to the published data more than two million fractures happen by osteoporosis which leads very high cost about $19 billion in the recent years. Because of the increased life expectancy, there have been more than 200,000 hip replacements in the USA which cost more than 10 billion a year. It is shown that even young patients are insisted to go on hip replacement surgery as they have lots of difficulties in their daily activities. Therefore, the American Academy of Orthopaedic Surgeons (AAOS) describes the most important reason that patients get consultation by orthopaedic doctor is to treat many of bone related disease fractures. Biomaterials are used to replace a part or whole of the tissue in a safe, reliable, economic, and physiologically acceptable manner. Synthetic materials should have biological, mechanical and chemical stability to be used as tissue replacing materials. The substituted artificial tissue may revitalize to the host bone for better remodeling. Therefore, required characteristics like proper bioactivity and bone formation [1-3]. In order to solve such bone disease and disorder using new techniques like chemotherapy, thermal therapy, and recently developed hyperthermia treatment has

been mostly introduced by researchers as shown in literatures. These types of treatment can support the formations and regenerations.

1.1.1 Osteoporosis

Osteoporosis is a common and its treatment is costly that imposes a significant burden in terms of disability and impaired quality of life. It is almost estimated that over ten million person over 50 years old in the USA have osteoporosis by 2010. With close investments forecast to around $50 billion cost for the USA government by 2040. Arbitrary continuous application of corticosteroid doubles the osteoporosis risk. Osteoporosis causes to loss the inner lining of bone and leads multiple fractures [3-5]. Osteoporosis causes bones to become weak and brittle — so brittle that a fall or even mild stresses such as bending over or coughing can cause a fracture. Osteoporosis-related fractures most commonly occur in the hip, wrist or spine. Bone is living tissue that is constantly being broken down and replaced. Osteoporosis occurs when the creation of new bone doesn't keep up with the removal of old bone. Osteoporosis affects men and women of all races. But white and Asian women — especially older women who are past menopause — are at highest risk. Medications, healthy diet and weight-bearing exercise can help prevent bone loss or strengthen already weak bones [5]. It has been found that osteoporosis with high risk of sudden fracture should be treated with substitution of bioceramics scaffold like diopside and akermanite or hydroxyapatite [5, 37-38]. Scaffold like bredigite-magnetite ($Ca_7MgSi_4O_{16}$-Fe_3O_4) can be substituted with removed necrosis tumour regarding to its proper advantages of biological and mechanical features as it is Mg-containing comparing to other calcium silicate magnesium bioceramics.

1.1.2 Bone Cancer

Bone cancer is an inconspicuous hostile threat that has the ability to destroy normal bone tissues. It takes the form of a malignant (cancerous) tumour within the human body. However, it is safe to say that not every bone tumor is malignant in nature. In fact, “benign”, which is non-cancerous, has a higher chance of being diagnosed as the likely ailment. Both bone tumours (malignant and benign), execute a similar mode of attack by compressing and growing within a normal bone tissue; however, benign tumours hardly become fatal because it avoids spreading or being destructive within the bone tissue, unlike its counterpart. The type of malignant tumor which starts up at the bone tissue is known as the “primary bone cancer”. On the other hand, “metastatic cancer”, which starts up from various organs or tissue of the body such as the prostrate, lungs, breast, etc., spreads to bones in the body. Usually, the name that is assigned to it reflects the tissue or organ it emanates from. Moreover, the type of cancer that spreads to bones is far more recurrent than the “primary bone cancer”. At the anatomical level, tumours that are gigantic in statue can be taken out by applying hyperthermia treatment or surgical operations. Consequentially, several complications arise due to bone substitutions. Therefore, the bioceramics that are utilized for bone substitution should be able to withstand the punishment that these bones undergo routinely as well as mimic their biological properties. Hence, the morphology of powders or bulk ceramics and the characterization of bioceramics, have gained widespread recognition amongst researchers of biomaterials. Statistics show that primary bone cancer is responsible for less than one percent of most type of cancers and so, quite rare. In addition, the United States, each year, are plagued with a diagnosis of about two thousand three hundred cases of primary bone cancer [1-3].

1.1.3 Bone Tumor

Cell division is a natural process that our cells must undergo. However, “bone tumour” occurs when there is disruption in the natural cell division process within the bone, causing the cell to divide out of control. This results in an abnormal mass or lump formation within the tissue. However, majority of the bone tumours that occur frequently are not cancerous in nature i.e. benign. Moreover, like stated previously, benign tumours are not fatal and won’t spread to other parts of the body. Now, with respect to the category the tumours fall into, there are various options available to treat this ailment; this ranges from surgical operation to mere simple observation. On the other side of the spectrum, there are some that are cancerous i.e. malignant. Furthermore, the treatment for this ailment becomes a coalition of various counteractive measures such as surgery, chemotherapy and radiation. This bone tumour disrupts the body and its effect, can be severely pronounce in any part of the bone i.e. from the core itself to the very surface, which is known conventionally as the bone marrow. Benign tumour as well as an advancing bone tumour, preys on healthy tissue, thereby weakening the bone, making it susceptible to bone fracture. Bone cancer that is cancerous, is in two categories i.e. either primary or secondary bone cancer. When talking about the primary bone cancer, it emanates directly from the bone itself, while the secondary bone cancer emanates from somewhere within the body, spreads uncontrollably, and then, converges to the bone; this is known as the “metastatic bone disease”.

1.1.4 Fracture and Trauma

There is a significant ongoing problem that plagues our healthcare institution; this problem results in a socioeconomic imbalance as well as presents a major clinical obstruction, and is responsible for high rate of complications and likely poor long-

term outcomes [1, 3]. This problem is known as “Fracture”, which is the non-union of bones that are long. There are several skeletal muscular tissues such as the ligament, tendons and muscles that are responsible for shock absorption and bone tissue protection. The bone alone, just plays a vital role in providing strength and stiffness to the body, while the tissue is responsible for load transmission between bones that are interconnected. The ductility of a bone changes to withstand the externally applied loading that cause bone fracture. Following the preliminary section of this thesis, the bone, in terms of its behavior and mechanical properties, were discussed in details and explained. Moreover, another significant feature of the bone to take note of, is its “self-adaptive capacity” i.e. the ability to shape its anatomical microstructure and property. Also, the environment (physiological or mechanical), has a profound effect on the bone shape, structure and composition; this adaptive ability is called “bone modelling”. This helps the bone withstand fractures as well as provide efficient counteractive repair measures. Now despite this inherent ability, bone fracture is quite frequent in occurrence; the reason being that the amount of load the bone is subjected to exceeds its strength. Failure occurs when the strength and stiffness of the bone plummets. As a result of this, preventing and pointing out the varying bone fractures, has become a vital topic in the circle of orthopedics research. Statistic show that the number of hip fractures globally, in 1990, was about 1.66million and this number is estimated to rise to about 6.26 million, in the year 2050. Immediately a fracture is detected, the healing process kicks in automatically to remedy the situation. Sites such as the bones, tendon, cartilages etc., are where the healing process takes place, and this can be influenced by the mechanical environment, which in turn, has a ripple effect on the stability and subjected load of the site in question. However, certain fractures cannot be fully

repaired. Also, there are delayed fracture and non-union occurrences, depending on the mechanical, geometric as well as the biological factors affecting the site. Therefore, this reason tends to justify the lack of fracture stabilization [1-4].

1.2 Biomaterials used in Regenerative Medicine and Tissue Replacement

1.2.1 Metals

In the field of dentistry and medicine, metal and its alloys have played a significant role in the manufacture of regenerative materials and prosthesis [6-7]. Now despite the fact that the body contains corrosive fluid that degrade metals, metallic alloys such as cobalt chrome, titanium, stainless steel etc., have been devised to be anti-corrosive, thereby making them suitable candidate for biomedical devices. Metallic alloys such as cobalt-chrome (Co-Cr) [9], titanium-6Al-4V and its alloys [8], and stainless steel (316 L) [6-7], are widely used in hospitals for performing replacement surgeries. On the other hand, metallic alloys such as silver (Ag) and gold (Au), are more traditional biomaterials used in dentistry [10]. Hydroxyapatite as well as silicate bioceramics are the coatings that are applied to the metals; this plays the role of mimicking the host tissue [8, 11]. What makes the metallic biomaterials differ from the ceramics and polymers is the mechanical strength it possesses i.e. its fatigue strength, toughness, compressive strength etc. Consequently, these metallic biomaterials have favorable advantages and some disadvantages [12]. Its no surprise that metallic biomaterials are more extensively accepted for load tolerance as compared to its counterparts.

1.2.2 Polymers

Polymer materials are most often utilized in the field of biomedicine. Now despite the fact that synthetic polymers are much easier to make use of, the natural polymer

is more degradable and compactable biologically. Therefore, it is essential in the field. Moreover, breaking down and blending both types of polymers, creates another polymeric material with a distinct mechanical property. Therefore, the quest for a new type of material has gained widespread interest in the last thirty years. By closely observing Table 1.1, the profound effect of blending both polymers together can be clearly seen. These new class of materials have been called biosynthetic or bio artificial materials. Note that the natural polymers are more biocompatible, whereas the synthetic polymer contains compounds and initiators that inhibit the natural cell growth [13-14]. However, these synthetic polymers possess excellent mechanical properties as well as thermal stability when compared to its natural counterparts. In addition, on a performance scale, the synthetic polymers are more superior and is simply easier to shape synthetic polymers to a desired shape unlike the natural ones, which might crumple when subjected to high temperatures. Therefore, there must be a balance between blends of natural and synthetic polymers, to ensure it is biocompatible, with an excellent mechanical and thermal property. Biopolymers suc as chitin, chitosan, collagen, silk, keratin and elastin, are the major biopolymers that are used for manufacturing the biomaterials. It should be noted that these biopolymers are the bodies of animals. Another type of biopolymers extracted from plants includes cellulose, starch and pectin. These can be easily blended with the synthetic polymers to create a distinct material. Also, strengthening measures can be taken by blending the polymers with minerals. These minerals grow in a polymeric matrix, that mimic the shape, size and crystal distribution, inherent to hard tissues. Collagen and elastin are usually insoluble in water as well as solvents that are organic. However, there is an exception, and that is the collagen that is extracted from young animal tissues. This type of collagen is soluble in dilute acetic acid.

Moreover, chitosan is also soluble in this fluid; however, its highest attainable concentration is low and it depends on the molecular mass of the biopolymer. Due to the solubility of both materials i.e. the chitosan and the collagen, in acetic acid, there is a higher chance that it can be blended with other water-soluble polymers [13-14].

1.2.3 Ceramics

During last four decades, the industrial revelation in the ceramic field leaded the improvement in many applications like tissue replacement. The ceramics are applied in many applications such as disease, regeneration, aerospace, and biomedicine. Availability and antibacterial behavior is the most common advantageous of ceramics. The short-term and long-term behavior and reaction of ceramics is possible to be predicated [15]. Bioceramics are the groups of ceramics that carries the bioactive characteristic of the ceramics that make them possible to be used in the medicine tools and implants. The bioceramics have some drawback like the low mechanical compressive or tensile strength because of the brittle character [16]. Bioceramics like calcium phosphate is one of the most common ceramics used in the bone tissue engineering. Calcium phosphates (CaPs) are widely used bioceramics in bone-tissue engineering due to their excellent bioactivity and compositional similarities to bone [17]. Among various CaPs, hydroxyapatite [HA, $Ca_{10}(PO_4)_6(OH)_2$] and tricalcium phosphate [TCP, $Ca_3(PO_4)_2$] are the most widely used ones in various biomedical applications, such as bone reconstruction and replacement, bone defect-filling, and coatings of metal prostheses because of their osteogenic property and the ability to form strong bonds with host bone tissues. Dissolution characteristics and excellent osseoconductive properties make TCP widely used as a bone cement and implant material [18]. TCP ceramics with improved mechanical properties and controlled resorbability can assist in designing

optimal biodegradable bone substitutes for spinal fusion and craniomaxillofacial applications. Use of such bone substitutes also avoids the second surgery required for auto graft harvesting.

1.2.4 Composites

The combination of two or more materials is known as a “composite”; a composite possesses a distinct desired property that differs from the independent materials. Materials that make up the composite can be identified within its structure as these materials do not dissolve into each other. Advanced composites (ACM) are also called advanced polymer matrix composites. What sets these materials apart are the unusual fibre strength, which possess a unique modulus of elasticity, high stiffness and weaker matrices bond, in contrast to other materials. These ACMs differ from the conventional composites such as the traditional concrete or reinforced concrete. Moreover, a low density and high fraction volume is usually associated with this high strength fibres. Some of the benefits of this ACM is a certain desired chemical and physical property, which includes a higher stiffness, strength and lower weight ratio, towards the reinforcing fibre direction, temperature, dimensional stability, chemical resistance, relatively easier processing and then, flex performance. ACM has even gained widespread usage in the aerospace industry, replacing its metal counterparts. Classification of composite is based on the matrix phase it belongs to, such as: ceramic matrix composites (CMCs), polymer matrix composites (PMCs), and then, the metal matrix composites (MMCs). Moreover, these types of materials are usually referred to as advanced materials. Their properties range from lower weight ratio, high axial or longitudinal stiffness value, high axial or longitudinal strength values, electrical properties and corrosion resistance. Animals and plants, both have natural composites [19-20]. Wood, for example, is a composite

that is gotten from cellulose fibres that are long, which is held together by a relatively weak substance known as the lignin. Cellulose can also be extracted from cotton; however, the absence of lignin means it will be very weak. Another surprising composite is the bones in our body. It is composed of a brittle hard material known as the HA and as flexible-soft material called the collage. The flexible soft material is a protein while the brittle hard material is majorly calcium phosphate [21]. Finger nails and hair also possess collagen. Functioning independently on its own, it won't be very effective in the human skeleton but when combined with hydroxyapatite, it gives the bone the necessary strength required to support the human body. Composites have been around for centuries. Examples are mud bricks (a mixture of straw and mud), which have great structural integrity and make excellent blocks for building. One more prehistoric composite material is concrete, which are lighter and tougher than fibre glass; however, it is much costlier to manufacture. These materials can be designed for usage in sport utilities or aircraft components. State of the art materials such as carbon nanotubes have also been used to manufacture composites as well. The advantage of this advanced material is that it is much lighter and stronger than its counterpart, which is gotten from carbon fibres. However, these advance materials are very costly but are significant in producing lighter aircrafts and automobiles. As a result, the fuel consumption level is dropped profoundly. Glass fibre reinforced aluminum is widely used in industrial applications. It is a new type of composite that is exceptionally stronger than the typical airframe aluminum frame. In fact, it is twenty percent lighter and twenty-five percent stronger than its predecessor. The fusion of reinforcement material and matrix produces a material that meets a certain mechanical property criteria. Moreover, composites have an inherent flexibility within its microstructure as result

of the complex shape it is molded into. However, the problem that arises is it is expensive but this expense, accounts for the efficiency of the product [19-21].

1.2.4.1 Ceramic Matrix Composite

In order for the material's structural toughness to be drastically improved, a special class of composites called the ceramic-matrix composites (CMCs) must be created. This composite has an inherent ability to withstand excessive loading conditions, which leads to fracture. This will result in a significant improvement in the stiffness and strength of the material. Moreover, the reinforcing phase plays a role in the ceramic by limiting the growth formation. Now this can take place in a number of ways, which includes: the formation of bridges across the crack face, deflecting the tip of the crack, redistribution of stress within the adjacent regions and absorbing the energy when the pull-out phase occurs. Furthermore, the morphology is vital in reinforcing the mechanical properties of the material [22-23]. The reinforcing material will perform much better when its aspect ratio is considerably higher. Therefore, thin-longer fibres that possess higher aspect ratio will reinforce much more better than particulates; this is because it has a value of 1 as its aspect ratio. Moreover, in other for the crack propagation to be truncated within the matrix, much of the load applied must be taken up by the reinforcing material. The bond that exist between the matrix and the fibre, will tell how well the matrix will be able to channel stresses to the fibers that are stronger. However, it should be noted that this bond is not excessive that it limits the mechanism that aid in its toughness i.e. fibre pullout and debonding [22].

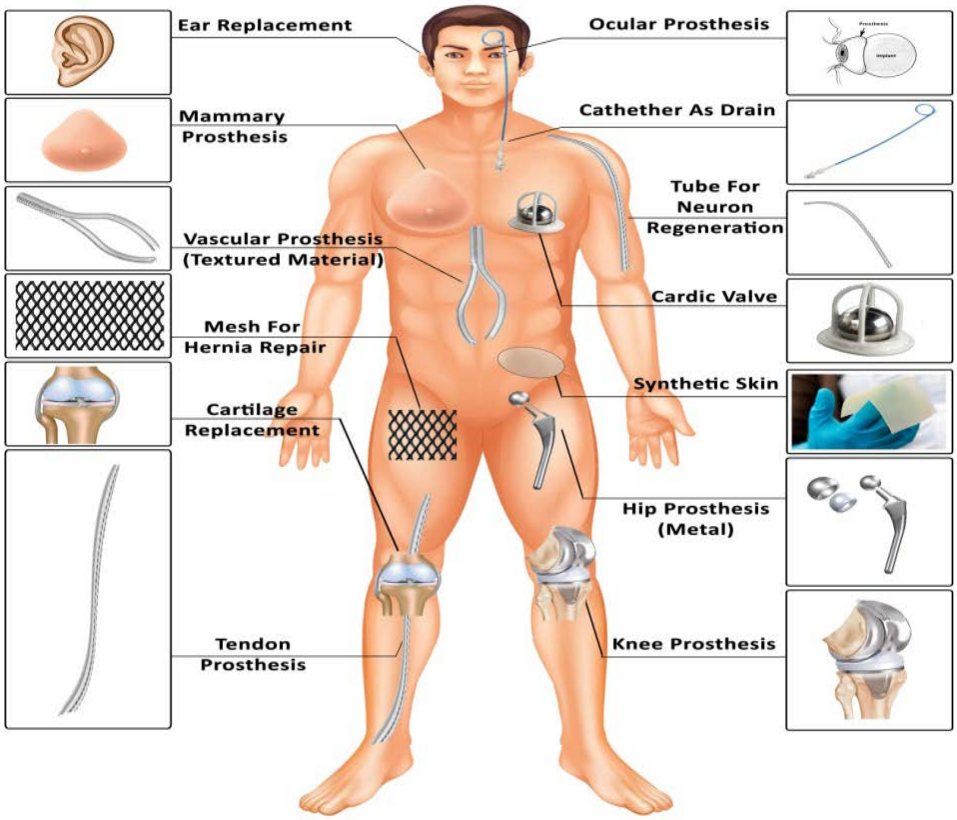

Figure 1.1: Application of biomaterials in the human body in different place implantation [304]

Higher volume fractions of reinforcement tend to improve mechanical properties. Furthermore, aligned fibers best prevent crack propagation, with the added advantage of anisotropic behavior. Additionally, a uniform dispersal of the reinforcing phase is also desirable, as it imparts homogeneous properties to the material. Ceramic matrix composites, e.g., stainless steel/HA, and glass/HA [24-25].

1.2.4.2 Metal Matrix Composite

In the last ten years, there has been a profound rising interest on “metal matrix composite” (MMCs), especially amongst the transportation or automobile industry, that have huge appetite for strength, corrosion resistance, stiffness and creep resistance. One of the benefits of using MMCs as biomaterials is because of their changeable mechanical properties as well as changeable corrosion resistive property

[26-27]. One of the measures that is put in place for controlling corrosive nature of magnesium is to increase the PH of its surrounding magnesium alloy by encapsulating it in a protective layer. Also, one element that is widely used for limiting corrosion in magnesium is calcium; this occurs when few tenths of its percentile weight is introduced [26-28].

1.2.4.3 Polymer Matrix Composite

A combination of resin or polymer with a fibrous reinforced dispersed phase, gives rise to a new kind of material called the “polymer matrix composite” or PMC. The PMC gained widespread attention as a result of its simple fabrication technique and low cost of production. However, the limitation of structure materials that are made from non-reinforced polymers is because of their low mechanical properties. Take for example, epoxy resin, which is one of the toughest polymers, has a tensile strength of just 140 MPa. Moreover, strength is not the only give in this polymer material; it also suffers from low impact resistance [29-30]. A continuous or short fibres fused together by a matrix of organic polymer, is the structural makeup of the PMC. Furthermore, PMC, unlike its counterpart-CMC (which provides high fracture toughness when reinforcement is undertaken), gives the material high stiffness and strength, when reinforced [23]. The essence of the PMC is to improve the load bearing capacity of the structure that is reinforced. Therefore, the transfer of loads within the structure and the bond of fibres are the responsibilities of the matrix. Advance composites and reinforced plastics, are the major two segments that make up the PMC [30-31]. And so, what sets this segment apart is its mechanical properties level, although there is not a clear defined line that’s differentiates them. Polyester resins that are reinforced with low glass fibre stiffness are example of reinforced plastics; this material is usually cheaper and assessable. On the other

hand, aerospace industries have thrived due to the incorporation of advanced composites within its aircraft design and engineering; this is due to its stiffness and strength, although it is quite costly. This material has been used in the aerospace industry for close to fifteen years and so, the assessment in this paper will be focused on this material [32].

1.2.5 Bionanocomposite

There has been a growing need to improve the bone problem discussed in most articles and reports in the field of biomaterials. The artificial bones that are usually encapsulated with fibrous tissues have a certain drawback and that is its inability to adhere adequately to its bone host [15, 16, 33-36]. Fusing both artificial bones and living tissue with a new bioactive compound, produces materials with better biological properties and densification, when combined with the HA ceramics. These bioactive materials are MgO, SiO_2 and $CaCO_3$. Examples of additives are Mg, Zr, Sr, TiO_2 and Fluorine. Akermanite, baghdadite, diopside and bredigite synthesized by the combination of three group phases of MgO, SiO and the CaO. This is done in order to put together a glass-ceramic material that has a better bone-bonding property as well as mechanical strength [37-41]. A coalition of these fillers and additive compounds, work together to reinforce and form the material into a granular shape with higher thickness. When a clinical investigation is conducted, the downsides of the biomaterials and scaffolds become quite obvious. Even when the material is subject to a small force, it crumbles under the loading. A significant number of trace elements like the Magnesium (Mg^{2+}), Sodium (Na^{+}), Zinc (Zn^{2+}), Strontium (Sr^{2+}) and Silicium (Si^{4+}) are found in the natural bone within the mineral phase [41-45]. Another medium for improving the mechanical properties as well as the vivo and vitro biological responses of materials significantly is by initiating cation substitution

in CaPs [6, 7, 15, 18]. From the various studies, it has been shown that the required mechanical properties of the material can be gotten from the dopants such as the sodium fluoride (NaF), silver(I) oxide (Ag_2O), calcium oxide (CaO), titanium(IV) oxide (TiO_2), strontium oxide (SrO), magnesium oxide (MgO), zinc(II) oxide (ZnO) and the silicon(IV) dioxide (SiO_2), when the optimum concentration is introduced in order not to affects its biocompatibility i.e. β-TCP [16, 18].

When considering Sr^{2+}, for example, Sr^{2+} results from instantaneous stimulatory effects on the osteoblast bone formation and inhibitory effect on osteoclast mediated bone resorption. Due to its profound impact in the area of bone remolding and modeling, Sr^{2+} has become widely used in osteoporotic drugs; this includes Sr^{2+}ranelate. The presence of this compound in CaP, helps in improving the functions of osteoblast as well as the bone formation process. On the contrary, an increased amount of strontium instigates mineral profile alteration as well as flawed bone mineralization. Mg^{2+} effect on mineral metabolism and bone was highly pronounced [41-45]. As a result, Mg^{2+} is a very vital bivalent ion linked to biological apatite. The advantages of Mg exchange with CaPs have received a profound recognition because of the role it plays in changing, qualitatively, the bone matrix, indirect influence on metabolic mineral, catalytic reaction promotion and biological function control [18, 42]. Another important element that is vital in influencing the calcification and formation of bone is silicon (Si). From past research, it has been uncovered that Si has the ability to stimulate cellular activities; this can be differentiation and proliferation of osteoblast like cells, mesenchymal stem cells' osteogenic differentiation, and the human osteoblast mineralization. Furthermore, Si^{4+} can be located within the connective tissues and bones of the body [18, 41-45].

Table 1.1: Comparison of biomaterials (metals, ceramics, polymers, composites) use and application

Biomaterials	Example	Advantages	Disadvantages	Application
Metals	Aluminum, Titanium alloy, Steel alloy (4340), Aluminum alloy (7075)	Flexible, stronger, Anti corrosion, easy fabrication	High corrosion in biological environment, high density, non bioactive,	Orthopedic plate, load bearing implant. Orthodontics wire
Polymers	Polystyrene, Polymethyl methacrylate	Easy Fabrication, low density, flexible, no oxidation, low toxicity, lower weight, colorful	High degradation rate, Low heat resistance, low mechanical resistance, some of them expensive	Biomaterials, Industries tools, Tubes, sutures, arteries, veins, cements, artificial tendons, teeth, nose, ears, heart valve, breast implants
Ceramics	Concrete, Soda-lime glass, Silicon carbide, Aluminum oxide	High Bioactivity, High corrosion resistance, Biocompatible	Low strength, complex technique, low toughness, non flexible, low impact resistance, difficult to reproduce	Hip joint, bone filler, coat on implant, tissue engineering, dental parts, endoscopy
Natural Materials	Collagen, Tissues, Grafts	Availability in the body, bioactivity, biocompability	Rejection by host organs	Heart valves, implant coating (dental, orthopedics) hip implants
Composite	Silica aerogels, Mullite-fibre composite	High strength, stronger, varied manufacturing technique,	leak of consistency and difficult fabrication methods, expensive	Bone regeneration, scaffolds, drug delivery

1.2.6 Magneto Ceramic

Ferrimagnetisms takes place when oxide materials or magnetic ceramics portray a distinct permanent magnetization property. Magnetic ceramics that are commercially

mass produced are used in the production of transformers, permanent magnets, information recording devices and telecommunication devices [46]. In this thesis, the properties as well as the composition of principal magnetic ceramics are explained; additionally, its role in the commercial industry is surveyed. Ferrites are widely used for making the magnetic ceramics; these are mostly minerals that are crystalline in nature and are made up of iron oxide combined with other varying metals [47]. Their organic chemical formula is $M(Fe_xO_y)$, where 'M' stands for elements that are metallic other than iron. One of the most popular magnetite is ferrous ferrite i.e. Fe_2O_4; it occurs naturally and is usually called "Iodestone". In the past, this magnetite where used for making crude compasses. Ferrites magnetic behavior is known as "ferrimagnetisms" and this differs from "ferromagnetism" (a magnetic property that is associated with iron). When talking about ferromagnetism, just a single lattice site is available and electrons without a pair spin in other to line up with the domain in question. Magnetic ceramic products are made from three preliminary classes of ferrites. This is with respect to its crystalline structure, which can be hexagonal ferrites, garnets and spinals. Moreover, because these materials have higher dielectric properties, they can be introduced into devices that electronic; this includes memories, resonators, capacitors etc [46-49]. In our present age, however, the $RFeO_3$ which is a rare ceramic magnetite, has been a closely studied material amongst researchers and biomaterial enthusiasts; the reason being their ease of applicability [48-50]. $RFeO_3$ is applied in sensors [52], solid oxide fuels [51], environmental catalyst [53] etc. There is measure that has been put in place to account for the degree of distortion affecting the optical, dielectric, and structural and properties of another compound, and this is the bond angle Fe-O-Fe. It is no longer a closely guarded secret that synthesized material at the nanoscale, produces

a more preferable property; this includes higher chemical reactivity, larger surface area, better electrical as well as magnetic features [46-47]. Therefore, orthoferrite ceramics synthesized at the nanoscale, brings about photocatalytic and magnetic features [46-48]. In other to ward off infections that arise in the prosthesis, some counter measures must be taken; these are as follows:

a) Engineering composites that are HA based, that possesses antibacterial phases. For example: Ag, Cu, ZnO, Fe_3O_4, and Ti etc.
b) Controlling the infected site by bombarding it with a magnetic or electric field that is external.
c) Introducing drugs that are nanoparticle into the site that is infected [46-53].

1.2.7 Bioceramic Properties

1.2.7.1 Mechanical Properties

There is a flaw that is inherent with bioceramics like phosphate and orthophosphates. These bioceramics usually have poor mechanical properties and are therefore, not viable for field operation because they lack the structural integrity to withstand certain loading conditions. Having the ceramic origin, any bioceramics made of CaPs possess poor mechanical properties that do not allow them to be used in load-bearing areas, such as artificial teeth or bones. For example, fracture toughness of HA, bioceramics does not exceed the 1.0 MPa $m^{1/2}$ (e.g. human bone fracture toughness: 2–12 MPa $m^{1/2}$). It decreases almost linearly with porosity increasing [54]. Moreover, the fracture toughness declines linearly with respect to the value of its porosity. However, when talking of the non-cubic bioceramics, the fracture toughness climbs to a higher value and drops drastically with respect the grain size reduction. According to [55], the fracture toughness of hot pressed HA that was pure,

having a 0.2-1.2 (μm) grain size, was closely observed by Halouani et al. By closely observing its behaviour, it was seen that the fracture toughness increased as the grain sized reduced by more than 0.4 (μm) and reverse was the case for decreasing fracture toughness. The fracture toughness value at 0.4 μm picked at 1.20 ± 0.05 (MPa $m^{1/2}$). Moreover, the amount of energy that was expended by the sample of the HA ranged from 2.3-20 J/m^2. Another interesting find was that when the porosity increased, the strength decreased [56]. It is also worth mentioning that porous HA bioceramics are considerably less fatigue resistant than compact ones. Both grain sizes and porosity have been reported to influence the fracture path, which itself has little effect on the fracture toughness of calcium phosphate bioceramics. Furthermore, no obvious decrease in compressive strength properties was found after calcium phosphate bioceramics had been aged in various solutions for different time periods [56]. As the scaffold implanted in humans body they are bearing various amount of loads, therefore the mechanical properties e.g. compressive strength and fracture toughness are the most important properties required to be addressed [36-37]. As it is investigated the incorporation of MNPs on silicate bioceramics may significantly enhanced the mechanical resistance of the scaffolds under static and dynamic loads.

1.2.7.2 Biological Properties

The most important differences between bioactive bioceramics and all other implanted materials are inclusion in the metabolic processes of the organism; adaptation of either surface or the entire material to the biomedium; integration of a bioactive implant with bone tissues at the molecular level or complete replacement of resorbable material by healthy bone tissues [54-57]. Bone-like apatite of bioceramics is a major profit to design a bone tissue. The bone-like apatite or term of bioactivity which can induce apatite on the surface of implant after soaking in the artificial

solution. The functional groups in the apatite make the apatite formation be ready to precipitate on the ceramic [58-59]. Apatite formation and nucleation investigated by surface modification and analysis. Different ceramics like Bioglass, natural HA (NHA), and A-W ceramic can bond with the living tissue easily. These bioceramics, which can easily join with real bone, is called bioactive ceramic. These bioactive ceramics are highly used in clinical surgery and bone substitution in the hospitals and clinics. However, these bioceramics might attach with the cortical bone with difficulties as they have higher fracture toughness and lower elastic moduli. Thus, it is recommended to introduce bioceramics with better mechanical properties. The bioceramics motioned above have good *in vitro* condition and the bone apatite formation can easily occur on their surfaces. The formation of apatite on the surface of these biomaterials is possible because of some functional groups like Si–OH, Ti–OH, Zr–OH, Nb–OH, Ta–OH, –COOH, and PO_4H_2 [56-59]. Such functional groups have special microstructure, which shows negative charge and leads the apatite formation to be created very fast. The apatite, which prepared on the surface of tissue, is containing calcium silicate, calcium titanate, and amorphous calcium phosphate. By knowing these informations creating a new novel bioceramics is possible and controllable. Hard materials can be produced by various techniques like those that mechanochemical, and mechanical activation combine with metals salt to enhance fracture toughness. In addition, soft materials can be prepared by sol-gel method like flexible polymer composite. Bone disorder cause lots of problems and pain for patient, which makes the life difficult for old people. In general, treatment of bone defect or disorder the best treatment is bone grafting in various amount for each person [56-58]. In the new world wide, bone grafting has attracted researcher's attention to the allogenic bones. Although the used of autogenous bones destroy body

organs, the amount of substitution should be controlled and limited [56-61]. Bone disorder cause lots of problems and pain for patient, which makes the life difficult for old people. In general, treatment of bone defect or disorder the best treatment is bone grafting in various amount for each person. In the new world wide, bone grafting has attracted researcher's attention to the allogenic bones. Although the used of autogenous bones destroy body organs, the amount of substitution should be controlled and limited.

1.2.7.3 Electrical Properties

The electrical behavior of CaPs bioceramics materials has been investigated in the wide range of biomedical application. For instance, the surface conduction of HA (dense and porous) has been utilized for the humidity with sensor applications, considering the room temperature conductivity was affected by dependent humidity. Some application of HA bioceramic as ionic conductivity like CO_2, alcohol and CO_2 for gas sensors [62].

The electric behavior of HA bioceramic as one of the important characterization technique to monitor the phylogeny of materials. As an example Valdes et al. [63], determined HA dielectric features to know the β-TCP decomposition. As the reports indicate the electrical behavior of HA ceramics greatly effect on biomedical applications like transaction of cells and hard tissues in a humans body. The electrical properties also has been investigated by various researcher to analysis the microstructure in HA [64] and study composites [65] such as HA–ZrO_2 [66] and HA–Ti [67]. The HA polarization can produce a full charge surface with the electric field up to 200°C temperature [62-64]. This surface might have the predominant impression on both *in-vitro* and *in vivo* evaluation of bone-like apatite. Moreover, the

bone-like apatite and growth resembles to be expedited on the charged surfaces (negatively) and decelerated at positively charged surfaces of HA bioceramics. Nakamura et al. [68] recently reported that both positive and negative charges accelerated the cytoskeleton reorganization of osteoblast-like cells. The major importance of investigation of the bioceramics as popular bone reconstruction materials can be their appropriate acceleration occurs by electrical currents in the injured or defect area. Proper electrical feature of scaffolds are required to support mimicking of host and guest tissue and control neuron behavior under stimulation of electrical, therefore, more proper guiding neural tissue to regenerate properly.

1.2.7.4 Thermal Properties

Thermal properties are another important parameter that can affect the properties of ceramics. These thermal properties include the duration of applied heat treatment and its temperature [69]. Studies has shown that synthetic ceramics like HA having a Ca/P ratio close to 1.67 remain steady even below the 1200°C mark i.e. when sintered at a moist or dry atmosphere [17,70]. The stability of ceramics is compromised due poor thermal resistance and so, it breaks down to form tricalcium phosphate i.e. TCP, when temperatures exceed 1200°C [70-72]. Therefore, great care must be taken when working with ceramics at high or low temperatures. The preparation of ceramic powders is done by various methods [16-18]. Now with respect to the method concerned, materials that portray different stoichiometry, morphology and crystallinity have been designed [15-18]. Moreover, these new properties have a profound effect on the biomaterial quality through the effect of mechanical integrity, dissolution behaviour, and thermal stability [72]. Another study conducted by Dezfuli et al. showed that the creation of Mg-bredigite composite wasn’t the only thermal event that occurred during the heating process but the cold

magnesium oxide that was heated at 600°C , experienced an exothermic reaction which commenced at 550°C and peaked at 592°C; this lead to an abrupt mass loss [73]. These ongoing researches were targeted at devising a fabrication methodology that was viable for structural bioceramics, that houses MNPs-matrix composite. And so, it is no surprise that an in-depth comprehension of the mechanism for degrading as well as the rate of degradation with respect to the decline in MNPs-bredigite mechanical property, will help in improving the MNPs-matrix composites' degradation related mechanical properties of control. This will prove significantly important in when these advanced biomaterials are applied. The mechanisms of the thermal, mechanical, biological, electrical and degradation of the MNPs-bredigite composites were proposed in this work. However, another critically important issue, i.e., their cell culture behavior in relation to degradation behavior was not addressed. The thermal conductivity of scaffold magnetite-bioceramic nanocomposite prepared by magnetite particles which incorporated into the ceramics matrix introduced two advantageous such as the micro structural assistance and may help the matrix with appropriate functionalizing and presenting thermal and magnetic behavior to the host tissues. The magnetite can released heat as they may insert in the AC field, therefore the scaffolds nanocomposite containing magnetite can properly release heat because of cortical bone thickness, which limits the thermal conductivity for tumour therapy.

1.3 Manufacturing Techniques of Biomaterials

Several manufacturing processes have been utilized to manufacture biomaterials scaffolds. Although various traditional manufacturing techniques such as solvent casting are available; the production of scaffolds using these methods lacks consistency and reproducibility [74]. Recently, with the use of modern techniques like rapid prototyping (RP), it is possible to mimic naturally-occurring scaffolds,

even with their complex structures. The purpose of this section is to provide a quick overview of some traditional manufacturing procedures, like material injections and solvent casting, and to expand upon new fabrication techniques, such as RP, to produce bone scaffolds for bone tissue engineering application. Even though advanced scaffold manufacturing techniques provide many advantages over conventional scaffold fabrication techniques, conventional techniques are still widely used for porous scaffold manufacturing. RP which is known as the SFF i.e. the Solid Free Form fabrication, are systems that have been put in place to define the various sets of manufacturing processes that are capable of utilizing CAD models directly to create free form components that are complex, without a defined information or tooling. When compared to the conventional subtractive machining process i.e. drilling, shaping etc., the RP system differs because it possesses the ability to join powder, liquid, and sheet materials to piece together a component. The Rapid prototyping machines can fabricate wood, plastics, metals, and ceramics by using a horizontal cross section that is thin from a CAD model; and this is usually done layer by layer. RP devices which includes FDM i.e. fused deposition modelling and 3d printing technology, make it possible for manufacturing process that make scaffolds that are porous, to be developed. This scaffold closely represents the living tissues' microstructure. A description of some of the more traditional methodology is presented below [75].

1.3.1 Modern Manufacturing Technique

1.3.1.1 Solvent Casting and Particulate Leaching

Solvent casting and particulate leaching (SCPL) method involves a solution of polymer (for example, PLLA) dissolved in an organic solvent (for example, chloroform). Salt particles such sodium chloride (NaCl) of specific dimensions are

then added to this solution to make a uniform suspension. This mixture is then shaped into its final geometry using a mold. The solvent is then allowed to evaporate then leaving the composite that consists of the particles with polymer as shown in Table 1.2. The composite is then placed in a water bath where the salt particles leach out and leave behind a porous structure. Solvent casting (i.e. particulate leaching) has shown promise in producing scaffolds at room temperature. In this method, the pore size and porosity of scaffolds can be varied by changing the size and morphology of the salt crystals. Scaffold properties, such as polymer degradation time and mechanical strength, can also be altered by changing polymer concentration and the amount of salt crystals. Although solvent casting has been effective to produce scaffolds sufficiently strong, it lacks in reproducibility and ability to provide desired pore geometry and morphology. In addition, the thickness of scaffolds produced by SCPL technique should be less than 4 mm to have a uniform pore structure [76]. Comparing some traditional and modern manufacturing techniques shows that 3D printing technology is more capable of answering customer needs in printing complex shapes in a short time period. The cost efficiency is also another benefit of 3D printing technology.

1.3.2 Rapid Prototyping of Ceramic Manufacturing

Three-dimensional printing i.e. 3DP was developed by MIT; it develops components by using an inkjet printing technique, which injects liquid binding solution on the powder bed, held by the movable platform [77, 85-87]. Various material types i.e. either liquid or solid, can be used to accomplish this printing task. Fine layers of powder are spread consistently across the platform in other to initiate the process. Materials such as PVA [88-90], calcium polyphosphate, TCP [91] and HA, are employed in this technology. Other materials include: HA and apatite–wollastonite

glass ceramic with water-based binder [95], MgO doping [93-94], TCP [92] and TCP with SrO, PLGA [97], calcium phosphate with collagen as the binder [96] and then, and farringtonite powder ($Mg_3(PO_4)_2$) [98]. In indirect 3DP, the materials that is employed as a replacement for gelatin performs is the chitosan and PCL [77, 99].

Reviewing several literature indicated that the 3DP machine has proper advantageous compared with other traditional techniques mentioned before like high cost of materials preparation, time consuming, requirement for expert operator and unable to design complex shape and design. In addition, the mass production of product with traditional technique has been investigated as a famous obstacle. However, the 3DP machine are highly automatically create and complex shape with proper required properties, thus the 3DP machine has been used and applied to fabricate the magnetite-bredigite nanocomposite for bone tissue engineering applications.

1.3.2.1 Stereolithography

One of the earliest rapid prototyping processes that was introduced by 3D Systems Incorporated, in the year 1980, was the stereolithography (SLA) [77-78]. When ultraviolet light is targeted at the liquid surface, the SLA photopolymerizes the liquid polymer, causing it to solidify [77]. The enhancing model is supported by a platform, which is designed to come close to the liquid's surface when actuated; following this, the first cross sectional layer of the model is solidified by an ultraviolet laser [78]. A second layer is added to it by lowering the platform by one cross-sectional layer thickness, recoating the first layer's liquid and finally, bombarding the new layer with ultraviolet light. It should be noted that this process reoccurs repeatedly, until the model in question is finalized. Normally, after all this has been done, the model is taken out, cleaned and cured by using an oven that possess ultraviolet radiation.

There has been various biopolymers that have been introduced into the catalogue of the SLA; one of such biopolymers is aqueous poly (ethylene glycol) (PEG) hydrogel solution. When the SLA is taking place, the dermal fibroblast cells that is wrapped within the solution concerned, can be adequately protected from harm by employing the use of hydrogel; this finding was verified through a conducted research on the SLA. Further research has shown the usefulness of bioceramics as opposed to the conventional usage biopolymers due to its biocompatibility [77]. In other to prepare the suspension of the bioceramics, the powder of the bioceramics is introduced into a photopolymer; this is usually done before the SLA processing takes place.

1.3.2.2 Selective Laser Sintering

In the year 1989, the University of Texas came up with something through revolutionary and it was called “selective laser sintering” or “SLS”. Most of its functionality is quite similar to that of the “3DP”, when the powder particles are fused together; the only difference is the use of CO_2 laser beams [79]. The essence of the laser is for scanning the polymers’ powdered surface within a two-dimensional pattern, in other for it to be sintered by raising the temperature higher than the transition temperature of the glass. Polymer powder form the building blocks for parts manufacturing in SLS, as lasers are passed across thin layers of it. When this laser is passed across the powder, the temperature increases causing the particles that are close to it to be bonded together and this action also takes place at the layer that follows it. After this action, an elevating platform holding the part in place, moves downward by one layer and then, a roller is utilized for deploying powder on the layer that was initially processed. The part is taken out of the machine and then post processed; this is done by using a CAPs solution to dissolve the particles that were unsintered, which will leave within its microstructure, micro-porosity. Moreover,

particulates like the CaPs and Ceramics have been widely used in the SLS material implant as binder for the polymer. Also, bone scaffolds have produced through the process of SLS from both the composites of the pol-L-lactide (HA-PLLA) and HA-particles; the selected binder in this case is PLLA. This is as a result of its lower melting point and degradation time, which is higher [80]. From studies that have been conducted, the modulus of elasticity ranges from about 140.47 to about 257.27 MPa, and then 1.57 to about 4.05 MPa, reflects its bending strength, which is quite close to the strength value of the cancellous bone. However, when the SLA is compared to the SLS, SLA has a smoother finish, higher porosity and dimensions with whither precision; which is a major setback for the SLS.

1.3.2.3 Fused Deposition Modeling

Another type of rapid prototyping technology is the FDM i.e. fused deposition modelling; this technology rapidly produces parts by using a filament material, which is extruded from a minute orifice that is temperature controlled; this filament material gives out a polymer that is closely molten in structure, depositing it on the movable platform; when this occurs, there is an instant solidification. The part is then built layer by layer, when the platform goes down so as to deposit this filament material on the layer that follows [81]. Scaffolds that have a finely uniform microstructure can be gotten by altering the trajectory of each layer as well as the space that exist between each material. In other words, multi-material scaffold manufactured by employing the use of varying deposition process as well as multiple heads. There have also been various processes used in rapid prototyping technology for the fabrication of scaffold and a high number of these processes are focused on spraying methodology, extrusion or material printing; this process normally requires multiple material feeders to create the complex scaffolds to optimize the composition

and geometrical make-up of the material instantaneously [81-82]. On the other hand, for complex designs to be made such as anatomical parts, 3D printers are employed in the process. The particles which emanates from the feed bed is delivered to the build bed via rollers and then, upper machine part moves towards the powder bed that is loose and prints consistently based what is defined by the computer aided design model. A heater is vital in the process, because it helps in extracting the moisture from the powder bed, especially the moisture that exists between the obtained shape and the powder [81-83]. This process repeats itself until the build platform moves downward to eventually a newer layer; the newer layer usually has a thickness lower than 20 (μm). Furthermore, another layer of powder is deposited on the last layer, then the printer head, with respect the part's geometry, employs a binder. This cycle repeats itself until the finalized component is manufactured. Moreover, there are composites that are highly regarded in the industry due to their biological and mechanical properties for regeneration of bone; this includes the PCL-TCP or polycaprolactone-hydroxyapatite (PCL-HA) [84]. The Table below highlights the advantages and disadvantages of these RP technologies.

Table 1.2: Advantages and disadvantages of common rapid prototyping techniques

Method	Advantages	Disadvantages
Stereo lithography	Hydrogel materials, high-resolution and accuracy, liquid build material can easily be removed from within complex scaffolding	Limited choice of materials, may require furnace post processing (e.g. bioceramics), high material cost, complex and expensive equipment
Laser sintering	Wide range of material choices, good mechanical properties, lower material cost, good accuracy	Materials may thermally degrade during the process, undesired porosity, hard to remove trapped powder, complex and expensive equipment
3D printing	Wide range of material choices, low cost, quick process, multi-material capabilities through multi print-heads	Hard to remove trapped materials, low to Medium resolution, powder particles may not bind well, binders are always necessary to bind powders
Fusion deposition modeling	No trapped materials, minimal material waste, low cost	Materials may thermally degrade during the process, lower range of material choices, medium resolution

1.4 Hyperthermia Treatment

In general, hyperthermia term means increasing the part of body temperature up to 5°C [100]. This increase in temperature causes the cancer tumor to disappear with applying of radiotherapy and chemotherapy. This leads the bone not to be suffered and damage by the hydrothermal therapy using biomagnetite particles. All the previous methods used for hyperthermia were applied on the skin surface such as microwave and laser treatment [102-103]. Hyperthermia leads the cancer capsule to have better influence and reaction along the treatment process. Cancers like sarcoma

and melanoma are the most common and known disorder in medicine. Hyperthermia consequences indicate that size of tumor has been reducing to half using hyperthermia and chemotherapy together [100-102]. From the research conducted by Tseng et al. [103], the incorporation of platinum and iron ions with the HA i.e. PT-Fe-HA, was shown to be extremely deadly to the A549 i.e. the human lung adenocarcinoma cell and the fibroblasts of rats, when subjected to hyperthermia under a predefined magnetic field; however, the study showed that the fibroblast cell wasn't affected in any way. Therefore, this can be used as a likely dual agent for cancer treatment during the chemo-hyperthermia therapy [103].

1.4.1 Magnetofection

Transfection reagents, nucleic acids and viruses are brought together with certain definite nanoparticles; this is known as the principle of "magnetofection". In other words, the process by which a external magnetic field is used as a catalyst to fuse the DNA with nanomagnetic particles is called magnetofection. However, in order for this to take place a special coating called the polycation polyethylenimine is applied to the magnetic particles [104]. Following the advancement in technology, there has been a huge breakthrough in magnetofection technology; methods such as mixed bacterial toxins, hot water bath, high frequency radiation, perfusion heating, magneticfluid hyperthermia, have been utilized in the fight against tumours [105-106]; note that all this process requires heat to work. When heating of nanoparticles of super paramagnetic is initiated, the heating process becomes completely dominated by the Brownian and N éel mechanism for relaxation; But there is limitation at work because the relaxation mechanism is only effective for particles less than or equal to 10nm [105-109].

1.4.2 Magnetic Heating

The key feature of magnetic hyperthermia is its inherent ability to channel the heat and keep it focused on the tumour site. Another feature to take note of is the usage magnetic particles that are sub domain [100]. The heating potential is strongly dependent on the particle size and shape, and thus having well-defined synthetic routes able to produce uniform magnetite nanoparticles (MNPs) is essential for a rigorous control in temperature [100-103]. The classical approach of hyperthermia consists of submitting the patient to electromagnetic waves of several hundred MHz frequencies. The thermo ablation of a tumour can be achieved by an electromagnetic wave emitted by a radiation electrode implanted in the pathological area. One important contribution of the hyperthermia treatment is the increase of perfusion in the tumour tissue which also increases the local oxygen concentration and thus results in optimal conditions for the γ-radiation to destroy the tumour cells [100]. The National Cancer Institute (NCI) introduces three different types of hyperthermia treatments. Disease part under electromagnetic waves with the frequencies of more than 100 of MHz. The thermo ablation of a tumor can be achieved by an electromagnetic wave emitted by a radiation electrode implanted in the pathological area. The data gather from clinical investigation indicate that hyperthermia term is useful and possible joining with radiation therapy. As the particle size increases, ferromagnetism is stabilized and hysteresis loss mechanism becomes the dominating factor in the heating process. Hysteric effects cease to exist above the magnetic ordering temperature, the Curie temperature, TC; thus, by adjusting the TC value heating can be controlled. This provides a basis for self-controlled hyperthermia treatment. The ferromagnetic materials with appropriate TC values can be used for self-control or self-regulation of the heating of the tumour area [100-111].

One of the most common application of magnetite particles used in the current research was the high rate of heat which magnetite (Fe_3O_4) released as they installed in the AC magnetic field. Also, the suspension of ferrofluid (in this thesis soaking of nanopowders in ethanol) investigated to consider the magnetic saturation and magnetization of each bredigite-magnetite nanocomposite.

1.4.3 Types of Hyperthermia Treatments

Hyperthermia treatments are divided in three categories according to the size of tumour. The types of treatment of hyperthermia are local hyperthermia, regional hyperthermia, general hyperthermia that is explained in the following subsections.

1.4.3.1 Local Hyperthermia

In the local hyperthermia with temperature (42–45°C) the heat utilizes to remove the tumour in small size and shape with different techniques that apply energy to cell or tumour. The techniques to apply energy are including microwave, radiofrequency, laser and ultrasonic wave-based [112].

1.4.3.2 Regional Hyperthermia

The second type of treatment is regional with covers large areas of defect tissue. In the regional hyperthermia treatment the part which be heated is a limb, jaw, mandible, maxilla bone tumour or another hard tissue. In this technique the energy applied using external applicators or regional perfusion [113].

1.4.3.3 General Hyperthermia

General hyperthermia treatment is an important technique to remove the defect part is whole body treatment. This method used for metastatic cancer that affects whole body. A Metastasis cancer is the extent of disease cells to new regions in the human's body frequently by the bloodstream. Hyperthermia is used to treat metastatic cancer that has spread throughout the body. In this method using fluid (alcohol or water) or

nano magnetic particle is so common. Also, magnetic fluid hyperthermia involves dispersing magnetic particles throughout the target tissue and then applying an alternating current (AC) magnetic field of sufficient strength and frequency to heat the particles by magnetic hysteresis losses or N éel relaxation [114-115]. Using magnetite particle in hyperthermia treatment is the recommended technique to remove the tumour cell and defect. It can reduce the effect of radiotherapy and chemotherapy for patients and help them to remove the defected part easier and with less side-effect. MNPs should be monitor and optimize by the surgeon [114-116].

1.4.4 Effect of Hyperthermia

One of the biggest challenges with chemotherapy is effectively delivering the drug to the tumor. Tumors have a blood reaction because the cells are so densely packed together [117-118]. When chemotherapy is infused into a patient, very small amount of drug actually get to the tumor. When any tissue in the human body is heated, it results in the dilation of blood vessels, which can support chemotherapy treatment as well as thermotherapy. Thus by applying heat to the tumor, the blood flow increased into that tumor which allows more effective delivery of the drug to the tumor. This is critically important for patients with solid tumours treated by chemotherapy. *In vivo* studies have shown that the combined use of hyperthermia and chemotherapy leads to increased cytotoxic effects of several anti-cancer drugs such as cisplatin, anthracyclines, cyclophosphamide, ifosfamide, nitrosoureas, belomycin, mitomycin and melphalan [119-121]. Knowing those common types of cancer drug and technique is not adequate to treat the bone cancer while the hyperthermia may have some disadvantageous like side effect on the healthy tissue as the defect part temperature rise up. Therefore, investigation of hyperthermia treatment is vital. In the current study, the effect of heating of magnetite particles in the novel

nanocomposite has been considered and the electrical and magnetic features were discussed in detail.

1.4.5 Hyperthermia and Radiation Therapy

Hyperthermia has the ability to kill cells that are under conditions of hypoxia (low oxygen), low pH and that are in the S-phase of cell division. The action of radiation is to damage the DNA of cancerous cells. The application of heat makes it challenging for these cancer cells to repair from this damage. The combination of hyperthermia with radiation may result in higher complete response rates in human's body, accompanied by improved local tumour control rates and better overall survival rates in many clinical trials [122]. Heating the tumour enhances the delivery of the drug to the cancerous cells by increasing blood flow into the tumour. Most importantly, hyperthermia damages the drug resistant cells and in some cases it reverses the chemotherapy resistance after repeated rounds of chemotherapy. In general, the most effective heat-drug sequence is drug treatment immediately before heat delivery. In other words, the hyperthermia should start soon after receiving the chemotherapy infusion. The application of heat devices increases the effectiveness or chemotherapy and radiation [122-123]. Néel or Brown or Hysteresis losses process of relaxation are major contributors for heat production results. Moreover, the value of the SAR is not only completely dependent on the nanoparticles' composition and structure but also, on the frequency and magnetic fields' amplitude (usually applied when measurements are taken); this plays a vital role in the value of the SAR [122-125]. Hyperthermia treatment divided into two important categories such as radiotherapy and chemotherapy to kill the tumor cell as shown in Figure 1.2. Hyperthermia reduces the cancer development resistance to chemotherapy or radiation.

Figure 1.2: Hyperthermia categories including chemotherapy and radiation therapy

Since the year 1957, there has been several conducted experimental investigations on the usability of magnetic materials to combat hyperthermia; bank of tissue samples which ranged from twenty to one hundred nanomillimeters particle size (Maghemite=γ-Fe_2O_3), was subjected and bombarded with a magnetic field of about 1.2 MHz [126-127]. Following this, equipment with a frequency of 100 kHz, was built to produce an array of magnetic fields measuring from 0 to 15A/m. Also, this hyperthermia facilities, put in place measures to monitor in real-time, the temperature levels of patients, in order to make sure that the higher limits of the temperature therapeutic threshold is exceeded; this will ensure that the thermal ablation is prevented, and also, the temperatures which are lower i.e. this lesser temperature that signal that the limit is not efficient, are surpassed. Furthermore, it was shown that this manufactured prototype performed optimally in treating tumours that resided within the human body [126]. Regarding to large number of published paper in hyperthermia treatment and technique there has been little works focus on hyperthermia treatment of magnetite nanocomposite as a scaffold structure for both bone regeneration and cancer tumour therapy.

1.4.6 Theory of Magnetism Physics

As the magnetite particle considered in the magnetic field with strength of H, each atom has its own individual reaction and response. The magnetite induction introduced by the following equation 1 as:

$$B=\mu_0(H+M) \quad (1.1)$$

Where μ_0 introduce the vacuum, permeability and M describe as magnetic moment per volume. In addition to that it is vital to know that most materials show magnetic behavior when they are in the magnetic field which called paramagnets. In addition, it is appropriate to say that ferromagnetic, and ferromagnetic materials show magnetic properties without being in the magnetic field. Recently in the 20th century another characteristic of MNPs has been discover called super para magnetism behaviour. In the case of magnetite nanoparticles, the most significant subject is the appearance and surface area of magnetic. Surface anisotropy appears due to the violation of the local environment's symmetry and the change in the crystal's field, which act on magnetic ions located on the surface. The magnetic fluid carrying the MNPs is delivered in one of four ways to the tumor.

The main parameter determining the heating of the tissue is the specific absorption rate (SAR); defined as the rate at which electromagnetic energy is absorbed by a unit mass of a biological material [126-129]. It is expressed in Watt per kilogram and is proportional to the rate of the temperature increase ($\Delta T/\Delta t$) for the adiabatic case as shown in equation 2:

$$SAR = C_e \frac{dT}{dt} = 4.1868 \frac{P}{me} = \frac{\Delta T}{\Delta t} \qquad \Delta t = 10 \tag{1.2}$$

Where P is the electromagnetic wave power absorbed by the sample, m_e is the mass of the sample, and C_e is the specific heat capacity of the sample. For classical high frequency irradiation by external antennas, the power deposition patterns lack selectivity. Another major difficulty in electromagnetic regional hyperthermia is the occurrence of local high temperatures (hot spots) because of the in homogeneities of electrical permeability and conductivity of the tissue, which cause variation of the

SAR [126-129]. This approach for localized thermotherapy induced by a magnetic fluid is already suitable for hyperthermia. The heating rate increased in the artificial tissue has been an interesting issue which leads the SAR to be developed compared to other technique, which can be used in the current work as a suitable technique and main parameter for evaluating the N eel and Brown relaxations. Also, the literature introduced that particles size of magnetite have an important effect on SAR ratio, therefore one of the purpose of the current study was to evaluated the effect composite morphology on SAR ratio.

1.4.7 Effect of Temperature on Anatomic and Live Tissue

Several studies employed NanoPlan® to calculate the expected temperature distribution within the treatment area for a desired magnetic field strength [130-131]. A clinical trial that employed NanoPlan® for *in vivo* temperature mapping, temperature distribution calculations and visualizations in the treatment area in relation to H (magnetic field) and the underlying magnetite particles distribution was performed by Wust et al.[132]. Another company has developed similar software, Sigma HyperPlan® to investigate the hyperthermia and distribution of heat. There have been several published papers, which show that increasing the temperature of disease body part can reduce the size of tumor. Therefore, the hyperthermia treatment may support the increase of tissue part with inserting magnetite particles in the artificial tissues, because as reviews indicated that magnetite in the AC magnetic field. The magnetite nanoparticles easily produce heat and affect on tissue parts. The range of increased heat is in the range 42-45°C in the live body part which do not consider (no side effect) all the host body parts.

In various contents of magnetite (Fe_3O_4), the releasing heat, scaffold apatite formation, and magnetic behavior of a novel bredigite-magnetite nanocomposite were evaluated. N´eel and Brown relaxations had not a significant effect on the specific absorption rate (SAR) of the composite samples. Indeed, magnetic saturation, *M*s, indicated a crucial effect on the releasing heat of the samples. There has been many published data gathered and are explained in chapter 2. The investigated research studies by other researchers and their gaps have been discussed in detail. This project has been performed contribute to gaps of those published works.

1.5 Objective of the Thesis

Due to the captivating property of “high saturation field” and “super paramagnetism”, there has been a profound interest in magnetic nanoparticles, also known as MNPs. However, the field of biomedicine has taken it up the notch by embracing this technology in areas such as the separation of cells, delivery of drugs, and have used it as a contrast agent for magnetic resonance imaging. However, MNPs have certain disadvantages, which are its tendency to accumulate into gigantic clusters which incites particles expansion that disrupt conventional biomedical process; this gigantic cluster is due to the anisotropic dipolar attraction. Therefore, the magnetite nanoparticle stability is very important as seen in chapter one and two. In order to fuse together proteins, antibodies, enzymes, tissue nucleotides etc., and channel them to tumours, organs etc., magnetic nanoparticles are needed as the binding agent. However, MNP needs to be prevented from accumulating, in order for its application to e successful; therefore, certain kinds of modification is required. In this thesis, in order to get that magnetic property and biocompatibility, the functionality of the bredigite is considered on the MNPs.

The objective of the current project was to develop a novel nanobiocomposite based on bredigite and akermanite bioceramics to solve the problems of tissue engineering including bone tumour and bone loss. In addition, the hyperthermia treatment as one of the most important treatment of bone cancer was discussed. According to the literature, the available bioceramics have weak mechanical properties, low chemical stability and low bioactivity.

In this work, the bredigite-magnetite functionalization is perfectly revamped on the MNPs to attain the physical performance such as magnetic property with biocompatibility and bioactivity. Among the different forms of MNPs, the maghemite and magnetite are able to fulfill the necessary requirements for the biomedical application. Especially, the magnetite nanoparticle exhibit super paramagnetism in nanoscale size. Beyond this limit, it exhibits ferromagnetism, the property which limits the applications in biomedicine. In precise, the reactivity of the MNPs greatly increases as their dimensions are reduced and may readily undergo rapid biodegradation when they are directly exposed to biological environments. Recently, bredigite is also known for its capability to bind a wide variety of molecules and most therapeutic agents for bone diseases. Thus, our research involves the synthesis of magnetic nanoparticles followed by functionalization or surface modification with bredigite. The work plan is executed with the following objectives;

1) To synthesize the pure magnetite nanoparticles within proper nanoscale size.
2) To control the agglomeration of magnetite.
3) To synthesize the bredigite bioceramic materials.
4) Fabrication of bredigite-magnetite nanocomposite through milling method.

5) To evaluate the structural and surface morphology of the as synthesized magnetite nanoparticles, bredigite and magnetic-bredigite nanocomposite.

Thesis Organization: The current thesis is composed of six chapters, and the references.

Introduction: Chapter 1 is the introduction chapter where the intension is to provide a background of bone disorders and materials used in treatment for bone tissue engineering with scaffold fabrications methods.

Literature Survey: Chapter 2 is the literature chapter consists of three sections materials properties (mechanical, electrical, thermal, and biological properties), silicate bioceramics and their composite and hyperthermia development during recent years. Moreover, each section in the literature chapter consists of several subsections.

Materials and Methods: Chapter 3 is the materials and methods chapter at which it introduces the materials preparation techniques, all the materials analysis such as mechanical, biological, electrical and thermal testing and technique are addressed in each sections.

Gene Expression Programming and Simulation: Chapter 4 represent the modelling and theory, development of 3DP machine and simulated scaffold porosity and compressive strength. The developed theory and formulations which are addresses in the Chapter 4 are assembled as prototype software given at end of Chapter 4.

Result and Disscusion: Chapter 5 represent the results and discussion of the prepared magnetite-bredigite scaffold nanocomposites. In this chapter, the results are discussed.

Conclusion: Chapter 6 presents the conclusions and the suggestions for the future work.

Chapter 2

LITERATURE SURVEY

2.1 Introduction

Due to trauma, bone cracks, tumor or illnesses like osteoporosis it became important to design scaffolds that are able to support or replace the bone and other soft tissues. Osteoporosis is a common disease and its treatment is costly that imposes a significant burden in terms of disability and impaired quality of life. The biomaterials engineers are motivated to design scaffolds with desired tissue properties like mechanical, tensile strength, and biological characteristics to mimic the anatomic tissue of the body. Many of these properties are mainly associated with the materials structure and their range of porosity, as well as the dimension of their pores and interconnectivity. Recently, a Ca, Si and Mg-containing ceramic, has been reported to possess apatite-forming ability, chemical and mechanical stability for bone regenerations. Mg-containing bioceramic have an excellent property in bone tissue reconstruction which support the thermal and electrical properties of the scaffolds. Bone reconstruction can be significantly accelerated by electrical currents in the injured or defect area. Proper electrical feature of scaffolds are needed to support mimicking and also control neuron behavior under stimulation of electrical, therefore, more proper guiding neural tissue to regenerate properly. Magnetite is a bioresorbable material that has been widely employed in the biomaterials domain and a product of drug-delivery operations.

2.2 Biomaterials for Bone Disease Treatment

In the biomedical engineering, the major focus is on properties of the materials used in implants. Metallic and nonmetallic implants are used greatly in orthopedic surgeries [6-8]. In general, bone tissues demonstrate a remarkable ability to recover from structural failure and lost physiological function [16], because of its strength and durability. Due to high strength properties, metallic implants are more applicable rather than nonmetallic [9-11, 133]. Titanium implants are most commonly used material with its great mechanical and biological stability after implantation [7-9]. However, the nonmetallic implants may have the ability to mimic the replaced tissue in the body with their biodegradable characteristic. Therefore, this advantageous make the non-metallic alloys as a superior implants rather than metallic prosthesis [7-9, 133]. There has been a huge leap recently in mechanical biocompatibility; this is with respect to the features of metallic biomaterials like fracture, modulus of elasticity, ductility or strength balance, wear resistance, fracture toughness etc. [134-136]. However, although most of these properties are essential and the control of the modulus of elasticity is more broadly researched; because of the value of the modulus of elasticity of the metallic biomaterial is higher than the bone itself, complications can occur resulting in bone atrophy or perhaps, poor remodeling of the bone [136]; implants, however, need to portray structural integrity and so, a balance must be satisfied [134].

2.3 Metallic Biomaterials

Alloys that are commonly used for making the orthopedic implants include: titanium [8,11], biomedical-grade stainless steel (i.e. 316L) [6-7] or cobalt chromium based alloys [9]. The most widely captivating metallic materials for biomedical applications as a result of its perfect biocompatibility, mechanical soundness and

non-biodegradable properties, are titanium based alloys or pure titanium (Ti) [8, 137-138]. However, there is a drawback to titanium and its alloy, and that is, its high coefficient of friction which causes wear debris to form; the repercussion of this inflammation and implants that tend to give under the applied stress [139]. Nevertheless, the life cycle of prosthesis can be prolonged by coating made from hydroxyapatite (HA) [140]. However, there was also a hiccup in its applicability, because this coating was susceptible to fatigue failure, meaning the implants will fail when subjected to the certain loads [141-145]. Therefore, there is a growing necessity to produce bioceramic tissue that are anti-corrosive; this is because osseointegration can occur when corrosion takes place [6-8]. The need for bone implants has been on the rise since the 20th century; from our history books, it is clear that bone implants were initially made from metals and the first ever metal plate was made by Lane in 1895, for bone fracture fixation [146]. As stated previously, metals had a major flaw and that was the corrosion problem as well as problems with strength [147-148]. However, with the advent of stainless steel in the year 1920, which showed structurally to have higher corrosion resistance, growing interest sparked amongst healthcare professionals [148]. From that timeline, an outburst of metal implants was being developed for surgical operations. 316 L, was one of the stainless-steel implants that was widely used, and it is still in use for surgeries like cardiovascular. CoCrMo alloys are more widely acceptable due to high wear resistance, particularly when diathrodial joint is concerned. A matchup of the material of the implants is as follows:

(1) Orthopedic bone fixation; the implant material includes Ti; Ti6Al4V; Ti6Al4V CoCrMo; 316L SS; Ti6Al7Nb.

(2) Cardiovascular Stent; implant material includes: 316L SS; Ti Ti6Al4V; CoCrMo. (3) Dentistry Orthodontic Wire Filling; implant material: CoCrMo; 316L SS; TiMo AgSn(Cu) amalgam; TiNi.

As stated previously, the implants' compatibility with the bone can be improved by using bioactive ceramics HA [148-149], while its compatibility with the blood can be increased by using biopolymers [150]. Therefore, it comes as no surprise when researchers are battling to find, and develop the perfect biomaterials that contain allergy-free elements and satisfy the criteria of nontoxicity. One of the outstanding breakthroughs that has been made is called temporal implants [148-151]. Metallic implants have higher density and are not magnetic; this present a problem with visibility on the MRI machine or X-ray machine. However, metallic implants perform optimally in terms of load bearing abilities than its counterparts- polymers and ceramics. Now, in the case of orthopedic implants, metallic implants are meant to have exceptional elasticity, toughness, fracture resistance and strength, with respect to the body part concerned. On the other hand, when total joint replacement is the order of the day, the metals need to be completely resistance to tear and wear; as a result, debris formation due to friction can be circumvented. Finally, any implants that will be sold commercially must be FDA approved [148-151].

2.4 Ceramics Based Biomaterials

In the past, some surgical implants were made entirely of ceramics as result of their strength to weight ratio and properties like low electrical and thermal conductivity. However, their usage has been limited due to its low ductility [152-153]. There is a bright side, however, to the usage of ceramics in dentistry; ceramics that are used in dentistry are designed majorly from titanium, aluminum and zirconium oxides. The

strength i.e. tensile, bending and compressive strengths, go beyond what the compact bone can dish out. It is about 3 to 5 times stronger. By combining these properties with a high modulus of elasticity, helps in producing an improved type of biomaterials [154]. Amongst the implant material used in the early 90's, Zirconia was widely accepted for dental prosthetic surgical operation. One of the first work on zirconia was done in 1975 by cranin and his co-workers. Osseointegration was another reason for the implementation of ceramic implants, while another reason was its low accumulation of plaque giving rise to an optimized management of the soft tissue and finally, the aesthetic was considered [152, 155-156]; these aesthetic replaced the conventional titanium implants. Three forms of crystals are cubic(C), tetragonal (T) and the monoclinic (M); this crystalline structure has zirconia within it. The stabilization of pure zirconia can be accomplished by mixing MgO and CaO. These outcomes in a multiphase material conventionally known as PSZ i.e. the partially stabilized zirconia. PSZ is a mixture of monoclinic, cubic and tetragonal phases; this is usually put together in order of hierarchical value. Moreover, Tetragonal zirconia polycrystals has high density, compression strength, high bending and lower porosity; this makes it feasible for biomedical usage [157]. Another important fact to take in is TZP is stabilized by Yttria [157]. Therapy methodologies involving metallic and bone implants, have become approved i.e. since its inception forty years ago. One of the closest biomaterials that mimic the chemical composition of the human bone is ceramic-based biomaterials. One research involved the coating of implants made of titanium with CaPs ceramic, in order to improve the implants load bearing properties as well enhance the bone development required for bone-implant osseointegration (Khandan et al. 2015) [8, 11]. In addition, it should be noted that bioactive behavior and higher

osteoconductivity are properties that ceramics carries; this makes it possible for cells to thrive on the surface of the implants. HA, TCP and silicate ceramics stand a better chance of properly fusing with living tissue; this is done by instantaneously producing a biological apatite layer on the implants' surface. Despite HA outstanding value, surface degradation as well as implant separation, could likely occur [15-17]. In order to prevent this from happening, HA must be coated with bioactive additives to improve its properties [6-8]; for osseointegration to occur much earlier [6-8].

2.4.1 Calcium Phosphate Based Ceramics

The third-generation of biomaterials was described by Hench and Polak: "biomaterials are meant to be new materials that are able to stimulate specific cellular responses at the molecular level" [158, 168]. The present biomaterials definition introduced, biomaterials as a product containing a bioactive behavior, which can be used in human body. Calcium phosphate (CaPs) can be found in various forms. CaPs shows biological properties like bioactivity and proper degradation compared to other bioceramics without CaPs. It is interesting that all of the CaPs do not have same biological properties and same degradation rate, due to their various crystallinity and microstructure. Between all types of CaPs, monocalcium phosphate monohydrate (MCPM) is the most important and soluble and highly acidic phase [158]. MCPM was obtained by water extraction of triple superphosphate. The solubility of MCPM is 783.1 g/L, and is entirely soluble [158-159]. Biomaterials open a new way of biotechnology to the world. The CaPs was used for artificial eye lenses, heart valve, artificial skin, dental and orthopaedic implant and breast prosthesis [89, 160-162]. The bioactivity, bioinert, and cellular responses are the main characteristic of CaPs to be considered [163]. Bioinert materials are the substance that reduces the interaction of materials with the

biological environment. The phenomena are regeneration of tissue around the implant without any side effect. Bioactivity and biodegradability of materials define as ability and tolerant of product to degrade or regenerate in the local environment [164]. Hydroxyapatite can be give as an example that regenerate apatite after soaking in the artificial liquid, simulated body fluid (SBF) or implanted into the body [164-165]. The third-generation of biomaterials was described by Hench and Polak: “biomaterials are meant to be new materials that are able to stimulate specific cellular responses at the molecular level” [166-168]. The present biomaterials definition introduced, biomaterials as a product containing a bioactive behavior which can be used in human body. The controlling of pH, Ca release, bone mimic, degradation, and bioactivity behavior are very important while describing biological behavior of CaPs ceramics. Also, the toxicity is more necessary to be investigated which is harmful to the body. Recently, challenge and development on access to better complex natural materials close to human body tissue which mimics the extracellular matrix (ECM) [168-169]. Recent achievement on biomaterials leads to create an advance and smart biomaterials [160-163]. In this thesis we developed new generation of calcium silicate with better properties compared to CaPs and introduced new nanocomposite.

2.4.2 Calcium Silicates Based Ceramics

The mechanical properties of ceramic based $CaSiO_3$ needs to be drastically enhanced in order for its medical applications to be realised. In order to successfully boost the orthopaedic applications, calcium silicate structures are fused with bioinorganic trace elements. Examples of these trace elements are: Zinc, Titanium, Magnesium and Zirconium; these trace elements have been fused into the structure of the Ca-Si [170]. The minerals which arises due to this is $Ca_2MgSi_2O_7$, also commonly known

as akermanite, $CaMgSi_2O_6$ (which is also commonly known diopside) [37], and $Ca_3ZrSi_2O_9$ (commonly known as baghdadite) [40-41, 171, 305]. These minerals have showed a high degree of enhancement, when tested within the *in vivo* and *in vitro* circle. These improvements far surpass that of the calcium silicate. This diopside belongs to the pyroxene group of solid solutions; the chemical formula of diopside is $CaMgSi_2O_6$. It has been widely applied in the field of biomaterials, coatings, solid oxide fuels, phosphors etc., for making interesting and useful materials [37]. Moreover, the synthesis of nanocrystalline diopside powder is made up of sol gel methodology [172-174], hydrothermal process and co-precipitation process [175]; however, these are usually restricted when employed on bulk synthesis, and are completely energy draining and time consuming. Moreover, in order to synthesize nanomaterials, a novel, powerful and economical method known as the high energy ball milling (HEBM) is employed; this approach is a Sol-Gel based approach [37, 177-179, 306]. Furthermore, in order for the medical usage of $CaSiO_3$ to be improved, its mechanical properties must be altered.

With respect to researches that has been conducted previously, fusing both the calcium silicate structure with the Zr ions, helps in synthesizing the baghdadite ceramic; the advantage of this manipulated material is that it is completely non-toxic, even when it comes in contact with the osteoblast [38, 41]. Moreover, akermanite has depicted properties in both *in vitro* and *in vivo* environments [38,180]. This material is highly respected and regarded as a result of its excellent controllable rate of degradation [182] and mechanical properties [38,181]. Sol-gel based methodology is used commonly for producing akermanite; according to Wu et al. [183], akermanite powder was created using the method of both sintering process and sol gel at about

1370°C for six whole hours. From their findings, the samples of the akermanite were fully capable of creating apatite within the solution, ten days after, in the SBF. Another research showed that akermanite powder was synthesized at for four hours at about 1350°C (Hou et al.) [184]. Within this research, apatite was formed as a result of a pore diameter of three micro-meter (3 μm**)**. Other authors used sol gel methodology in combination with sintering for three hours at 1300°C, to create powder samples of akermanite (Wu et al.) [185]. From their study, they were able to point out that even a minute amount of impurity could ruin the process of forming apatite. Furthermore, the preparation of akermanite bioceramic spheres where carried out through the use of the container less processing techniques [186]. Another author was able to create akermanite powder by using the sol gel process, extracted from eggshells (Choudhary et al.) [187]; but there was a problem that arose during the experiment as akermanite that is pure couldn't be synthesized when it was sintered at 1200°C for 6 hours. And so, the combination of this research tends to suggest that egg shell will do well as a close auxiliary to calcium carbonate for synthesizing bioceramics. Furthermore, other author (Kazemi et al. 2017) used the facile method to synthesize diopside; they used egg shell powder which served as a calcium source [37]. Diopside, of recent, has become an important material due to its applicability in areas such as scaffold [37, 41], coatings [8,11], biomaterials [41], solid oxide fuels [189] and nuclear [188].

According to a research conducted by Kulakov et al., it was shown that an exceptional osseointeration takes place with Zr implants; moreover, coating material of Zr can be introduced into the bone implants [190]; this coating material is majorly zirconia ceramics. On the other hand, huge bone defects can be taking care of by

baghdadite, which has been proven to aid in closing up gaps [171]. On the plus side, baghdadite coatings will improve the stability, chemically, of the samples in questions [41,191]. There is also a profound increase in the bonding agent at the surface; moreover, there exist a higher potential for in vivo bone formation as well as in vitro Hp formation at the SBF solution [41,191]. Ceramics which have been shown to have excellent apatite forming potentials within the SBF solutions i.e. having ionic concentration that match closely or resemble the plasma of the human blood, are Ca, Si, bredigite ($Ca_7MgSi_4O_{16}$) and Mg [192-194]; moreover, cell growth can be drastically improved from the products gotten from the dissolved bredigite i.e. within a specified concentration. Furthermore, other authors (Wu et al.) were able to synthesize pure bredigite ($Ca_7MgSi_4O_{16}$) powders by making use of the sol gel methodology [192]; also, these powders had dimensions ranging from 1-10mm and were made up of polycrystalline particles. By closely evaluating the formation of hydroxyapatite within the simulated body fluids (SBF) as well as its profound effects on the ionic products (i.e. on the osteoblast formation on bredigite dissolution), the *in vitro* bioactivity of the bredigite powders can be scrutinized. From the study result, it was shown that the nanocrystalline HA was induced by the bredigite, when it has been soaked for about ten days. Elements like Si, Mg and Ca ions that are present in the bredigite dissolution, instigate the osteoblast proliferation with a specified range of concentration [192-197]. From the research, it can be seen that the fracture toughness, modulus of elasticity and the bending strength are: 1.57 MPa $m^{1/2}$, 43 GPa and 156 MPa, respectively. On another study conducted in 2008 by Huang et al., the simple combustion methodology was utilised as a means for creating the $Ca_7MgSi_4O_{16}$ (i.e. nanocrystalline bredigite) [193]. Furthermore, on another research conducted recently by Mirhadi et al, mechanical activation was used as means for

preparing the nanocrystalline powder; this was accomplished, using calcium carbonate, talc and a mixture of amorphous silica powder; this then annealed at a temperature for one hour at about 1200°C. Note that a single phase bredigite powder having a crystalline structural size of 65nm, for about 20 hours, was synthesized. Moreover, researchers (Eilbagi et al.) fabricated bredigite by developing scaffolds composite that have an average pore size with an appearance porosity of 63.1–75.9%, ranging in size from 220-310 μm and appearance density of 1.1± 0.04 g/cm^3; however, despite the three-dimensional pure HA scaffolds that portray attractive features, it showed weakness in its mechanical property and so, Eilbagi et al, made this scaffolds composite by utilizing well adapted secondary components; it should be noted that this varied with respect to the bredigite content [196]. From the study, it was seen that an increase in the content of the bredigite resulted in decrease in the micro pore size of the scaffolds; this showed that the sintered scaffolds was optimized. As a matter of fact, the modulus of the scaffolds and the compression strength rose due to the bredigite content of 0 to 15 wt.% [196]. These new scaffolds portrayed better biodegradability potential and higher bioactivity, when the content of the bredigite increased. Furthermore, the test on toxicity proved the HA bredigite scaffold, having a 15 wt.%, brought about an increase in cell proliferation as opposed to the HA scaffolds and the control (i.e. the tissue culture plate). Therefore, bone regeneration can be greatly improved by a three-dimensional HA bredigite scaffolds; therefore, this HA bredigite scaffolds are well suited for performing the task of the HA scaffolds [196-197]. Table 2.1 reports various methods for production of akermanite, diopside, and baghdadite as well as their crystallization temperatures. It is clear that the crystallization temperature is dependent on the production method and the starting materials. The Table 2.1 also shows that for all three compounds

presented in our study the crystallization temperatures are lower than those reported in other researches.

Table 2.1: The previously reported methods for preparing akermanite, diopside, and baghdadite bioceramics.

Product	Processing methods	Starting materials	Crystallization Temperature (°C)	Ref.
Diopside	Co-precipitation process	$Ca(NO_3)_2{\cdot}4H_2O$; $Mg(NO_3)_2{\cdot}6H_2O$; $Si(OC_2H_5)_4$(TEOS)	845	[28]
Diopside	Solid-state reaction	$CaCO_3$, MgO, SiO_2	882	[48]
Diopside	Sol–gel	$Ca(NO_3)_2{\cdot}4H_2O$, $MgCl_2{\cdot}6H_2O$ and $Si(OC_2H_5)_4$	751	[26]
Diopside	Sol–gel	$Ca(OC_2H_5)_2$; $Mg(OC_2H_4OC_2H_5)_2$; $Si(OC_2H_5)_4$ (TEOS),	840	[49]
Baghdadite	Freeze-casting	Silica gel, ZrO_2 and CaO	900	[50]
Akermanite	Sol-gel	Eggshell biowaste (as calcium source), $Mg(NO_3)_2{\cdot}6H_2O$; $Si(OC_2H_5)_4$(TEOS)	900	[31]

2.4.2.1 Biological Properties of Bioceramics

After implantation of bioactive ceramics in the human body, a series of biochemical reactions occurs at the interface of the material and host bone whereby a layer of bone-like apatite forms on the interface, stimulating bone regeneration [198-199]. A first step in this process involves the release of Na^+/Ca^{2+} ions from bioactive ceramics and the formation of Si–OH groups at the surface of the material. This is followed by Ca^{2+} and PO_4^{3-} ions being absorbed from body fluids forming an amorphous Ca–P deposition on the surface of the ceramic. With increased implantation time, a crystallized Ca–P (apatite) phase forms. Finally, a matrix is

produced stimulating the formation of new bone tissue [199]. Generally, silicate bioceramics with high Ca contents possess improved apatite mineralization in SBF. The incorporation of other metal ions, such as Mg, Zn and Zr into binary oxide silicate ceramics will decrease their apatite mineralization. Furthermore, it is found that dissolution may play an important role in influencing the apatite mineralization of silicate ceramics [198-200]. Firstly, the ion exchange of Ca^{2+} and other metal ions in the silicate ceramics with H^{+} in SBF resulted in the formation of a hydrated silica layer on the surfaces of the ceramics and provided favorable sites for phosphate nucleation [200]. Then, Ca^{2+} and PO_4^{3-} ions in SBF will re-mineralize and form amorphous calcium phosphate and the subsequent formation of crystal apatite by incorporating OH^{-} ions from SBF. Apatite formation and nucleation can be investigated by surface modification and analysis with various instruments like SEM and FTIR or TGA. Different ceramics like Bioglass, natural hydroxyapatite (NHA), and A-W ceramic can bond with the living tissue easily [17, 200]. These bioceramics which can easily join with real bone is called bioactive ceramic. These bioactive ceramics are highly used in in tissue replacements. However, these bioceramics might attach with the cortical bone with a difficulty as they have higher fracture toughness and lower elastic module comparing to the cortical bone. Thus, it is recommended to introduce bioceramics with better mechanical properties. The CaPs and silicate bioceramics have good *in vitro* environment and the bone apatite formation can easily occur on their surfaces. The formation of apatite on the surface of these biomaterials is possible because of some functional groups like Si–OH, Ti–OH, Zr–OH, Nb–OH, Ta–OH, –COOH, and PO_4H_2 [199-201]. Such functional groups have special microstructure, which shows negative charge and leads the apatite formation to be created very fast. The apatite which prepared on the surface

of tissue is containing calcium silicate, calcium titanate, and amorphous calcium phosphate. By knowing this information's creating a new novel bioceramics is possible and controllable. Hard ceramic tissue materials can be produced by various techniques like mechanochemical, and mechanical activation combine with metals salt to enhance fracture toughness. Also, soft materials can be prepared by sol-gel method like flexible polymer composite [198]. Once the apatite nuclei are formed, they can grow spontaneously by consuming the calcium and phosphate ions in the surrounding fluid because the body fluid is highly supersaturated with respect to the apatite [198, 202-203]. Mechanism of integration of bioactive ceramics with living bone [198]. As a result, the surrounding bone comes into direct contact with the surface apatite layer. When this process occurs, a chemical bond is formed between the bone mineral and the surface apatite to decrease the interfacial energy between them. It can be concluded from these findings that an essential requirement for an artificial material to bond to living bone is the formation of a layer of biologically active bone-like apatite on its surface in the body. The CaPs offer the advantage of being custom tailored to the patient and directly applied to the target based on computed tomography (CT) scan of the defect site [18, 208]. The systematic variation of scaffold architecture as well as the mineralization inside a scaffold/bone construct can be studied using computer imaging technology and compute aided design and computer aided manufacturing (CAD/CAM) and micro CT [205-208].

2.4.2.2 Mechanical Properties of Bioceramics

One way of manipulating osteogenesis, is by the mechanical properties of bioceramics. In fact, osteogenesis is vital in improving gene expression that is osteogenesis related as well as improving the bone regeneration in HA scaffolds that are *vivo* related [205-207]. From several researches, it can be seen that the

mechanical strength of silicate bioceramics with respect to the fracture toughness is considerably higher than that of the HA ceramics that is usually made by the method of low pressure sintering [197]. These materials are known to have a similar modulus of elasticity and bending strength, ranging from 50-150 MPa, to that of the human bone [197, 204-205]. Moreover, another material that has an improved mechanical strength, when contrasted with the low pressure sintered silicate ceramics (SSC), is the spark plasma sintering-SSC; this could be either the dicalcium silicate or the wollastonite [197]. When the bending strength of SPS-SSC, was analyzed, it proved to have a higher value, during a dry assessment state, than that of the bone. In addition, the SPS-SSC, has a fracture toughness that is similar to the value dished out by the human bone [40, 197]. As stated previously, the mechanical properties of calcium orthophosphate bioceramics is poor. From one study, Hydroxyapatite ceramics possess a fracture toughness of about 1.0MPa $m^{1/2}$, unlike the human bone, which ranges from 2-12MPa $m^{1/2}$ [197-200]. Looking at another fracture toughness experiment conducted by Halouani et al. [55], on pure hot-pressed Hydroxyapatite, the highest value at 0.4 μm was 1.20 ± 0.05 MPa $m^{1/2}$ at 0.4 μm; this was when a grain size ranging from 0.2-1.2 μm was considered. Furthermore, dense HA bioceramics have a compressive, bending and tensile strength value of 120–900 MPa, 38–250 MPa and 38–300 MPa respectively [58-61, 206]. Moreover, HA bioceramics that is porous has value ranging from 2–100 MPa, 2–11 MPa and 3 MPa respectively. Another vital fact to consider is that a decrease in porosity will result in an exponential increase in strength [58-61]; but by altering its geometrical structure, it is quite possible to alter its strength. Furthermore, calcium orthophosphate bioceramics' fracture toughness does not change considerably with respect to a change in porosity or grain size.

2.4.2.3 Electrical Properties of Bioceramics

There has been a growing interest, amongst researchers, on the unique feature of HA's electrical properties with respect to AC and DC [209]. On one study (Hoepfner and Case), the effect of the porosity on the permittivity of HA, at room temperature, was closely observed; this was done in order to paint a picture of behavior with respect to an electrical field subjected to it; from the observation, bone growth improved as well as an improvement in the fracture healing process [210]. Another research (Zakharov et al.), inspired by the electrical stimulation of implant, took into account the dielectric loss of HA and permittivity temperature dependency (i.e. at temperature ranging from 20-50°C) [211]. On another research conducted by Nagai and Nishino, porous and dense HA ionic conduction at the surface was closely evaluated, in order to utilize it in humidity sensors [212]; one factor that was taken into account was that the relative humidity is directly proportional to the temperature conductivity. Due to its likely use as carbon monoxide gas sensor [112] or carbon dioxide [111], and alcohol [111], HA ionic conductivity has been a hot research field amongst scholars. Moreover, in order to study the micro structural evolution of HA as well as HA–Ti [67] and HA–ZrO_2 [66] composites, electrical measuring analysis has been used as the yardstick to carry out the study. Furthermore, the dielectric properties of HA were also utilized to paint a picture of the TCP-$Ca_3(PO_4)_2$ decomposition; this was with respect to the water content removal of OH^- ions at high temperatures [19]. This following process was carried out by Valdes et al. [63]. The presence of surface charges on HA bioceramics was shown to have a significant effect on both *in vitro* and *in vivo* crystallization of biological apatite. Furthermore, bone growth appears to be accelerated on negatively charged surfaces and decelerated at positively charged surfaces of HA bioceramics. In addition,

polarization of HA bioceramics was found to accelerate the cytoskeleton reorganization of osteoblast-like cells. Further details on the electrical properties of calcium orthophosphate-based bioceramics might be found in literature [209-211].

2.4.2.4 Thermal Properties of Bioceramics

From the bank of fine ceramics provided by nature, there are some that transmit heat effectively and have high conductivity levels, while for some, the case is opposite. Example of good transmitters of heat is silicon carbide and aluminum nitride. The temperature and period of heat treatment, are vital variables to consider, which influence the HA property. Temperatures higher than 1200°C, decrease the thermal stability of HA; this causes a decomposition to occur forming secondary phases such as the TCP. Therefore, it should be noted that low and high temperature heat treatment on bovine bone, is vital in order not to threaten the HA phase stability [212]. Another fact to consider is that the temperature of the densifications process as well as its grain size can be profoundly reduced by employing hot isostatic pressing (HIP), hot pressing and HIP post sintering; also, an increase in its density can also take place by employing these measures. The benefits of this, therefore, range from a higher thermal stability to a smoother microstructures of calcium orthophosphates. HIP, hot pressing and conventional sintering methodology, can be replaced by microwave sintering. Additionally, the forming process for the manufacture of calcium orthophosphate bioceramics are: injection moulding, slip-casting, tape-casting, centrifugal settling or viscous plastic processing [54, 213]. Also, this is to add to the consolidation methods, at high temperature, that was discussed previously. The fabrication of bioceramics that had no thermal decomposition whatsoever or thermal dehydration was created by utilizing an advance methodology called

“hydrothermal hot pressing” [214]. More details on the process of sintering can be observed in [54, 215].

2.4.3 Synthesis of Magnetite Nanoparticles

From various researched literatures, a good number of artificial approaches have been highlighted for the production of magnetic nanoparticles. In addition, with respect to these approaches, co-precipitation method stands out as one of the most efficient and easiest path for producing the magnetite nanoparticles [46-49, 216]. One underlying benefit of this approach is that it can scale up to larger productions with ease; but there is a drawback, and that is in terms of the particle size supply control, which is restricted. This is because the growth of crystals can only be influenced by the kinetic factors. Another thing to point out is that co-precipitation techniques, has proved useful in size control of magnetite nanoparticles; these nanoparticle size range from about ten to forty nanometres [216]. However, with the use of a magnetic field, magnetite nanorods having the property of anisotropy, was synthesized by employing the method of co precipitation [217-218].

2.4.4 Synthesis of Magnetite-Ceramic Composite

There has been certain composite that aid with hyperthermia therapies of bones that are plagued with cancer. The magnetite/hydroxyapatite (MNPs-HA) composite helps with heat generation from magnetite that has been introduced to an alternating current magnetic field. The following composite also acts as an efficient binding agent to the bones. The mixture of magnetite powder having a concentration of magnetite, at a temperature of 120°C, ranging from ten to fifty percent by mass, when subjected for 24 hours to a saturated vapour pressure and a hydrothermal treatment of α-tricalcium phosphate (α-TCP), was made from an HA composite/MNPs. Furthermore, the composite had submicrosized pores of 400 μm

and micro sized pores of 0.2 μm in size [219]. Moreover, magnetite particles of 20-30nm made from carbon nanotubes (CNT) was made by in situ thermal analysis, for the very first time, with Fe as the precursor. The decisive characteristics of composites was drawn from the different processing variables and CNTs properties; from the analysis, SEM was employed to observe the characteristics of the microstructure and the measurements of the relative density; from the observation, an excellent coverage of the CNTs within the matrix and percolation property, will bring about electrical conductivity improvement [220]. Another good example of an excellent bioactive material is sintered HA nano-iron oxide; as a matter of fact, the ability of this material to adipose tissue-derived stromal as well as hold up lines of osteoblast cell, shows its importance in performing therapy. It can also be fabricated into stem cells, which will make it an important asset in engineering skeletal tissues; this is as a result of the activities of cell proliferation as well as non-cytotoxicity [221]. Several types of silicate-magnetite and calcium-magnetite bioceramic composite have been compared in Table 2.2 with the advantageous and their disadvantageous. The earliest work belongs to Farzin et al. in 2017 [297] that produce Hardystonite –Magnetic for hyperthermia application and for cell cancer therapy under AC magnetic field for regeneration of bone defects.

Table 2.2: The previously reported methods for calcium and silicate composite containing magnetite ceramics [221, 297-302]

Researcher	Composite	Advantageous	Disadvantageous	Application
Farzin et al. [297]	Hardystonite -Magnetic	Drug delivery system, excellent compressive strength (1.8-2.5 MPa)	High porosity	Regeneration of bone defects
Wu et al. [298]	Bioglass-Magnetite	Proper magnetic strength, high porosity (83%)	Low compressive strength (46 ± 5.4 kP)	Regeneration of large-bone defects
Meng et al. [299]	Poly-lactide/Hap-Magnetite	Enhanced the proliferation	Low porosity	Osteogenic responses of pre-osteoblast cells
Li et al. [300]	Magnetic bioactive glass-doped Mg ferrite	Proper hyperthermia	Weak compressive strength	Thermoseeds for hyperthermia
Ebisawa Y et al. [301]	Wollastonite-Magnetite	Bioactivity, coercive forces of the magnetite-containing glass-ceramics	Growth of particle size	Tumour treatment
Luderer et al. [302]	Lithium ferrite-Hematite-glass	Proper coercive force (500Oe)	Difficult process	Hyperthermia of cancer
Current work	Bredigite-Magnetite	Proper compressive strength, bioactivity, hyperthermia term	--	Bone restoration, Bone cancer therapy

In another study, the useful properties of graphene have been looked into [222-224]. In the circle of lithium battery engineering, the nanotubes of graphene play a role not just limited to lithium storage materials, but as electronic conductive matrix; this is in order to boost the graphene performance electrochemically. On one study conducted, a magnetic-controlled conductive switch was designed by making use of a multifunctional and flexible graphene hybrid paper sheet; this study was undertaken by Liang et al. [224]. While on another research (He and Gao), a firm super para magnetism, excellent solubility, high electrical conductivity, improved solubility

and excellent process ability, was the assessment made of the integrated properties of graphene sheets that were multifunctional [225] ; from the assessment, it was clear that this material showed true promise to be used in MRI technology. Another research, highlighted the importance of graphene composites for drug administration and immobilization; this was uncovered by Zhou et al [226]. Also, ongoing research has uncovered the likelihood of dispersing a matrix of nanoparticles polymer or magnetite nanoparticles encapsulated with a biodegradable polymer layer, to serve as the conveyors of drug targeting [227]. It has been seen that nanoparticle composite of magnetite or polymers have a lower value of *in vivo* toxicity [227-228]. An evaluation of a glass based magnetite-wollastonite was undertaken and incorporation of a sol-gel glass system at proportions that vary [36]. Now, with respect to the physio-chemical properties as well as microstructural or structural properties of the combined materials, their inherent ability for heat production i.e. when subjected to AC magnetic field and the implants' bioactive property was discussed. As a matter of fact, the textural properties of the biomaterial are directly correlated to its bioactivity and so, the porosity and specific surface area's high value, will bring about an improvement in the composite's reactivity [36]

2.5 Developments in Biomaterial Manufacturing Technique

The ability to design and fabricate biomaterials like scaffolds is critical in tissue engineering applications. Applications for example, defects in the craniomaxillofacial complex cause by cancer, trauma, and congenital defects. Proper restoration of these defects requires functional nerves, vessels, muscles, ligaments, cartilage, bone, lymph nodes and glands to be compatible. Fabrication of complex scaffolds such as internal channels or hanging features is easily achievable with 3D printing technique. Kim et al. created highly porous scaffolds in combination with

particulate leaching techniques by 3DP and demonstrated cell ingrowths into the scaffolds [229]. Also, room temperature processing conditions allowed the incorporation of temperature sensitive materials such as pharmaceutical and biological agents into scaffolds [230]. Lam et al. fabricated starch-based scaffolds by printing distilled water, demonstrating the feasibility of using biological agents and living cells during fabrication [231]. Another favorable characteristic of 3D printing technology is multi-"color" printing where each color ink can be positioned on a precise location. This feature offers the exciting potential to simultaneously arrange multiple types of cells, deposit multiple extra cellular matrix materials, and exert point-to-point control over bioactive agents for biological tissue manufacturing. In this respect, 3DP may be more flexible for printable material selection than other SFF technologies. Currently in literature and mainstream media, the term "3D Printing" is being used to refer to all SFF technologies (e.g. fused deposition modeling, selective laser sintering, etc.) [77]. A number of Additive manufacturing (AM) techniques have been developed or modified to include cells in the fabrication process, among which biolaserprinting [234-235], stereo lithography [236] and robotic dispensing [237]. Recently, the very first use of AM directly *in vivo* was reported [234, 238].

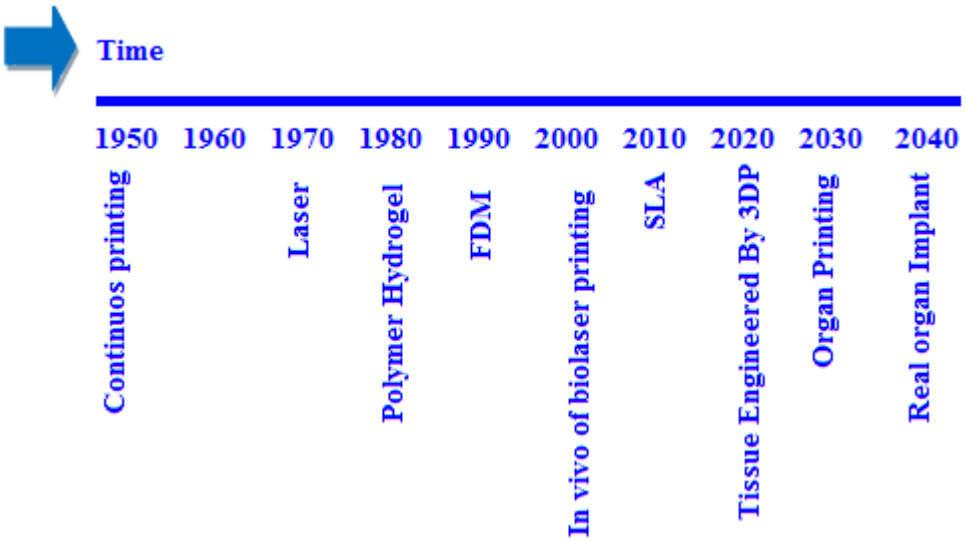

Figure 2.1: History of additive manufacturing and its application in tissue engineering; the introduction of technologies and major scientific findings [234].

2.6 Biomedical Engineering for Hyperthermia Treatment

In 1993, two study was conducted by Jordan et al. [240] and Chan et al. [239], demonstrated the use of magnetite particulates for treating hyperthermia. As an added bonus to this research, the efficiency rating of super paramagnetic crystals was shown; these super paramagnetic crystals were able to attract the energy of an AC magnetic field and give out heat as a by-product. One interesting point to note is that healthy cells are not more sensitive to the rise in temperature than its counterparts, the tumour cells [241-242] and so, this property can be exploited in vivo by drastically raising the temperature of the tumour cell in order to annihilate the hyperthermia pathological cells [126]. A profound heat loss that is given off when the reversal magnetization process is initiated is a result of the magnetic nanoparticles being bombarded by an AC magnetic field. Moreover, due to the influence of an external magnetic field on the MNP, which results in the rise in temperature, there has been a growing need in its application in biomedicine and chemistry [126]. Moreover, thermo sensitive magnetic nanoparticles, hyperthermia as a cancer therapy, and the magnetically application of controllable catheters are all

crucial examples. Therefore, enhancing the temperature is more beneficial if the enhancement is achieved by a low MNP value. And so, the value of the MNP specific loss of the magnetic material must be considerably high. Especially when target precision is minimal i.e. for example the tumours targeting. Even in the 21st century, science hasn't found a concrete solution to the cancer problem [126,243]. In organic nanocarriers, however, have shown true promise with their versatility and biocompatibility properties; these inorganic nanocarriers are silica based material. These materials, have shown to have a good range of biomolecular conjugations and polymers and also, these materials have a lot of features locked within its design that give out certain favorable functionalities; this includes the imaging for transonic purposes, passive/active targeting and treatment of hyperthermia [126,243-244]. Furthermore, mechanical milling techniques which serve as an economic route for diopside preparation, bredigite and akermanite scaffold, which is made using the three-dimensional printing methodology, hasn't been proven as a concrete methodology for fighting hyperthermia.

2.7 Global Regulatory Strategy and Intended Use and Standard

Before applying the artificial specimens in the human's body, after *in vitro* evaluation, these materials should be considered in long-term implantation for the bones and muscles of rabbits, rats, and dogs. Normally, researchers used two species like the rabbits and the dogs. Now when considering the rabbits' implants, the standards usually call for about four healthy rabbits per period of sacrifice with usually one control and then the two test materials are introduced into paravertebral muscles of the spine at each side. However, no standards are put in place for testing of devices on a long term. As stated earlier, the standard for long-term testing of implants hasn't been established by the American Society for Testing Materials

(ASTM) yet; however, F1439, that is the Standard Guide for Performance of Lifetime Bioassay for the Tumorigenic Potential of Implant Materials, gives us some guidelines as to the type of testing to carry out [307]. Now with respect to all these various applications, the biomaterials are regulated indirectly by the intended usage of the final product. Therefore, the regulation is correlated with the risk associated with its intended usage [307].

Chapter 3

MATERIALS AND METHODS

3.1 Introduction

This work aims to study the effect of magnetite nanoparticles amount on bredigite as one of the silicate bioceramics powders and consider its relevance on the development of porous scaffolds, especially on their final structural and surface characteristic.

In this current work, our plan comprised of three main areas: (1) fabrication and design and (2) Simulation, and (3) Characterization and Testing. We will expand on these areas below:

a) Preparing the bredigite-magnetite nanocomposite through combining the bredigite powder and magnetite powder with (0 wt.%, 10 wt.%, 20 wt.%, and 30 wt.%).
b) Mixing the prepared powder with water and printing it with 3D printer.
c) Then depowering and sintering are used to develop the materials strengths.
d) Then the materials are tested mechanically and biologically to achieve suitable scaffold tissue for cancer bone repairmen.
e) Furthermore, the objective function is used to achieve the mechanical, thermal, electrical and biological characteristics.

1) **Fabrication and Design:** Synthesis of MNPs-bioceramics (MNPs-Ak, Di, and Br) scaffold nanocomposite prepared by mechanical activation (MA)

process to reach simultaneous enhancement in cells growth and mechanical stability, chemical stability, proper thermal behavior. The preparation method to built scaffold is choosing from additive manufacturing (3DP).

2) **Simulation and Gene Expression Programming:** The compressive strength and porosity of diopside as a case study simulated to meet the required mechanical and biological properties for tissue engineering applications. The final product must have proper reaction in humans body, therefore the optimum sample will be choose from the nanocomposite sample with various amounts of MNPs (0 wt.%, 10 wt.%, 20 wt.%, and 30 wt.%) which was prepared with mechanical activation process called High Energy Ball Milling (HEBM). The homogenous MNPs-Bioceramic scaffold nanocomposite prepared by mechanical activation (MA) process which has to attain simultaneous improvement in bone apatite formation, mechanical and electrical properties.

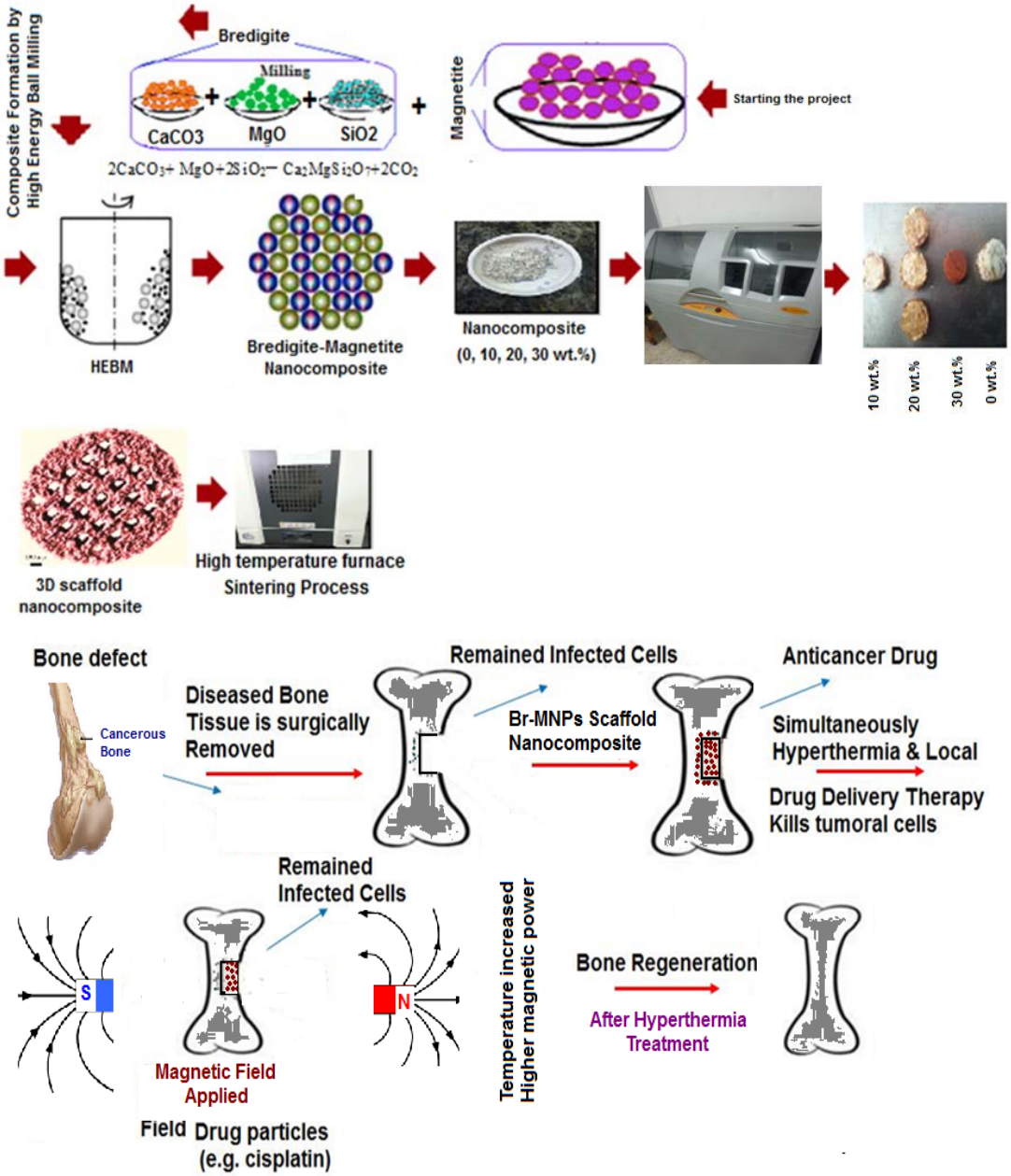

Figure 3.1: Schematic of preparation of scaffold nanocomposite with 3D printing, materials preparation, 3D printing of scaffold and hyperthermia application

3.2 Material Preparation

3.2.1 Bredigite

Bredigite powder was produced by a simplistic and cost-effective technique, mechanical activation (MA) method. The bredigite was fabricated using starting materials such as talc with chemical formula ($Mg_3Si_4O_{10}(OH)_2$), pure amorphous silica (SiO_2) and calcium carbonate ($CaCO_3$) powder purchased from Merck

company with 98% purity. The relevant percentages of $CaCO_3$ and SiO_2 were combine with $Mg_3Si_4O_{10}(OH)_2$ to obtain the proper molar ratio of Ca=7 Si=4: Mg=1 that addresses to the stoichiometric proportion for bredigite ceramic. The combination of three salt then milled in HEBM using Retsch milling machine (Islamic Azad University of Najafabad) under ambient environment with three zirconia balls with diameter size between 10-15 mm with 30 g weighting of each balls (Figure 3.2). The ball-to-powder ratio (BPR) set 10:1 rate with a milling process, the rotational speed of the milling desk selected at 650 rpm in HEBM process. Then, the milled samples were kept in the furnace for 4 h at 1300°C with cooling and heating rate of 10°C/min (Figure 3.3).

Figure 3.2: Schematic of planetary HEBM technique to synthesize based materials

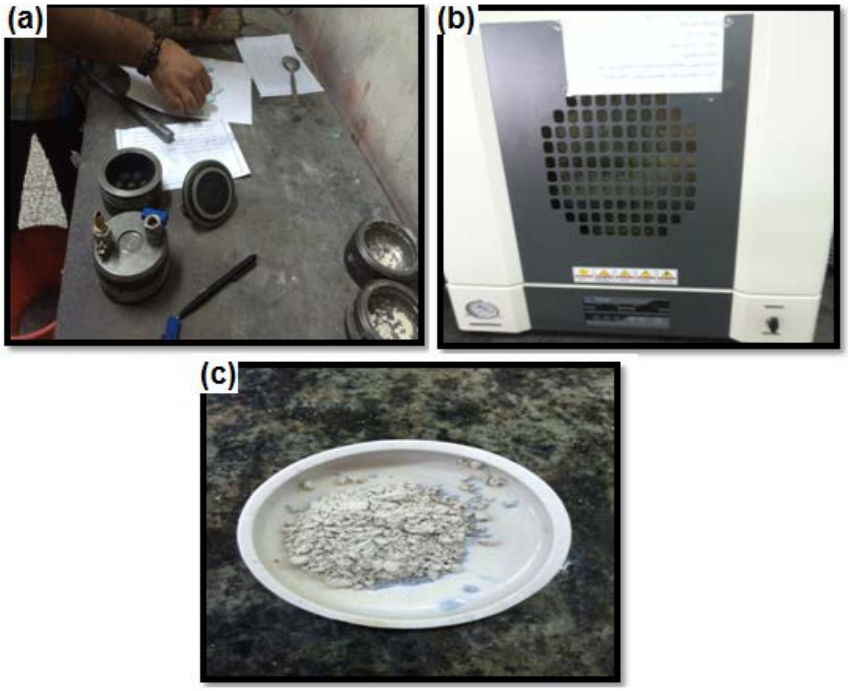

Figure 3.3: Process of synthesising bioceramic with planetary HEBM (a) cleaning zirconia cups from Retch Company, (b) furnace for sintering process (c) synthesized powder

Table 3.1 indicates the experimental parameters and weight of the raw materials for akermanite, diopside and bredigite used in the current research.

Table 3.1: Parameters of preparation of diopside, bredigite and akermanite using milling, parameters (vial speed, BPR, sintering temperature, weight of powder).

Milling Parameter	Akermanite	Bredigite	Diopside
HEBM speed (rpm)	650 rpm	650 rpm	400 rpm
BPR weight ratio	10:1	10:1	10:1
Maximum sintering temperature (°C)	1200°C	1300°C	1200°C
Total weight of powder (gr)	10 gr	11 gr	10
MgO	1.54	1.42	1.38
SiO_2	4.62	3.94	4.4
$CaCO_3$	3.84	4.64	4.22
Reference	[38]	[303]	[37]

3.2.2 Akermanite

Also in this thesis, the akermanite powder was synthesized using starting materials including magnesium oxide, silicon dioxide and calcium carbonate (eggshell source) as the starting materials for akermanite. The calcium carbonate source derived from eggshells source for economical reason which heated in oven for more than 2 hours at 100-110°C. The heated powders were selected and weighted according to the following reaction and condition given in the reaction 1. The primary surface activation of the prepared powders occurs using HEBM for 6 hours with the following conditions (BPR ratio=10:1, rotational speed=650 rpm) according to the following chemical reaction.

$2CaCO_3 + MgO + 2SiO_2 \rightarrow Ca_2MgSi_2O_7 + 2CO_2$ Reaction 1

The resultant powder was divided into two parts. The milled powders were heated to 900°C for 3 hours in a furnace with heating rate of 5°C/min. Through the heating process in the furnace, sampling was conducted at three various temperatures e.g. 500°C, 700°Cand 900°C for phase characterization with XRD technique and FTIR analysis performed on pure synthesized akermanite. In order to evaluate the effect of sintering time on the bioactivity and morphology of sample, the holding time at 900°C increased to 5 hours and the obtained results were assessed and explained in the Result Chapter section (5.1.1.2).

3.2.3 Magnetic Nanoparticles

Magnetite nanoparticles (MNPs: Fe_3O_4) made with the sol-gel technique (Pharmacy Department, EMU, North Cyprus) (Figure 3.4). In this research, MNPs produced by combining a base to an aqueous compound of Fe^{3+} chloride ions at molar ratio of 1: 2. In this work, citric acid used for process control agent (PCA) duty and inserted to

the starting blended to inhibit from two important events like agglomeration and cold welding in the milling process and action. The prepared materials in the previous step then were heated in 1200°C for 3 hours with heating and cooling rate of 10°C/min.

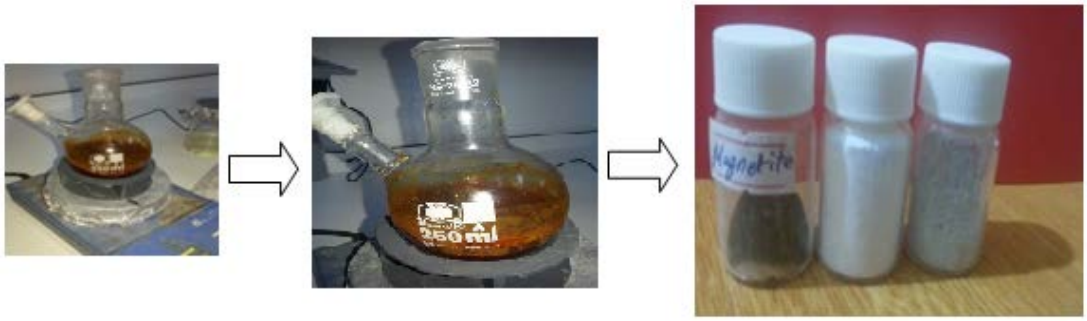

Figure 3.4: Prepared magnetite powders by sol-gel method

3.2.4 Nanocomposite Properties

A nanocomposite powder with various amount of MNPs (0 wt.%, 10 wt.%, 20 wt.%, and 30 wt.%) with bredigite (as matrix) was mixed via planetary HEBM in alumina cup with zirconia ball (diameter=10-15 mm, each weighing 30 g, alcohol medium) for 30-60 min as shown in Figure 3.5 The prepared powders were combined with alcohol medium to produce perfect homogeneous compound. The compounds were kept in an incubator as a maturing sample for the subsequent procedure avoiding from dirt and agglomeration appearance.

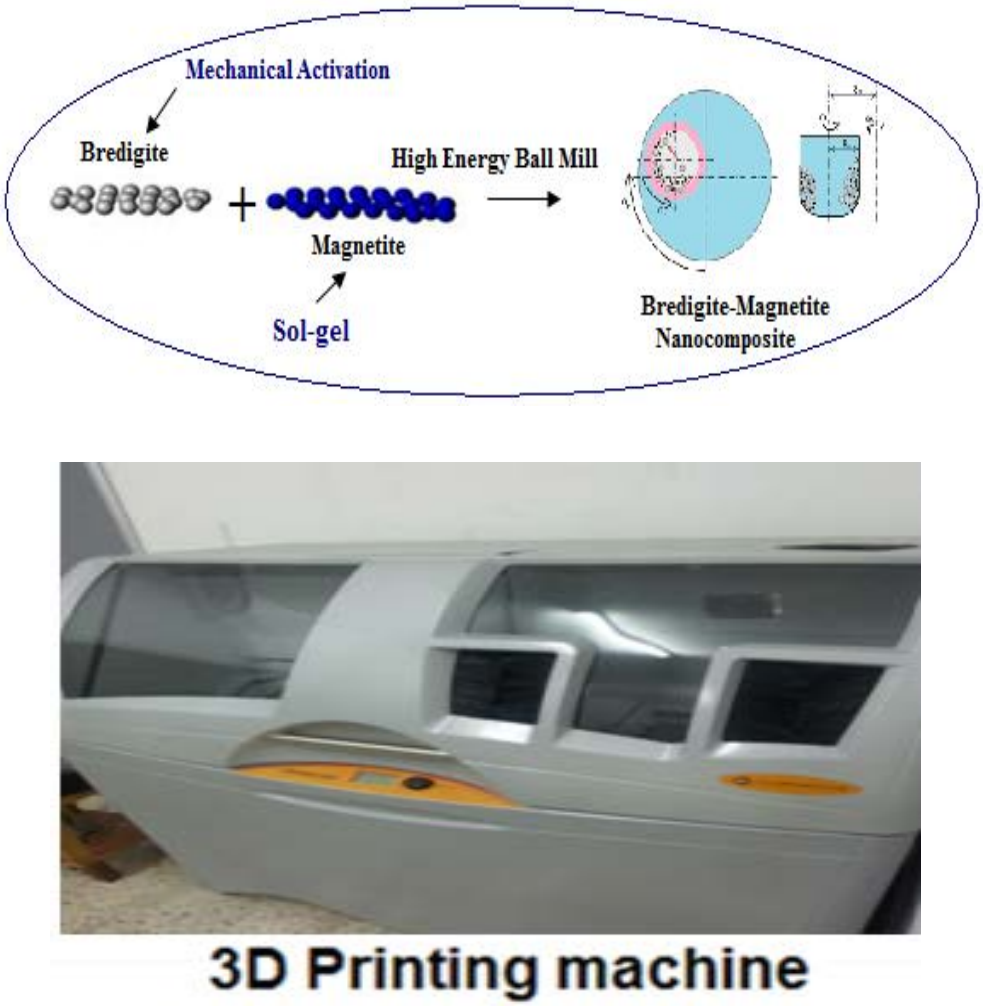

Figure 3.5: Preparation of bredigite-magnetite nanocomposite with milling process

3.3 Scaffold Preparation

To prepared the scaffold in this work 3D printer machine was used. The produced nanocomposite with (0 wt. %, 10 wt. %, 20 wt. %, and 30 wt. %) MNPs in bredigite powder were mixed with binder and Zb63 and then inserted into the machine feeder due to design the scaffold shape.

3.3.1 Three Dimension Printing Machine

Rapid prototyping (RP) technologies have been expanded and frequently employed in tissue engineering. At first stage, a product needs to be scanned using a computed tomography (CT) scanner and converted and then modeled using Computer-Aided

Design (CAD) software package. The CAD model is transformed to file with the stereolithography (STL) format into the computer as shown in section (4.4) and section (4.5). The software program can interpret the STL files and prepare the accurate slices of the model based on the chosen layer thickness. This process is repeated layer by layer until 3D product manufactured similar to the ultimate object. In this project, four different scaffold nanocomposites were fabricated with cylindrical shapes by 3DP machine (Z Corporation) with dimension of 12 mm height, 6 mm diameter, and 0.6 mm pore size were obtained. In this study, the nanocomposite with 98% water and Zb63 “clear binder solution” (commercially formulated 2-pyrrolidone solution) as binder were inserted into the 3DP machine (see Figure 3.5 and Figure 3.6). The Zb63 has been known as a hazardous product, which leads the pH of the binder solution set at 9.8 in the room temperature with density of 1 g/cm^3 and similar viscosity to the water.

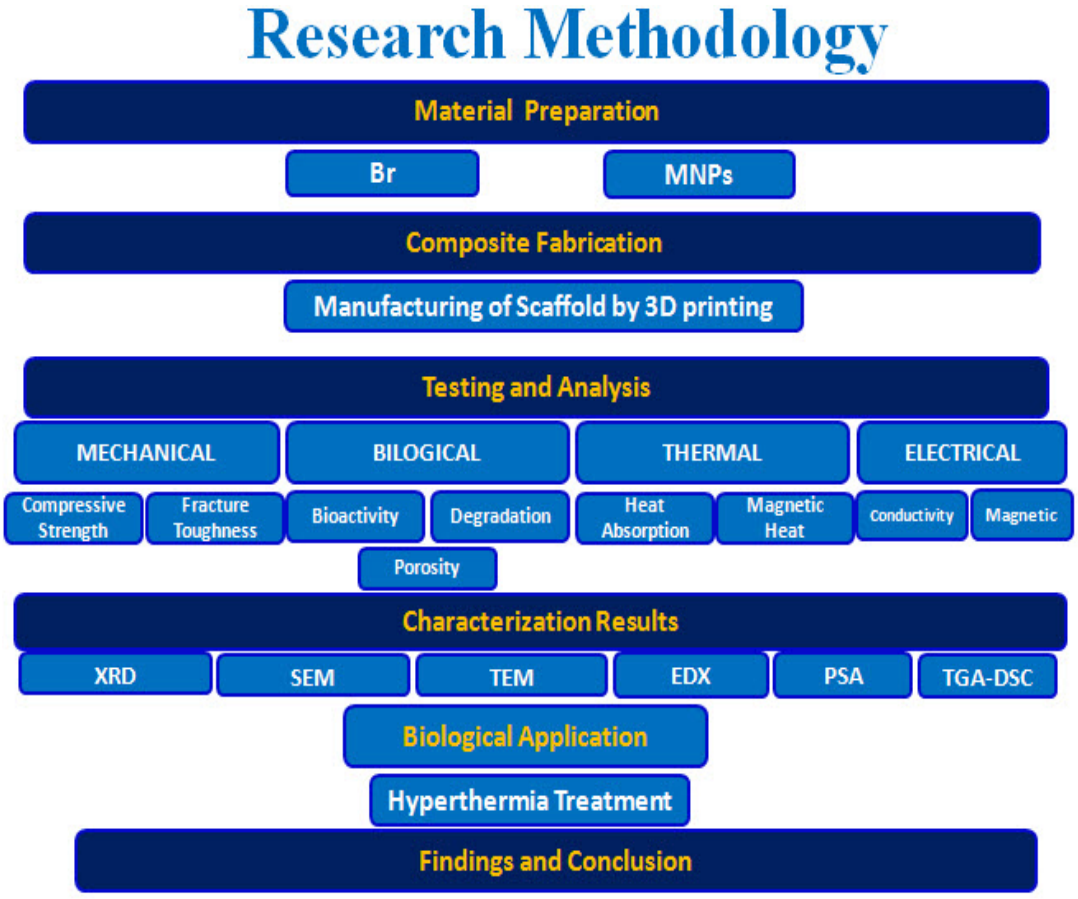

Figure 3.6: Schematic of the research work

The scaffold nanocomposite specimens were then sintered for 1 h at 550°C and 2 h at 650°C. The following sintering process leads the scaffolds nanocomposite to have better strength and do not let them to destroy easily.

3.4 Mechanical Testing of the Scaffold Nanocomposite

3.4.1 Compressive Strength

The compressive strength (CS) of each scaffold nanocomposite was measured using a compressive strength testing machine digital (universal testing machine Instron mod. 1195). The CS was measured from the stress–strain curve (first linear curve slope). Cylindrical specimens with dimensions12 mm×6 mm (Height × Diameter) using a computer-controlled universal machine with a selected 0.5 mm min^{-1} as a rate of ramp. The appropriate ASTM standard No. C0020–00R0522 was used. Based

on that, if D is the diameter of the sample as D=6 mm, with applied force load of F=2.5 kN and speed of 1 $mm.min^{-1}$ externally preloading were evaluated in the following equation 1:

Compressive Strength =CS (kg/cm^2) = Force/surface area (3.1)

The compressive modulus was determined based on the slope of the stress–strain curve in the elastic region.

3.4.2 Fracture Toughness and Bending Strength

The fracture toughness and bending strength of scaffold nanocomposite measured according to the previous worked performed by Guazzato et al. [248]. Therefore, the bending strength performed on the bredigite-magnetite scaffold nanocomposite.

The fracture toughness was determined by the indentation-strength (I-S) method using an applied load of 10 Kg. For each set of conditions, at least 3 samples were examined for both the strength and the fracture toughness measurements [293].

The three-point test performed on mechanical bench test (3 Point Flexural Test Machine) at a cross-head speed of 0.5 mm/min with applied load of 0.5 KN to the cell. The samples were polished with silicon carbide paper (grits= 1200) before the test. The bending strength was measured using the following Equation 2 [250]:

Bending strength=$3P_{max}L/2bh^2$ (3.2)

where P_{max} is the highest value of load on the load–displacement curve, L is the length of the support span, b is the width, and h is the thickness of scaffolds nanocomposite. The three-point bending and load–displacement curves of the samples the areas below the curves were introduced by the sample cross-section (bh)

to gain a quantitative measure of the fracture toughness [251]. The standard for the fracture toughness test chosen was ASTM D5045

3.4.3 Porosity

The porosity of the all four scaffold nanocomposites was checked by Archimedes principle. The porosity was calculated according to the following equation 3 [249].

$$\text{Archimedes principle porosity} = (M_{wet} - M_{dry})/(M_{wet} - M_{submerged}). \quad (3.3)$$

Where M_{dry} is the dry mass of scaffold, M_{wet} is the mass of prewet scaffold, and the $M_{submerged}$ is the mass of scaffold soaked in SBF. Briefly, the sintered scaffold sample soaked in the SBF solution and then the sample removed from the liquid and weighted. In the next step the weight of the dried sample (insert in oven T=110°C) and then again weighted and inserted into Formula 3.

3.4.4 Surfaces Profilometry

Tour measurements were taken for each sample and then their average will be determined. The roughness of the surface can be described using a number of different measures, for example R_a by roughness tester. The surface roughness of the scaffold nanocomposite as a cylindrical shape was measured by profilometry using a Mitu-loyo SURFTEST 301 profilometer. Three slices of the scaffold were measured for each surface condition to obtain an average roughness value R_a.

3.4.5 Conductivity Measurement

The scaffolds nanocomposites conductivity was recorded using a Digital Keithley Instruments, (Multimeter and USA). For conductivity evaluation, two steel blades were located with 1 mm gap between the nonconductive substrate. Then, the scaffolds nanocomposite with the dimension of (H=1 mm and D=6 mm) were inserted in the empty space between the mentioned blades. The scaffold

nanocomposite resistance measurement (R) was offered 3 times for all four specimens, and the average was recorded. The conductivity (σ) of scaffold nanocomposite was calculated by using Pouillet's law equation 4 [252]:

$$\sigma = \frac{L}{R \times A} \tag{3.4}$$

Where L is the height which is 1 mm in the current study, D is the diameter which is 6mm, and A known as scaffold nanocomposite surface area that is $A = \pi \times (D/2)^2$.

The magnetic power (magnetization) of the scaffold nanocomposite samples were measured at a relative high field in a superconducting quantum interference device (SQUID) magnetometer. Amount of 20 mg of the nanopowders was applied to test the magnetization changes along certain time versus Temperature. The magnetic properties of scaffold nanocomposite were measured using vibrating sample magnetometer (VSM) at room temperature. To measure the range of magnetic properties which induced heat, scaffold nanocomposite were crushed into small pieces and then were grounded to obtain sample powder. The heating of magnetite was conducted using high intensity generator with power in the range of 700-100 KHz. A two ml of powder were soaked in water in a small glass then inserted in the water-cooled copper coil with the diameter of 25 mm. Since the magnetite particle considered in the magnetic field with strength of H, each atom has its own individual reaction and response. The magnetite induction introduced by the following equation 5 [252].

$$B = \mu_0 (H + M) \tag{3.5}$$

Where μ0 is the vacuum permeability and M is described as magnetic moment per volume. In addition, it is vital to know that greatest materials show magnetism action when they are presented in the magnetic field which called paramagnets. Besides, it is true to say ferromagnet, and ferrimagnet materials show magnetite properties without being in the magnetic field. MNPs has the most significant point is the appearance and surface area of magnetic.

3.4.6 Applying Hyperthermia

After investigating the mechanical properties of bredigite-magnetite scaffold nanocomposite the hyperthermia was applied to the scaffold nanocomposite. The optimized scaffold nanocomposite with compressive strength, fracture toughness and also conductivity was inserted into hyperthermia evaluation. The hyperthermia behavior of scaffold nanocomposite was evaluated using Alternating current (AC) magnetic field with various frequency values of 100-400 KHz and a maximum reaction 300 W (power=5). The magnetic field amplitude was set as 28 kAm^{-1}. A thermometer with precision of 0.1°C was used to measure the scaffold nanocomposite heat and the transfer temperature. The manual hyperthermia tool should be installed in a silent place without any vibration or distractive wave as it is sensitive device to frequency waves. Specific absorption rate (SAR) is the rate that introduces the rate of energy wave's absorption in the body which is dependent on thermal effect/transfer. Due to check the SAR of the magnetite nanopartciles, homemade manual device was prepared to measure the SAR rate. The samples were evaluated in the in water (C_{water} = 4185 $JL^{-1}K^{-1}$) as ferrofluid. To reach increase the heat to higher than 42°C, the initial current density of (20-40 W/Kg) should be met in the target area (here all scaffold nanocomposite surface, however; in real tumor case, better on the area which the tumor exists). The electrical tissue binderies and

physiological characteristics also the differences in blood vessel speed can reach to 40°C in hyperthermia process. It is clear that frequency waves have great intensity but the influence of mechanical force and energy is better attaining in the process [122, 126, and 255]. In this work, we present a novel bredigite-magnetite scaffold nanocomposite. The sample with 30 wt.% magnetite nanoparticles show a significant improvement in mechanical investigations. Also, the sample with 30 wt.% magnetite temperature increased more than other sample with 0 wt.%, 10 wt.% and 20 wt.% MNPs in the nanocomposites. We found that incorporation of magnetite nanoparticles into bredigite network might enhance the SAR ratio without any hysteresis and no super paramagnetic. The primary findings shows that as the magnetite amount increased the particles agglomeration increased to cluster more than 1 µm. The finding in result sections shows that application of hyperthermia by using heat, chemistry of materials and geometry analysis can be treated as Figure 3.7 represented.

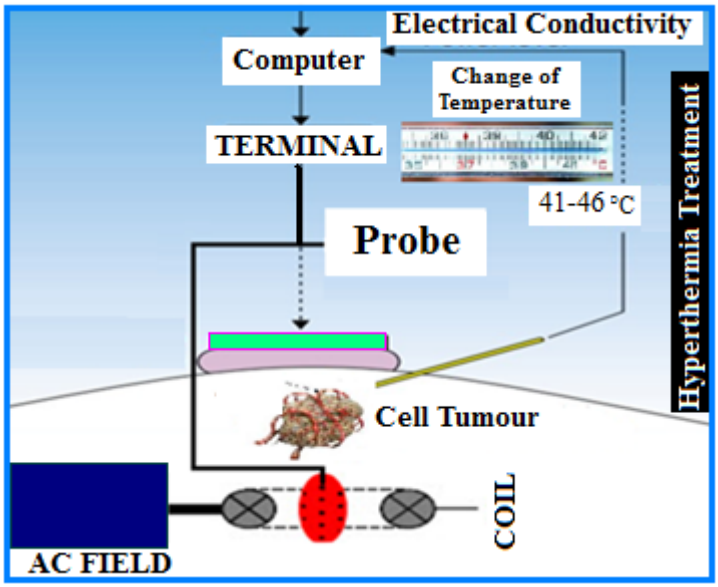

Figure 3.7: Hyperthermia effects using copper coils and field generator

3.5 Biological Testing of the Scaffold Nanocomposite

3.5.1 Wettability Study

It is shown that the surface wetting in SBF solution influence on the roughness of the surfaces. There are two main parameters in wettability of surfaces like 1) surface roughness 2) charge (zeta potential) that can effect on it. Therefore, in biomaterials engineering, two important criteria like roughness and wettability are important due to the bone regeneration of host, guest tissue and cells with proteins. It is important that all silicate bioceramics indicate negative zeta potentials, which is indicative of a negative surface charge [11, 253, and 294-295]. In this thesis, the main research is to evaluate the effects of surface roughness on wettability and the precipitation apatite on bredigite-magnetite scaffold nanocomposite. The contact angle/wettability test was performed to investigate the scaffolds nanocomposite wettability value. The scaffold nanocomposites were tested with the sessile drop method to consider the wettability by depositing SBF on scaffold surface (Millipore, USA). The results were captured using optical tools, and camera to analysis Θ angle. The theoretical wettability formula was used as the following equation 6:

$$\text{Cos}(\Theta)=(\gamma_{SV}-\gamma_{SL})/\gamma_{LV} \quad (3.6)$$

Where γ_{SV}, γ_{SL} and γ_{LV} are interfacial surface tensions of solid–gas, solid–liquid and V liquid–gas, respectively. The wettability test performed at room temperature of 25 ± 1°C and relative humidity (RH) of 35 ± 5%, by a low-energy electron beam irradiation, for various exposition times 400-1200 second with step of each 200 second like our previous work [11, 253].

3.5.2 Bioactivity Study

The bioactivity evaluated the *in vitro* for scaffold nanocomposites in simulated body fluid (SBF). The SBF solution was prepared according to the norm ISO 23317:2012, pH 7.40. The preparation method of SBF solution is briefly summarized here. After immersion of the scaffold nanocomposite during 4 weeks time, the bioactivity can be recognized by the content or amount of (Ca-P or Si) film layer formed/precipitate on the surface of the tissue. In this research the SBF solution created with the procedure explained by Kokubo test [79]. The SBF solution was fabricated with exact amount of the salt consequently, NaCl (8.026 g), $NaHCO_3$ (0.352 g), KCl (0.225 g), $K_2HPO_4 \cdot 3H_2O$ (0.230 g), $MgCl_2 \cdot 6H_2O$ (0.311 g), $CaCl_2$ (0.293 g) and Na_2SO_4 (0.072 g) in distilled water (1000 ml). The fluid was then buffered to pH 7.4 at 37 °C with trihydroxymethyl aminomethane (6.063 g) and hydrochloric acid (40 ml).

Table 3.2: Compounds of the blood, PBS and SBF solutions

Composition (g l^{-1})	Blood (m. mol^{-1})	PBS (m. mol^{-1})	SBF (m. mol^{-1})
KH_2PO_4	--	0.2	--
NaCl	6.8	8.0	8.035
KCl	0.4	0.2	0.225
$CaCl_2.H_2O$	0.2	--	--
$NaH_2PO_4.H_2O$	0.026	--	--
$Na_2HPO_4.H_2O$	0.126	--	--
$MgSO_4$	0.1	--	--
$NaHCO_3$	2.2	--	0.355
Na_2HPO_4	--	1.15	--
$MgCl_2.6H_2O$	--	--	0.311
$K_2HPO_4.3H_2O$	--	--	0.231
Na_2SO_4	--	--	0.072
$CaCl_2$	--	--	0.292
HCl (1.0 mol l^{-1})	--	--	39 ml
Tris-hydroxymethylamino	--	--	--
pH	7	7.2-7.4	--
Methane	--	--	6.118

3.5.3 Biodegradation Study

The rate of degradation and its controlling their behavior known as a crucial part in bone tissue regeneration, and has been extensively studied up to now. In general, the accurate degradation rate of the biomaterial found the opportunity for the cells to lay down their individual extracellular matrix and reconstruct the damaged tissue and at the same time to ensure that the scaffold does not serve longer than demanded. The phosphate buffered saline (PBS) was created to investigate the biodegradation rate

after 28 days of soaking in the PBS. Table 3.2 displays the quantities used to produce the, PBS and SBF solutions in this thesis. The prepared scaffolds nanocomposite were placed in falcon tube vials containing 10 ml PBS and SBF separately to measure the degradation rate and bioactivity ratio (bone-like apatite). The dried sample was weighing before and after testing to measure means of weight change (weigh loss) and water uptake for each bredigite-magnetite scaffold nanocomposites during the degradation/apatite formation period. The mass loss (%) and water uptake (%) were calculated according to initial and final weight of the samples. The bredigite-magnetite scaffold nanocomposite primary weight was measured before (W_0) and after soaking (W_t) to define the rate of specimens degradation. The degradation rate (weight loss) was estimated using the following equation 7:

$$\text{Degradation} = (W_0 - W_t)/W_0 \times 100\%. \quad (3.7)$$

Whereas, the pH of soaking liquid was measured by an electrolyte-type pH meter.

3.5.4 Inductive Coupled Plasma Atomic Emission Spectroscopy (ICP-AES) Study

In this study, Inductive Coupled Plasma Atomic Emission Spectroscopy (ICP-AES) was used as an analytical method to detect trace of metallic and nonmetallic powder in the various solutions with ICP-AES analysis. The intensity of Ca, P, and Si (the main element in the silicate bioceramics) elements within the scaffold nanocomposite samples were soaked for predetermined time intervals were considered in SBF solution. The true densities of the magnetite-bredigite scaffolds nanocomposite were measured using Archimedes principle according to the equation 8 [246-247].

$$\text{True Density} = \text{wt.\%}_{\text{MNPs}}.\rho_{\text{MNPs}} + \text{wt.\%}_{\text{bredigite}}.\rho_{\text{bredigite}} \quad (3.8)$$

Figure 3.8 shows the falcon tubes of bredigite-magnetite scaffold nanocomposite soaked in the SBF for 4 weeks in the bain marie bath.

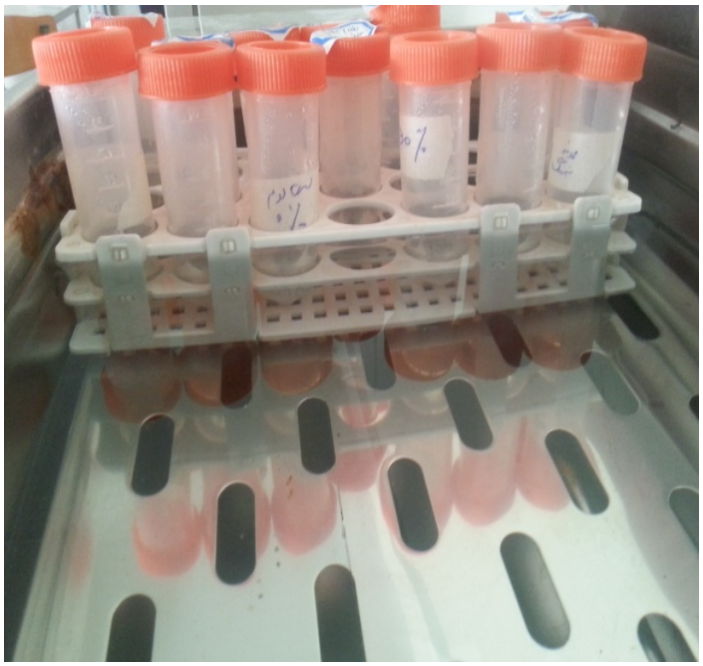

Figure 3.8: The falcon tubes and samples soaked in the SBF and PBS solution for 4 weeks in the bain marie bath (similar to human's body condition)

3.5.5 Effect of Feed Rate on Porosity and Compressive Strength

Porosity value and compressive strength of bredigite-magnetite scaffold nanocomposite have a critical role in the formation of bone in the laboratory and animal testing. Porous structures can create favorable conditions for cells to grow and nutrients to transfer, while the scaffold may afford superior compressive strength when inserted in the body. Therefore, investigation of porosity and compressive strength of bredigite-magnetite scaffold nanocomposite concerned by feed rate of 3DP machine. The 3DP machine pump, inject air with high pressure into the syringe. The syringe is fixed according to the machine motion system, and can be plugged to a wide range of needles. Then, due to the pressure, the depositing solution is flowing via the needles, and printed on the substrate. In the current project, we found out that

nozzle diameter have great impact on surface quality of the prepared scaffold nanocomposite. The nozzle diameter is greater than 0.2 mm up to 0.5 mm (diameter of nozzle 0.2-0.5). The motion accuracy in the axis depends on steeper motor and steeper drives used in the controller board, also types of Belt and pulley applied in the machine. Process parameters optimization involves setting for layer thickness, the water/Zb63 binder saturation, and time of required for drying. Fabrication of scaffold using 3DP regularly endures an unstable depowering plane, i.e., excluding loose powder from the porous interconnected structures. This is the main difficulty in manufacturing scaffolds with complicated structure by 3DP machine. This can be minimized with exact process parameters optimization. Process parameters may vary with particle size of the powder, and the type of the binder (whether the binder is aqueous or purely organic). The parameters of each process require optimization including modification of thickness of sprayed layer, the velocity of the roller, the saturation of the binder, and the layer drying time. Therefore, in this study we evaluate the federate, the layer roughness and layer thickness.

3.6 Materials Characterization of Scaffold Nanocomposites

To more fully discover how the materials phase, morphology, and microstructure influence on the all the properties of bredigite-magnetite scaffold nanocomposite supporting information required to performed by X-ray diffraction, Scanning Electron Microscopy, Energy-dispersive X-ray spectroscopy, Differential Scanning Calorimetric, Thermo gravimetric Analysis, and particle size analysis technique. The XRD used for phase characterization, SEM used for investigation of morphology of sample before and after soaking in the SBF, and nanocomposite powders. Also, the PSA used for analysis the size of bredigite powders. The TGA and DSC applied to

investigate the thermal behavior changes of bredigite-magnetite scaffold nanocomposite in various temperatures.

3.6.1 Phase Characterization

X-ray diffraction (XRD) (Philips X'Pert-MPD, Cu Kα radiation (λ1= 0.15423 nm) in the range of 10–80°, 40 kV, 35 mA) techniques was applied to the specimens to investigate the phase structure of bredigite-magnetite nanocomposite (0 wt.%, 10 wt.%, 20 wt.% and 30 wt.%). The XRD instruments were applied for analyzing the experimental results for samples containing different percentages of MNPs powders (IAUN, Najafabad, Esfahan and Iran).

3.6.2 Morphology Characterization

Scanning Electron Microscopy (SEM) were performed to observe the morphology of bredigite, magnetite, bredigite-magnetite nanocomposite with (0 wt.%, 10 wt.%, 20 wt.% and 30 wt.%) magnetite's, and morphology of bredigite-magnetite scaffold nanocomposite before and after soaking them in the SBF and PBS solutions. In addition the influence of sintering process (before and after sintering process) on the bredigite nanopowders (10 h milling and 4 hours at 1300°C sintering) was assessed with SEM technique. The prepared powders and scaffold nanocomposite (before and after soaking in the SBF and PBS liquid) samples were coated with thin layer of sprayed gold (Au) using a high vacuum for 2 min with the 40 kV accelerates voltage. The SEM tools was equipped with Energy-dispersive X-ray spectroscopy (EDX) microanalysis (FEI Quanta 200, Iran) to examine the Ca, Si, Mg, Fe and P ions contents from means of three spots on the surface specimens. The primary founding of the results indicate that the sintering process enhance the microstructure of the bredigite powder while it can increased the chemical and mechanical stability of the powders in the scaffold nanocomposite structure. The shape and size of prepared

samples were visualized by means of transmission electron microscopy (TEM, Hyundai, 100 keV). Fourier transform infrared (FTIR) spectroscopy (IR Affinity- 1, Shimadzu) was used for the examination of the functional groups in the bioceramic samples.

3.6.3 Thermal Characterization

The change in physical and chemistry of materials properties can be evaluated with increasing heat temperature or time to record the mass reduction or some transition like; vaporization, sublimation, and absorption and desorption. Also, to investigate amount of heat needed to develop the temperature of samples is essential. The thermal characterization of bredigite nanopowder was performed using Thermo gravimetric Analysis (TGA) and Differential Scanning Calorimetric (DSC) analysis. Samples weighing 5 and 7 mg separately was tied in aluminum crucibles with lids. The TGA and DSC analysis done at a heating rate of 10°C/min in the nitrogen atmosphere. TGA analysis is conducted by raising the temperature slowly and proposing weight against temperature. TGA was carried out on dried with a heating ramp rate of 10°C/min, starting form 50°C to 1500°C as a heating temperature to consider its water loss temperature. The basic data showed that from 500°C to 100°C the sample mass reduced 20 mg. Therefore, materials contents remain almost constant in the higher temperature.

3.6.4 Particle Size Characterization

The size of the particle characterized with particle size analysis (PSA). The PSA reports the distribution of powders by intensity and the mean size of the powders. Also, the PSA result can be used for BET analysis to found out about the morphology of the powders. The samples were analysis in the condition that temperature was 20°C, and test run for 70 second with ethanol as a dispersant

[viscosity (cp) =1.2000)]. The specific surface area of the prepared bredigite-magnetite scaffold nanocomposite powder was measured (N_2 was gas adsorption isotherms) for Brunauer–Emmett–Teller (BET) results. The powder particle size assumed as D (particle diameter), ρ (density of bredigite powder) can be calculated from the following equation Eq. (9) which ρ known as density.

$$D = \frac{6000}{S(BET) \times \rho} \quad (3.9)$$

3.6.5 Data and Statistical Analysis

The test and outcomes were expressed with ± standard deviation (SD) for $n = 3$ for all the samples. In addition, the data were analyzed and compared with support of one-way ANOVA. The significant differences of tests were monitored and highlighted when $P < 0.05$.

Chapter 4

GENE EXPRESSION PROGRAMMING AND SIMULATION

4.1 Gene Expression Programming

In this research, A Gene Expression Programming (GEP) used as one of the most important branches of the artificial intelligence (AI) for simulation of diopside scaffold. Using the GEP, two equations were described to predict the compressive strength (CS) and porosity (P) of the diopside scaffolds with the minimum error. The 3D diagrams extracted from the model were used to evaluate the combined effect of the process parameters on the compressive strength and porosity of the scaffolds [249]. The GEP model presented in this work has a very low level of error and a high level of the squared regression for predicting the compressive strength and porosity of diopside scaffolds as a case study.

The correlation between artificial intelligence (AI) and gene expression programming (GEP) is important and interesting issue in the materials science field. Researcher found out a wide range of application in GEP for those aspects of engineering which are under the influence of process variables and different setting parameters [256]. In the current study, the compressive strength, total porosity of silicate scaffold nanocomposite was modeled. A square regression (standard approach in regression analysis to the approximate solution) of the current study achieved was around 1 from both training and testing datasets (datasets from current

work and previous works). All the outcomes (compressive strength and porosity size) were compared to those obtained and acquired from case studies experiments diopside and bredigite powder as based materials in this work. The 3DP machine setting parameters (the additive range (0-30 wt.%) with step of 10 wt.%, layer thickness values (80, 110, 118, and 150 µm), and delay time (50, 100, 300, and 500 ms) were optimized and enhanced using design of experiment (DOE). In this study, DOE is a systematic method to find the relationship between factors affecting a process and the output of that process. In other words, it is used to find cause-and-effect relationships. The optimization and model used to predict a suitable value of input variable and output of DOE result. The basic GEP algorithm was developed by Ferreria in 2001 [257] that have the advantageous of coding simply, fast convergence speed and strong ability to solve the complex problems. Symbolic regression or function finding is one of the useful applications of the GEP models [256-257]. The aim of using GEP is to attain an expression that operates completely for all fitness events within a specific error for the accurate obtain value. Because of the complexity of the connection between the response variables and casual factors, prediction of the response variables based on mathematical model and simulation with empirically measurements is important. Stimulated models using bee colony [179], the Artificial Bee Colony (ABC) algorithm [258] were introduced by Karaboga for optimization of several criteria and parameter in year 2005 [259]. The ABC algorithm uses less control parameters; it has been found that its performance is better than other algorithms like Genetic Algorithm (GA), Particle Swarm Optimization (PSO), and evolution strategy (ES) [258].

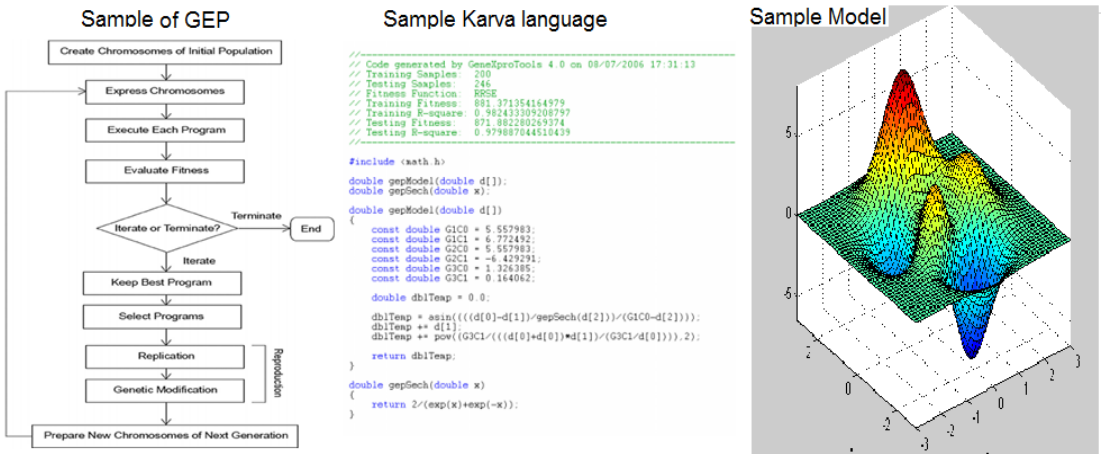

Figure 4.1: Connections of Algorithm, Karva Language, and simulated model

4.2 Gene Expression Programming Theory

In order to determine how efficient a given computer is efficient in executing a given job, a fitness function and established set of guidelines, known as the "gene expression programming" or GEP is used (an evolutionary algorithm that produces computer programs or models). Moreover, it is a special type generic algorithm, where every computer program is expressed as an individual. There are three phases that make up the generic programming i.e. the crossover, mutation and reproduction. According to Koza [261], independent methodology in generic programming is gotten from the genetic algorithm. When considering the reproduction selection means, a removal of minute percentage of tress with the lowest fitness range should be undertaken and then, the ones left out should be chosen trees, which is with respect to the system of selection [261]. In the crossover phase, swamping of chosen parts of two trees is undertaken; and so, fusing together info from both parents is used for developing the fitness of the next generation. Following this is the mutation phase, this aids with the development of non-local attributes of the search as well as fight against convergence that occur prematurely [94]. By employing the use of the Karva language the mathematical code of the gene can be highlighted; this Karva

language, the language of ETs or genes. A diagrammatic illustration of the encoded chromosome as a linear string possessing just one gene is shown in Fig. 4.2. Moreover, Fig. 4.2 also expresses the mathematical expressions and the ET. By closely viewing the data shown in the Figure, it can be seen that ET is converted to karva language. Furthermore, this methodology makes use of noncoding or coding parts which is close to the biological gene sequence. As a matter of fact, linking functions are used for the fusion of the genes; these linking functions are subtraction, addition, division and of course, multiplication. One crucial advantage that is offered by the GEP is that phenotype can be deduced with respect to the genes sequence; this is known as the Karva language. Another fact to consider is that in GP, the genotype as well as the phenotype are acts as expression trees. However, in GEP, the translation process of the genotype is what brings about the phenotype. Unlike the classical GP, the benefits of the GEP is that there is a strong distinction between the genotype and phenotype. Take for example, the equation given as $[(b\times a)-c)]+\sqrt{(d-e)}$ can be expressed by an ET or two gene chromosome; this is depicted in Fig 4.2. below.

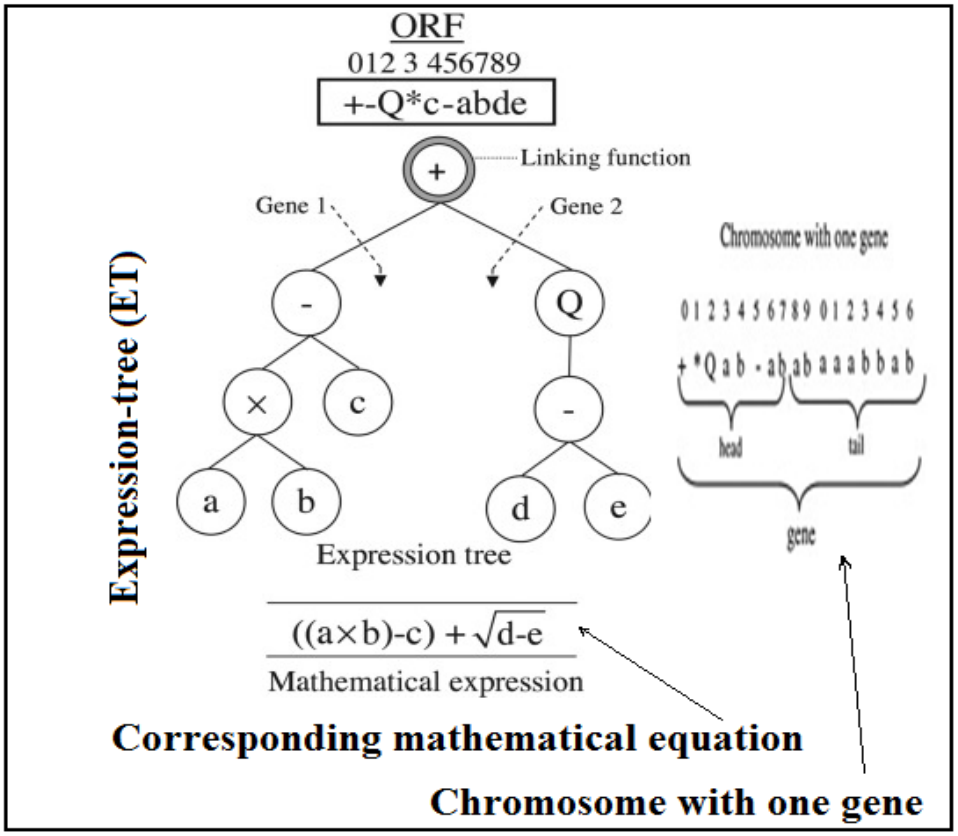

Figure 4.2: Chromosome with one gene and its expression tree and corresponding mathematical equation.

Usually, a mathematical model is illustrated from the conception of one or more genes by chromosomes. Additionally, Karva language, which could be illustrated in two various language i.e. the ETs language and the language of genes, is shown by mapping out a mathematical code of gene. Furthermore, the head and tail are basically the two major parts of a gene. When the head is considered, variables, mathematical operators and constants make up its building block; this is used for the mathematical expression encoding. An example of this includes: +, −, *, /, √, sin, cos, 1, a, b, c, etc. On the other hand, the tail is basically made up of constants and variables, conventionally called “terminal symbols”. Example of this is 1, a, b, c etc. Also, it should be noted that extra symbols are employed if the terminal symbols are unfit to properly depict its expression mathematically. The encoding of two

chromosome genes as well as its ET expression, is illustrated in Fig 4.2; it should be noted that these are linear string also. Moreover, when GEP is taken into account, the encoding of individuals takes place and it is expressed as fixed length of linear strings i.e. the chromosomes or genome. Following this, varying shapes and sizes of nonlinear entities are depicted with respect to the encoded individuals, by utilizing the GEP tools; this is conventionally known as the genes. These genes or sub-expression trees are used for the systems environment simulation through the use of the GEP equations. And so, the translation of the tree language expression to the mathematical formula is the means at which this equation is gotten [262]. In Fig. 4.3., the schematic illustrates the translation of ET language to a mathematical formula. Moreover, linking functions is accomplished by piecing together sub expression tress or genes; these linking functions are: subtraction, multiplication, addition or division.

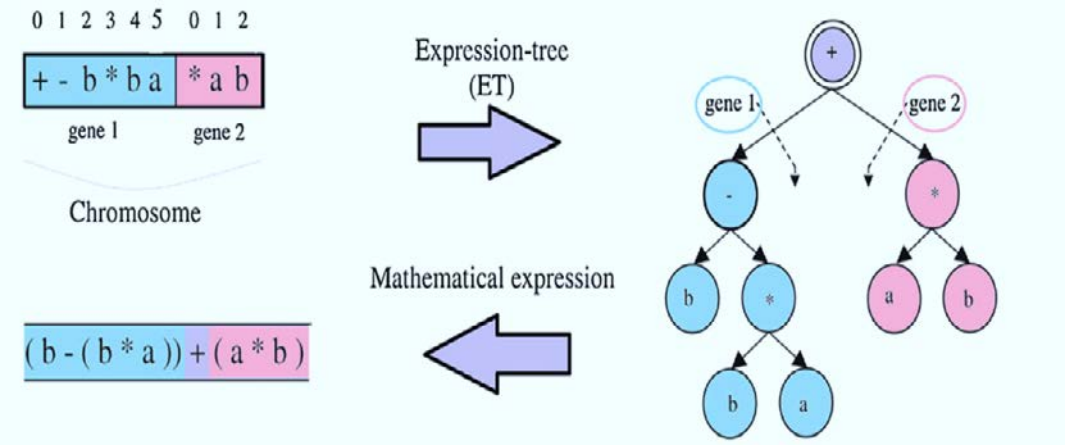

Figure 4.3: Process of translation of ET language to mathematical formula

Regarding the potential of GEP in simulating the engineering parameters and processes, the compressive strength and also the total porosity of the diopside scaffolds was simulated. In order to introduce the system conditions to the GEP model, a database of the process parameters was prepared, by which GEP can

understand the changes in the process parameters and their effect on the properties of the scaffolds.

4.2.1 Gene Expression Programming Language

The genes languages as well as the language of the ETs are the major two languages that are in use in the GEP. Furthermore, a GEP toolkit is utilized for encoding individuals of a computer program that is made; the GEP tools encode the individuals fixed lengths of linear strings i.e. chromosomes or genomes. Another fact to take into account is the selection process that the ETs undergo; these ETs are the chromosome's expression and the process of selection is usually authenticated by the value of its fitness in creating individuals that are new. Additionally, the genetic operator is responsible for the alteration of the chromosomes during the phase of reproduction. And as stated previously, the Karva language is responsible expressing the mathematical code of the gene [262].

4.2.2 Modified Gene Expression Programming

Ferreira [257] developed the basic GEP algorithm in 2001, which has inherited the advantages of the traditional genetic algorithm (GA) and genetic programming (GP). It has been applied to many fields for its simple coding, fast convergence speed and strong ability of solution problems. One important application of GEP is symbolic regression or function finding, where the goal is to find an expression (equation) that performs well for all fitness cases within a certain error of the correct value [5]. The "function finding" application of GEP can be extremely important within the pharmaceutical field. To evaluate the efficiency of the algorithm and obtained parameters, a case study was conducted. A square regression of about 1 was obtained from training and testing datasets. Also, the results were compared to those acquired from case studies (Diopside powder as based materials). What is important

in any modeling process is that whether or not the model is accurate. There are certain criteria to evaluate the accuracy of the model, those criteria that guarantee the superiority of one model over another model. The Mean of Square Error (MSE), the Mean Absolute Error (MAE) and Relative Absolute Error (RAE) are among these criteria. The Compliance of predicted data with the experimental data also examined by the numerical value of the squared regression (R^2) which is important parameter to measure the accuracy of the model. Errors and regression value are obtained from Equation (1-4) [249]:

$$RAE = \frac{\sum_{i=1}^{n} |t_i - o_i|}{\sum_{i=1}^{n} \left| t_i - \frac{1}{n}\sum_i t_i \right|} \tag{4.1}$$

$$MAE = \frac{1}{n}\left[\frac{\sum_{i=1}^{n} |t_i - o_i|}{\sum_{i=1}^{n} t_i} \right] \tag{4.2}$$

$$RMSE = \frac{1}{n}\sum_{i=1}^{n} \left(t_i - o_i\right)^2 \tag{4.3}$$

$$R^2 = \frac{\left(n\sum t_i o_i - \sum t_i \sum o_i\right)^2}{\left(n\sum t_i^2 - \left(\sum t_i\right)^2\right)\left(n\sum o_i^2 - \left(\sum o_i\right)^2\right)} \tag{4.4}$$

where t_i is the target parameter, o_i is the output parameter and n is the number of datasets.

Table 4.1 shows the applied settings for the presented GEP model. As can be seen in the current table, the number of genes, which are equal to the sub-expression trees, is 3 and the linking function is addition.

Table 4.1: Applied Settings for the presented GEP model

Parameter Definition	Values
Chromosomes	30
Head size	8
Number of genes	3
Linking function	addition
Mutation rate	0.044
Inversion rate	0.1
One-point recombination rate	0.3
Two-point recombination rate	0.3
Gene recombination rate	0.1
Gene transposition rate	0.1
Constants per gene	5
Weight of functions	7
Lower bound	10
Upper bound	10

The database used in this work was obtained from the previous work [249] and the experimental tests (Table 4.2).

Table 4.2: The database used in this work was obtained from the previous work and the experimental tests done in this work [36-38, 249].

Scaffold	Spacer Concentration (%)	Compressive Strength (MPa)	Total Porosity (%)	Ref.
Diopside	60	8.17	53	[263-264]
Diopside	70	5.37	61	[263-264]
Diopside	80	4.07	64	[263-264]
Diopside	60	2.04	62	[263-264]
Diopside	70	1.62	74	[263-264]
Diopside	80	1.22	83	[263-264]]
Diopside	80	1.41	80	[263-264]
Diopside	80	0.98	85	[263-264]
Akermanite	75	0.9	81	[38]
Akermanite	75	0.9	81	[38]
Akermanite	75	0.86	82	[38]
Akermanite	75	0.82	83	[38]
Diopside	75	1.56	81	This work
Diopside	75	1.51	82	This work
Diopside	75	1.47	83	This work

4.3 Artificial Intelligence and GEP

Evolutionary mechanisms are exploited in order to update these candidate solutions or particles; the reason being to give rise to a more better and acceptable solution. As a matter of fact, the mechanisms that have been proposed are identical to what usually takes place in nature. When considering how nature works, every single particle models itself to its best experience in life and following this, adapts and moves on to a better experience of its neighbours. The database that has been obtained is split into two categories i.e. the testing datasets and the training, the reason being to improve the GEP model's accuracy. The training datasets functions within a model introduced to it by, making it possible for the model to learn the conditions that make up the process circle or environment. About the learning rate of the model, the dataset to be tested is placed into the GEP model and then the model takes note of the accuracy through the process of learning. In order to maximize the performance of the database, those variables that contribute greatly to the system's performance must be greatly detected. Variables like the spacer size, spacer concentration, etc., are important things to look into when evaluating the compressive strength and the diopside scaffolds. In addition, the porosity and compressive strength of the scaffolds are taken as the output variables; this is known as the symbol for performance for these specified structures. The GEP, in this scenario, initiates an alliance between the output and input variables. The formula captures value from the input variables and output variables; where the input variable is the variables process and the output variable is the compressive strength and porosity.

The proper diopside powder to spacer ratios was considered in such a way that a final porosity of 80–90% was obtained. Eq. (5) helps to determine the proper weight percentage:

$$W_{spacer} = \frac{V_{spacer} \times \rho_{spacer}}{(V_{spacer} \times \rho_{spacer}) + (V_{diopside} \times \rho_{diopside})} \quad (4.5)$$

where W_{Spacer} and V_{spacer} are the weight percentage and volume fraction of the spacer, respectively (the required porosity is determined based on the V_{spacer}). $V_{diopside}$ is the volume fraction of the diopside. $\rho_{diopside}$ and ρspacer are the density of the diopside and the spacer, respectively. The densities of diopside and sodium chloride are 3.26 and 2.17g/cm^3, respectively.

$$\text{Interconnected porosity} = \frac{W_w - W_d}{W_w - W_s} \times 100 \quad (4.6)$$

In the first stage, the obtained powder mixture was stirred by a mixer for 1h and then the sunflower oil (in the amount of 2wt.%) was added to the powder mixture in order to stabilize the homogeneity.

In the final stage, the temperature of the obtained scaffolds was reduced to the environment temperature at a rate of 10°C/min. The Archimedes technique was used to estimate the porosity of the prepared scaffolds. Eq. (7) helped to determine the interconnected porosity of the scaffolds:

$$\text{Total porosity} = 1 - \frac{W_d}{\rho(W_w - W_s)} \times 100 \quad (4.7)$$

Where ρ is the true or theoretical density of the diopside and is equal to 3.26 g/cm^3.

4.4 Modeling Observations

As mentioned before, there is a need for a database in any modeling process to solve a complex problem. From the total number of data presented, 11 of them are assigned to the training dataset and the remaining 4 data are assigned to the testing dataset from 17 total data. The expression tree diagrams obtained by the GEP model to simulate the compressive strength and porosity of the scaffolds are shown in Figs. 4.4a and 4.4b, respectively**.** In these diagrams, C0 and C1 are the constants produced by the model and d(0) to d(3) are the input (process) parameters, which are applied concentration, and spacer size, respectively. The formulas extracted from these diagrams (shown in Fig. 4.2 and Fig. 4.3) are as follows:

$$\begin{aligned} CS = &(\sqrt{((\sin(d(1))+(d(2)/d(1))))}/\exp((\operatorname{atan}(-9.686737)+d(3)))) \\ &+\operatorname{atan}(((\cos(8.351806)/d(2))+(d(0)-(8.351806\times d(3))))) \\ &+(\operatorname{atan}(((-2.019592\times d(1))-(-2.019592-d(0))))\times\operatorname{atan}((\sin(d(3))\times d(3)))) \end{aligned} \tag{4.8}$$

$$\begin{aligned} TP = &\operatorname{atan}(((\cos(d(1))\times((d(2)\times d(1))+4.534271))\times d(1))) \\ &+((-4.534271+\cos((d(1)-(1.035278\times d(2))))+d(1)) \\ &+((\sin((d(0)-2.001647))\times((-3.93216-d(3))\times(-3.93216)))\times\sin((d(3)^2))) \end{aligned} \tag{4.9}$$

The compressive strength and total porosity value were represented in Eqs. (8) and (9) [249], as a dependent output variables. These dependent variables are related to the independent variables (input values or process parameters). To predict the compressive strength and porosity values, the values of input (process) parameters are placed into Eqs. (8) and (9), respectively. By checking the Table 4.2, it can be concluded that the tested value for compressive strength and total porosity as input variables are recorded to be 1.47MPa and 83%, respectively. Therefore, it is possible to measure the accuracy of our model for predicting the porosity and compressive

strength from equations (5-7). The values of errors and R^2 of the GEP model related to the training and testing datasets are presented in Table 4.3.

Table 4.3: The values of errors and also R^2 of the GEP model related to the training and testing datasets

Symbols	Compressive Strength Modeling		Porosity Modeling	
	Training	testing	Training	Testing
R^2	0.961	0.9595	0.9867	0.948
MSE	0.0234	0.0671	0.98	0.76
MAE	0.0543	0.543	0.754	0.7521
RAE	0.09	0.021	0.342	0.432

This means that the presented GEP model has the error values of 0.08 MPa for predicting the compressive strength and 0.05% for predicting porosity in the scaffolds, which were indeed very interesting results.

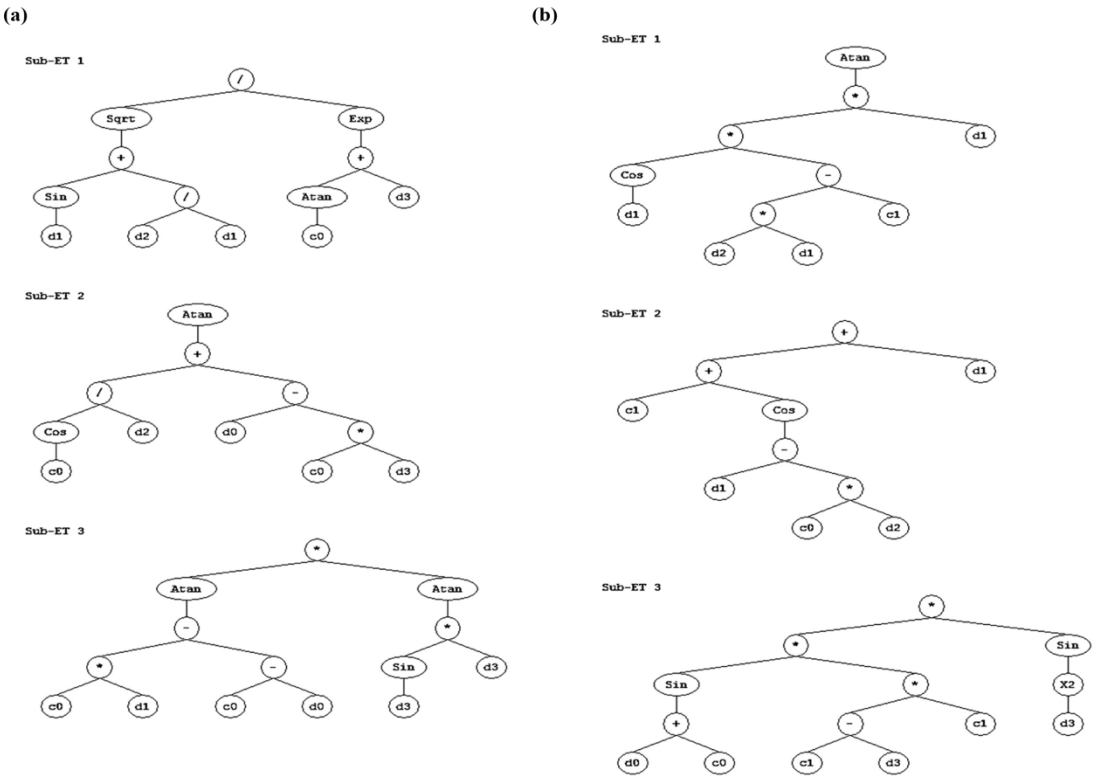

Figure 4.4: The expression tree diagrams obtained by the GEP model to simulate a) the compressive strength and b) porosity of the scaffolds.

The adaptation of the experimental data and the predicted one related to the prediction of the compressive strength and porosity for both training and testing datasets are shown in Fig.4.5 (a-b) and Fig. 4.6 (a-b).

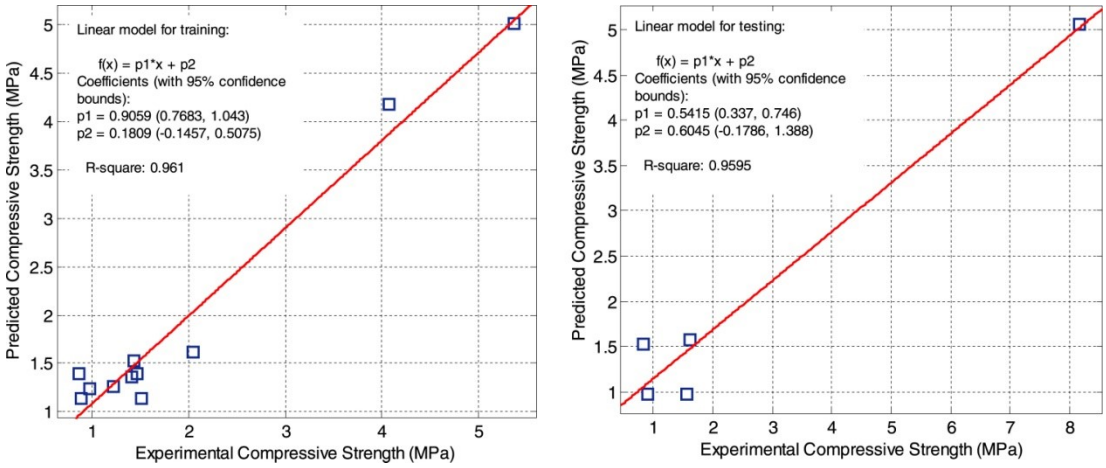

Figure 4.5: The adaptation of the experimental data and the predicted one related to the prediction of the compressive strength for a) the training and b) the testing datasets

The outcome shows the relation between the predicted and experimental values of compressive strengths (see Fig. 4.5) and total porosity (see Fig. 4.6.) for both training and testing datasets, respectively.

The GEP model could predict the compressive strength very close to the experimental values according to our previous work [249]. The accuracy of the model to predict the compressive strength and total porosity of the scaffolds was measured by Equations from 1 to 4. The values of errors and also represented at R^2 of the GEP model obtained from the training and testing datasets are presented in Table 4.3.

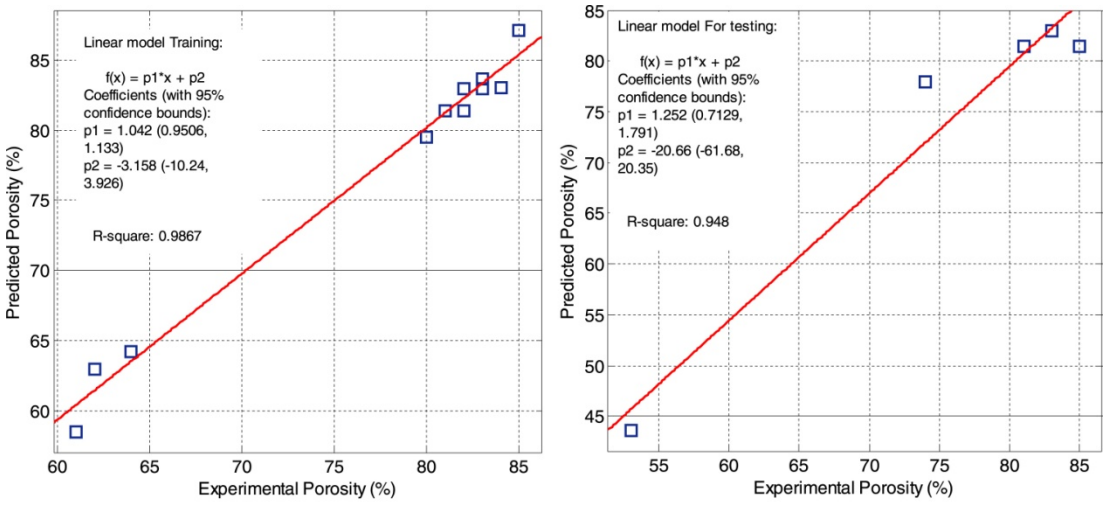

strength for a) the training and b) the testing datasets

Figure 4.6: The adaptation of the experimental data and the predicted one related to the prediction of the porosity for a) the training and b) the testing datasets.

From Table 4.3 and Fig. 4.5 and Fig. 4.6 it can be concluded that the GEP model presented in the current project have a very low level of error and a high level of the squared regression for predicting the compressive strength and porosity of diopside scaffolds.

The effect of input and output (compressive strength and porosity) were depicted in Figure 4.7 (a-f) in graphical chart. From the Figure 4.7 is seen that maximum porosity obtained when the spacer concentration and size of the particles increased (MNPs and salt) to a higher value (more than 20 wt%. to sample with 30 wt.%).

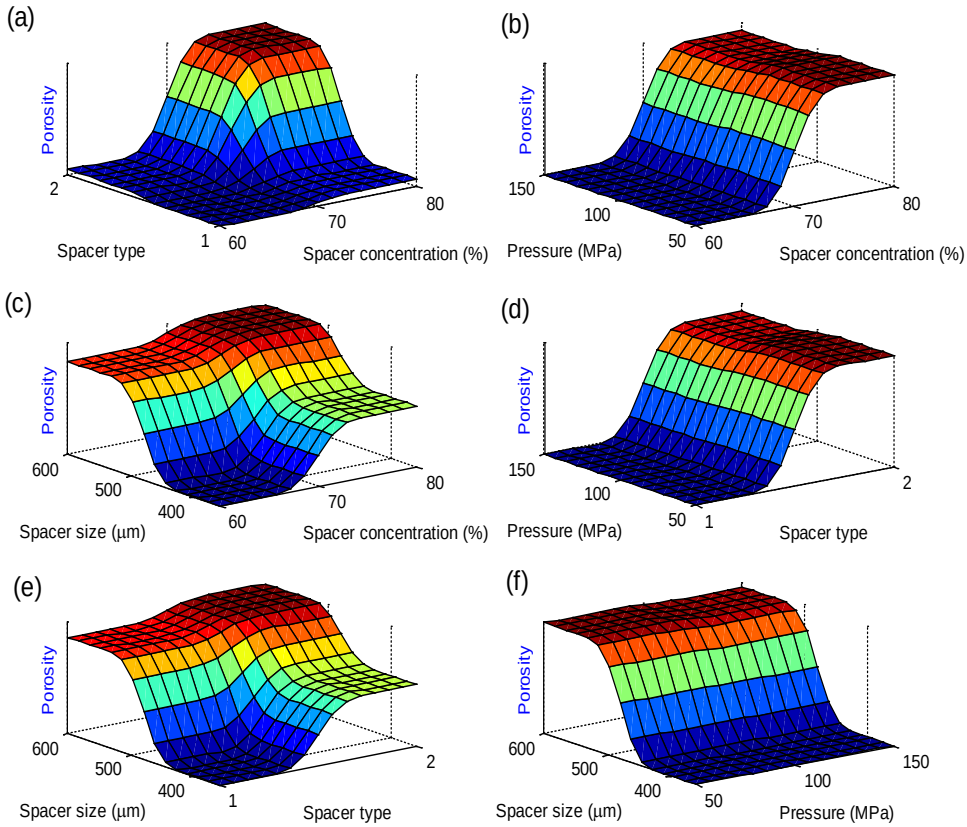

Figure 4.7: 3D charts by which the effect of any process parameters on the porosity of the diopside scaffolds are separately examined [249]

The results shown in Fig 4.7 shows that optimum amount of MNPs and salts should be applied and the scaffolds structure may collapse in higher or lower values during the sintering process. Figure 4.7 indicates the effect of spacer size and introduces that higher porosity obtained when the size of particles and spacer amount increased. Although higher porosity for the scaffolds, obtained which leads to lower compressive strength of the scaffold but it should have proper balance between porosity and compressive strength of the scaffold.

In this work, we found that scaffold nanocomposite with 30 wt.% magnetite powder have a proper porosity and compressive strength. As Figure 4.8 shows the distribution of particle is vital for enabling a well-packed, smooth powder bed for printing and also for dictating the intrinsic micro-porosity and resolution of the

printed material [296]. Then, the bredigite and magnetite powder was collected in ranging 30–150 μm to remove particulate that was too large for accurate printing and too small to avoid agglomeration. A cylindrical scaffold nanocomposite with 13 pore size on the top surface indicated better mechanical stability according to the solid work and our experiments.

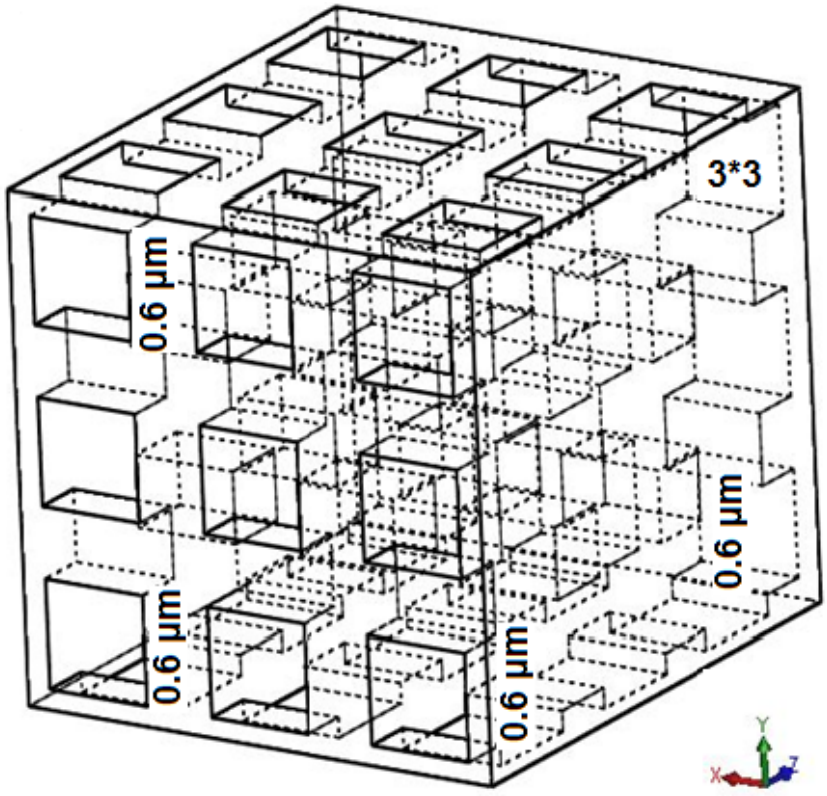

Figure 4.8: 3D image from micro-CT scans of 3 mm scaffolds were used to measure the printing accuracy relative to the ideal CAD image

4.5 Study the Feed Rate effect on Porosity and Compressive Strength

An injection of pressurized air into a given syringe is accomplished by the means of the 3DP machine pump. A motion system was responsible for holding the syringe in place and it can be configured to work well with broad range of needles. As a result of the intense pressure, the needles give out the solution to be deposited which is

imprinted. The most vital part of the machine is the smart pump. The value of the smart pump can be presented to automatically dispense material within a broad range of one to a million centipoises; this is done or accomplished with accurate timing, controlled air pressure, valve opening and height adjuster.

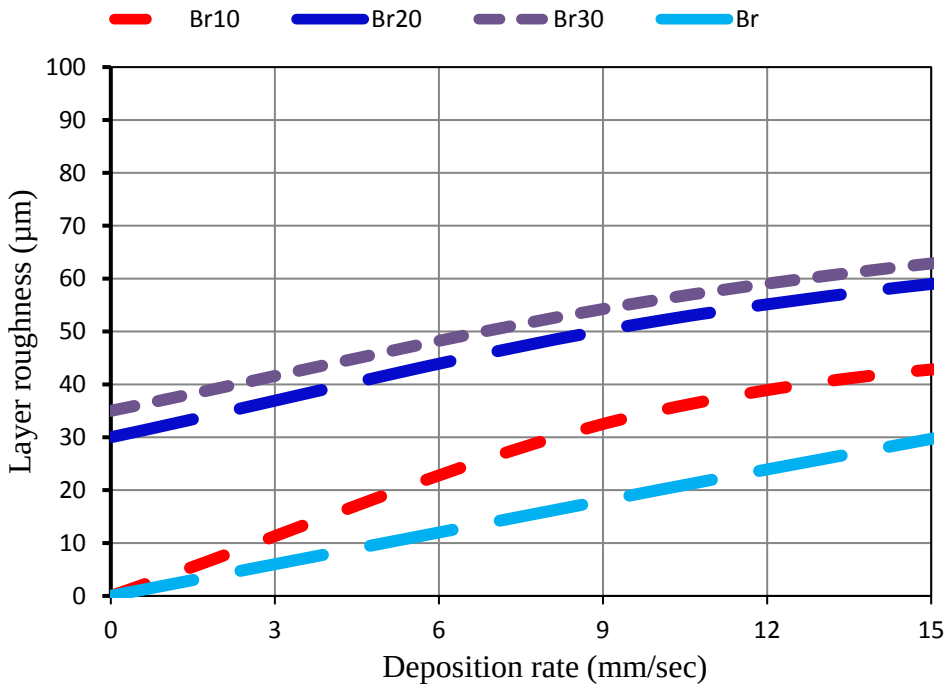

Figure 4.9: Line thickness at travel feed rates of 5, 10 and 15 mm/sec for various concentrations of MNPs (0 wt. %, 10 wt. %, 20 wt. % and 30 wt. %) in bredigite.

Figure 4.9 shows that as speed and feed rate increased from 5 mm/sec to 15 mm/sec may cause a significant increase in layer roughness. In addition, increase in MNPs concentration from 10 wt. % to 30 wt. % cause a significant decrease in thickness and increase roughness of the samples.

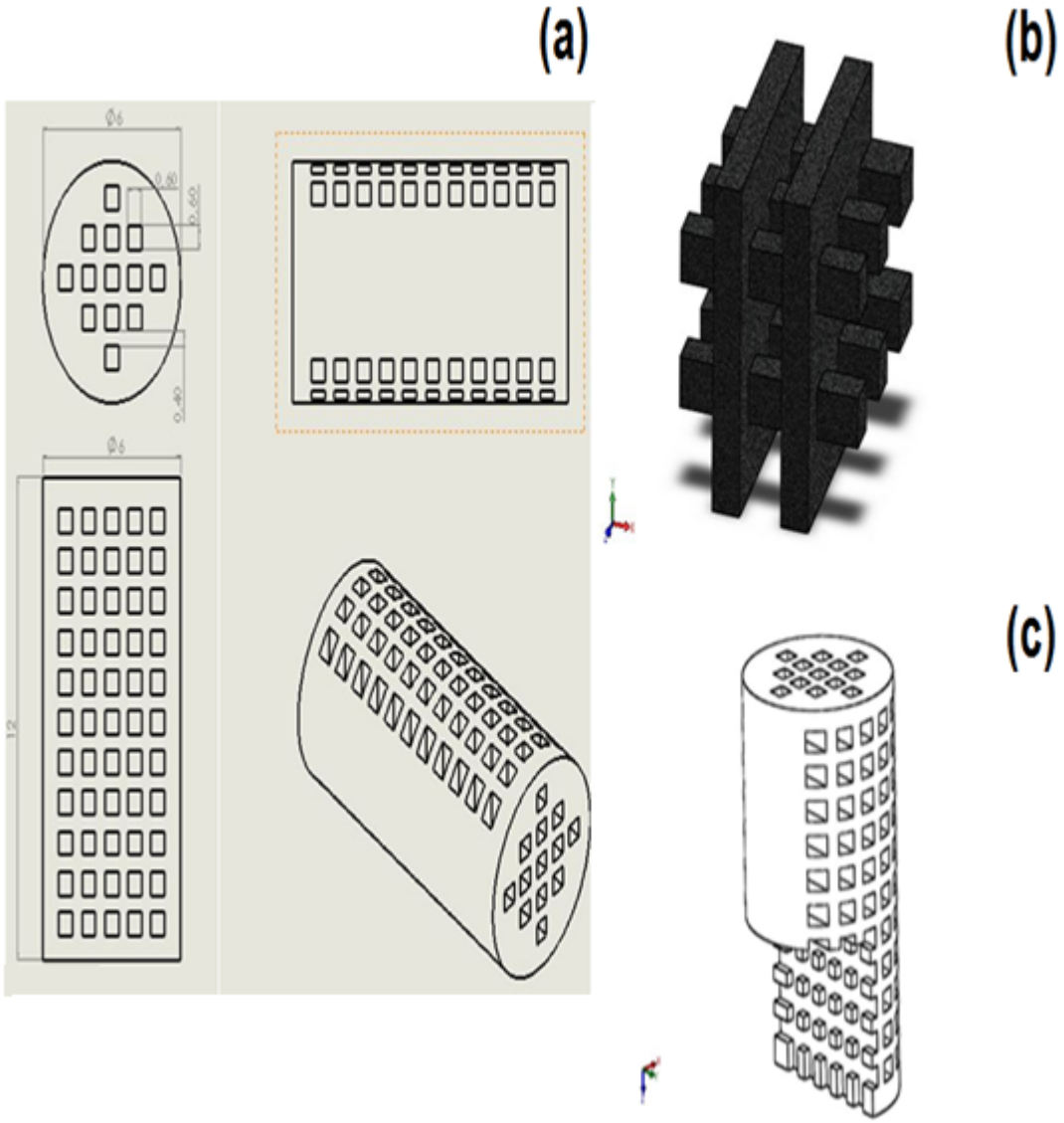

Figure 4.10: The schematic of three-dimensional nanocomposite in Cartesian coordinate for optimum sample designed by solid work a) full view, b) cross section of the centre, and c) sample which cross section occurred

Figure 4.10 show the cross section of scaffold nanocomposite prepared in the current study. It shows that scaffold nanocomposite walls are strongly stable and have uniform channel distribution as the modeled represented in Figure 4.10 (b-c).

In order for the manufacturing machine to be optimized, there are two methodologies that are utilized i.e. the operation variables are altered indirectly to boost the parts that are given out and then, the machine design is improved. Moreover, the producers

limit the operation parameters internally as well as the constructive alterations. However, employing the use of a software compensation which is an input alteration, has shown to be perform outstandingly i.e. without the modification of the machine, in various types of machine.

The result of 3DP machine observation indicate that when the 3DP machine starts to spray the powder with binder to produce 3D scaffold the suitable feed rate for the scaffold is 5 mm/sec up to 15 mm/sec. As the investigation shows with increasing the feed rate the scaffold thickness began to be decrease. However, adding more MNPs to the silicate bioceramic caused higher porosity in the sample with 20 wt.% MNPs. The scaffolds nanocomposite thickness is in the range of micrometer from 100 to 650. The optimum thickness can be set and calculated from training data and experimental data.

4.6 Observation of Machine Parameters

In the 3DP process, there are a number of variables which were stated initially that determine the scaffold's product efficiency i.e. the thickness of the layer, roller speed, feed rate and the bed temperature. Various levels of influence exist on every single variable (e.g. federate, speed, and layer thickness); moreover, the final scaffold nanocomposite can be a combination of these accurate parameters. Also, these observations indicated that instead of launching an examination which utilizes a one-factor-at-a-time test, the 3DP variable can be optimized by making use of the factorial design and basic observations. In addition, the levels, factors and the responses were also uncovered in any previous study.

The levels represent the precise value of the factors, while the factors represent the experimental variables that are controllable and finally, the responses are the experimental results. The 3DP machine is unique due to its ability to manufacture complex geometrical structures. Also, the system can be fully integrated with the CAD, to design products that exhibit complex structures. Another thing to consider is the three pumps that exist in the 3DP machine; this enables the product to be completely feasible. The feed rate for this project which is about 5 mm/sec to 15mm/sec is necessary for the production of the scaffold; this is accomplished by the spraying the powder with the 10 ml binder for better strength and proper stability. Therefore, it should be noted that an increase in the thickness of the scaffold will directly result in a decrease in the federate. Nevertheless, a twenty percent MNPs that has a high porosity within its sample results when more MNPs is added to the Br. There is however, no vivid connection between the layer thickness and adding more and more MNPs. From the study, the porosity of the sample is dependent on the compressive strength; an increase in the compressive strength will inversely affect the porosity, due to the structure of the pores and the channels that is fabricated from the scaffold itself.

Moreover, a range of 80 to 150 μm expresses the thickness of the scaffold. In fact, the training data as well as the experimental data help in designing the optimum layer. Moreover, when the sample has higher clearance, lower layer thickness and less roughness, the height of its layer precision can be significantly improved. And so, in this paper, the layer thickness of the 3D printer ranges from 80-150 μm. In order for the architecture of the 3DP to be outstanding, the binder is mixed; the time taken for the hardening process of the binder to occur at 150°C should be 60 minutes.

Moreover, hot press air is used as a medium for removing the extra powder samples. Following this, the 3DP sample at a sintering temperature is applied again; at 650°C, the samples are sintered at maintained for one to two hours. Finally, the heating and cooling rate as well as its dwell time i.e. at 5°C/min was both taken as two hours.

Chapter 5

RESULTS AND DISSCUSION

5.1 Materials Characterization

In this section, the results of the phase, morphology, microstructure of the powders and scaffold nanocomposite samples, are studied in detail. Moreover, a suitable homogeneous bredigite-magnetite (Br-MNPs) scaffold nanocomposite blends, were fabricated by using a 3DP machine. By Fusing the MNPs with the Br ceramics powder, a structural and physio-chemical change to the resultant pure Br scaffolds occurred.

5.1.1 XRD Analysis

5.1.1.1 Phase Characterization of Bredigite Powder

The bredigite powder was prepared by a simple and economical method known as the mechanical activation (MA) technique. Through the process of sintering, the prepared milled bredigite (Br) specimen was kept in the furnace for 4 h at 1300°C at a cooling and heating rate of 10°C/min. Figure 5.1 depicts the XRD pattern of the bredigite ceramic powder; from the Figure 5.1, it can be seen that the XRD pattern conforms to the standard card of the bredigite powder that has a chemical formula of $Ca_7MgSi_4O_{16}$ (Joint Committee on Powder Diffraction Standards (JCPDS) 0-360-399) i.e. with no additional peaks to the MA technique.

Table 5.1: The Composition of silicate bioceramics

Composition (wt %)	Akermanite	Bredigite	Diopside
MgO	1.54	1.42	1.38
SiO_2	4.62	3.94	4.4
$CaCO_3$	3.84	4.64	4.22

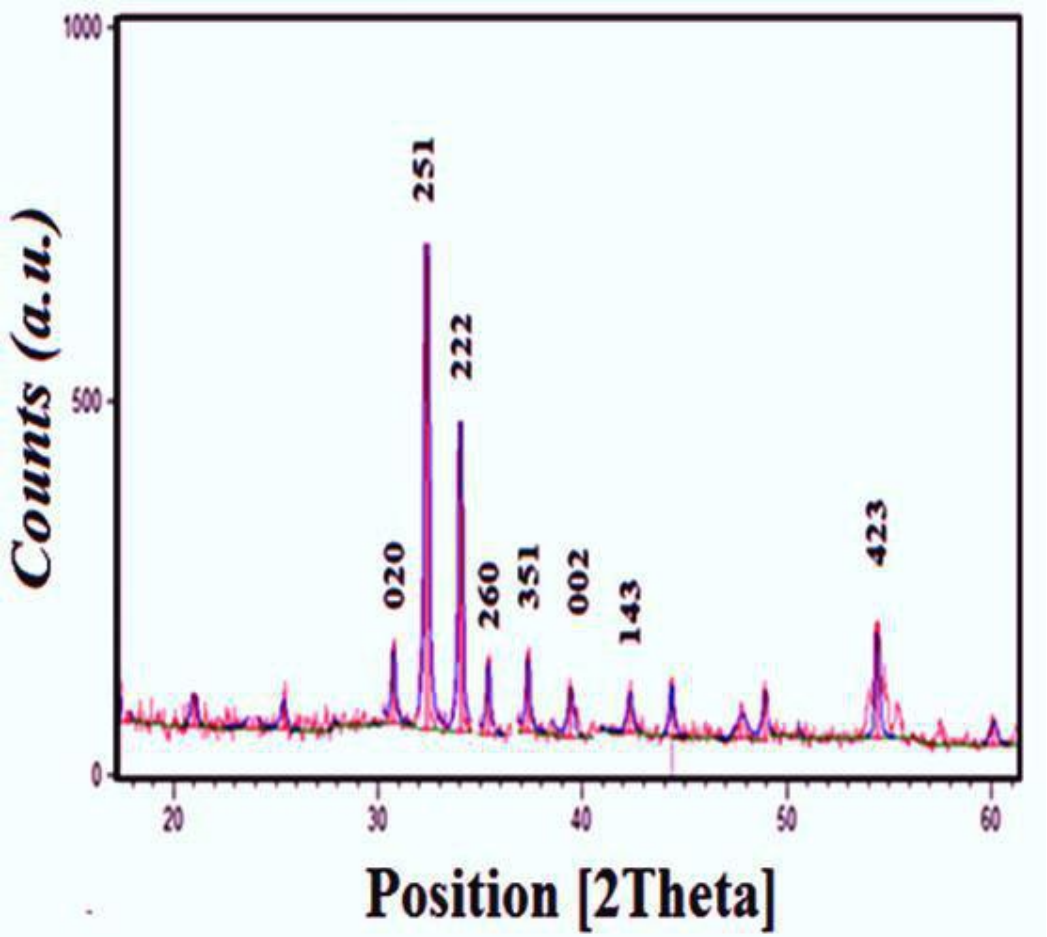

Figure 5.1: XRD pattern of prepared bredigite powder synthesized by HEBM after 10 hours and sintering temperature at 1300°C for 4 h.

Figure 5.2 demonstrates the XRD pattern of the sintered bredigite-magnetite scaffold nanocomposite containing (0, 10, 20, and 30 wt.%) MNPs. Figure 5.1 represents the sharp peaks of the bredigite peaks, which appear between 30-35°.

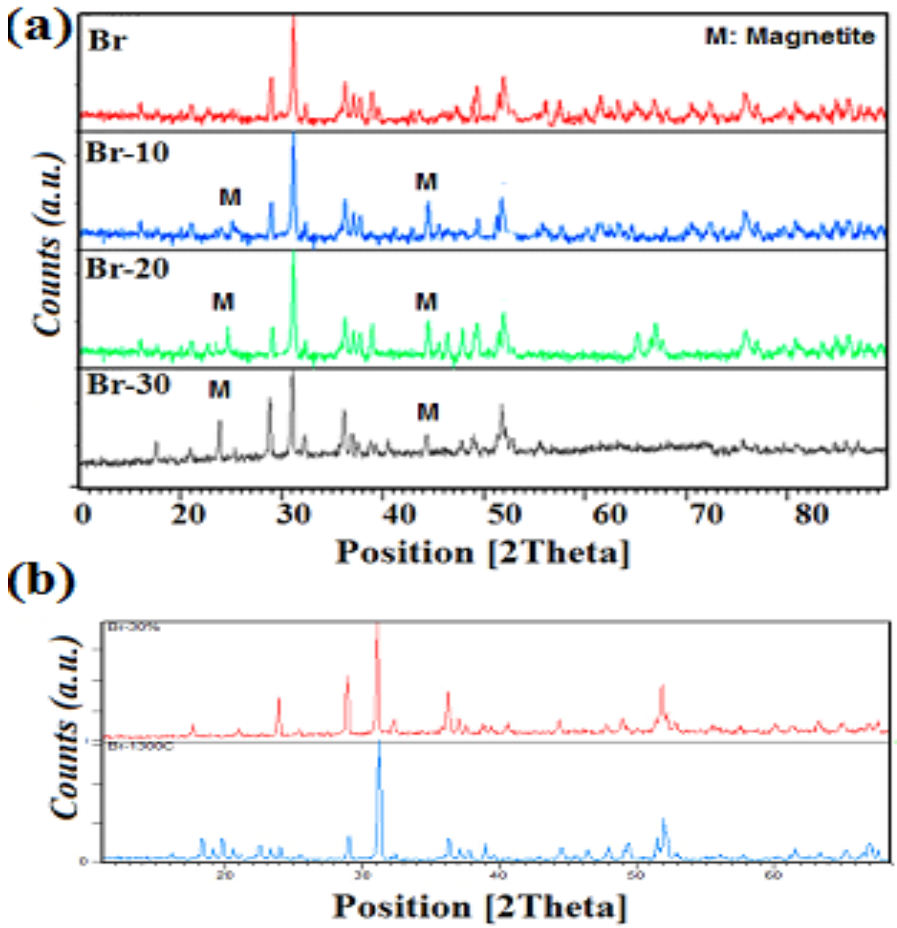

Figure 5.2: XRD pattern comparison of prepared bredigite powder a) with various amount of MNPs (0, 10, 20, and 30 wt. %), and b) Br powder compared with Br-MNPs 30 wt.%

Figure 5.1 showed that at 1300°C, an increase in the temperature produced some extra nanocrystalline phase within 2 h at an orientation of 37° and 54°. These additional peaks are the resulting impurities from CaO and Carbon. Table 5.1 shows the elements that synthesize the bredigite, akermanite, and diopside ceramic powder from their stoichiometric values. After four stages, the bredigite ceramic powders were successfully synthesized. In the first stage, after 5 h of milling, the similarity of the XRD pattern was about 35% i.e. when compared to the original pattern. Then continuing on with the milling process for 8 h, the similarity reached a value of 40%. Finally, after 10 h of milling and sintering at a temperature of 1300°C for 4 h, the bredigite was fabricated. The bredigite PSA result indicates the nanocrystalline size

of the bredigite (see Fig. 5.3). The size of the prepared powder was measured by using the PSA technique; moreover, the average particle size was less than 100 nm.

Table 5.2: Parameter used to synthesize the Br with through HEBM

Milling (h)	Ball (g)	Weight (g)	T (°C)	Similarity (%)	Sintering (h)	Ave. PSA
5	86.5	10	1100	35%	--	≤300 nm
8	85.0	10	1200	40%	-	≤250 nm
10	84	10	1100	45%	3-4	≤200 nm
10	85	10	1200	50%	3-4	≤200 nm
10	80.5	10	1300	65%	4	≤100 nm

The results of Table 5.2 indicates that the decrease in the weight of the ball during the milling process will result in a reduction in the crystallite size. Also, it has been proven that size of the balls has prominent influence on the quality of the synthesized powder. The PSA result and BET data showed that the average particle size of the bredigite particles were regular and spherical in shape i.e. with respect to the PSA and TEM analysis.

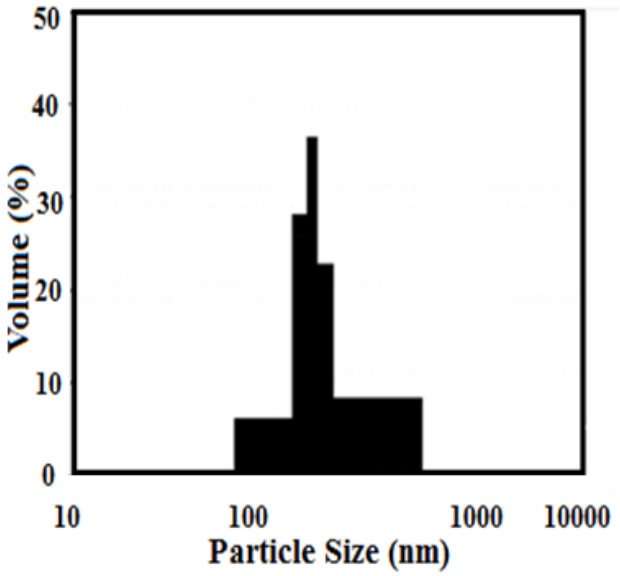

Figure 5.3: The PSA result for bredigite powder produced by HEBM technique.

It should be noted that the bredigite powders' mean crystallite size affects the calcined powder. The crystallite size of the bredigite powder can be found by using the broadening of XRD peaks and Scherrer equation 1 [17].

$$Xs = \frac{K.\lambda}{\beta\ Cos\theta} \quad (5.1)$$

Where K, known as shape factor, is equal to 0.89 and λ is the wavelength in nanometer. Also, β is the line broadening at Full width at half maximum (FWHM) in radians, theta (θ) is the Bragg angle in degree and X_s is the crystalline size (nm) of the areas. The four highest and sharp diffraction peaks for the bredigite (i.e. (020) (251), (260) and (222) planes) were chosen in XRD patterns, in order to calculate the crystallite size. The crystallinity of bredigite nanopowder, having various amounts of MNPs, was calculated by using equation 2.

$$Xc=(V_{251/222})/I_{222} \quad (5.2)$$

Where I_{222}, is the intensity of (222) diffracted plane and $V_{251/222}$ is the intensity of the hollow between the (260) and (020) diffracted planes of bredigite.

Table 5.3: Crystallographic parameters of the bredigite phase

Samples	Crystallinity (Xc %)±5	Crystallite Size (nm) ± 3
Br	44.8	45± 3
Br 10% MNPs	43.2	63± 3
Br 20% MNPs	41.1	52± 3
Br 30% MNPs	42.9	60± 3
HA-Br 5[196]	--	38.2 ± 2.7
HA-Br 10 [196]	--	25.7 ± 2.8
HA-Br 15 [196]	--	23.2 ± 3.1

By comparing the study results to similar work performed by Eilbagi et al. [196], it was clearly seen that the crystallite size of HA composite containing 5, 10 and

15 wt.% bredigite, were reported to be around 38.2 ± 2.7, 25.7 ± 2.8 and 23.2 ± 3.1 (nm), respectively [196]. However, in this study the data showed that the bredigite-MNPs crystallite size was 45, 63, 52, and 60 (nm), indicating that higher values for crystallite size can be ascertained. The change in the crystallite size is due to the presence of the MNPs having an amorphous structure, which depict higher crystallite size compared to that of the HA-bredigite composite. This shows that the bredigite nanopowder have a great influence on the density, grain size, porosity and compressive strength of the HA composite.

5.1.1.2 Phase Characterization of Akermanite Powder

Figure 5.4 (a-c) shows the XRD patterns of the Akermanite powders produced by HEBM after a duration of 6 h and proper sintering process at three different temperature (500, 700 and 900°C). As seen in Figure 5.4a, after 6 h milling, only the raw materials peaks were recognized. Figure 5.4a also indicates that no chemical reaction occurred in the starting materials i.e. even when subjected to a sintering temperature of 500°C. Following this, at 700°C sintering temperature, some peaks such as merwinite and calcium oxide were observed as shown in Figure 5.4b. Additionally, in the second stage, some additional peaks from raw materials disappeared after sintering at 700°C. At the end, pure akermanite were synthesized at 900°C after heating the samples in the furnace for 3h. Also, it is important to note that in the final stage, the merwinite was totally removed from the XRD patterns as shown in Figure 5.4c.

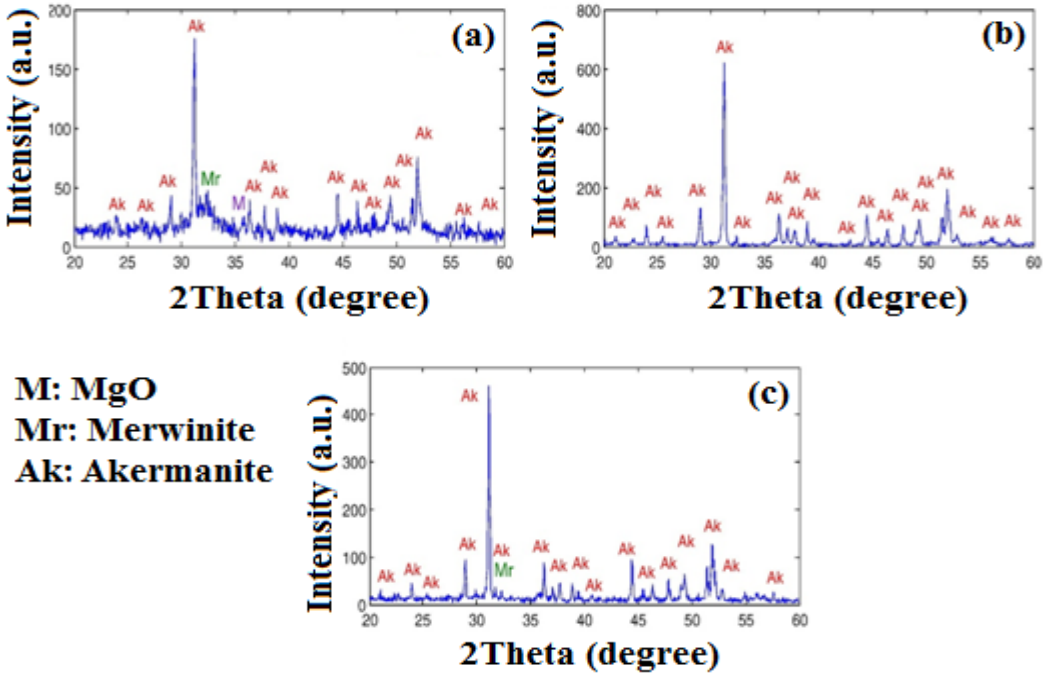

Figure 5.4: XRD patterns of the akermanite powders milled and sintered at various temperatures a) 500°C, b) 700°C and c) 900°C

5.1.1.3 Phase Characterization of Magnetic Nanoparticles

Figure 5.5 illustrates the XRD patterns of the milled MNPs powder that was sintered at 1200°C temperature. A comparison between the profile of X-ray diffraction (milled for 10 h), is illustrated in graph below.

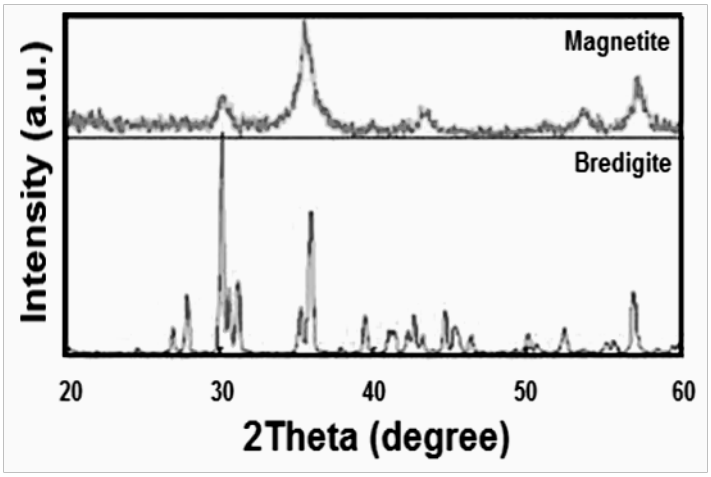

Figure 5.5: XRD diffraction patterns of MNPs sample compared with bredigite bioceramic

The XRD pattern of the magnetite and bredigite nanopowder are shown in Figure 5.5. In Figure 5.6, an illustration of the MNPs and Br powders in a glass cup is depicted. The results express the broadening of diffraction lines as well as clearly demonstrate the decline in the peaks intensity due to an increase in temperature of 1200°C and the influence of the strain during the milling process.

Figure 5.6: Nanocomposite and magnetite powders prepared by HEBM and sol-gel technique

5.1.2 Geometry and Size Evaluation

In this research, the TEM technique was applied in order to capture the morphology of the produced bredigite nanopowders and magnetite nanoparticles. The TEM micrograph helps in investigating the geometry and size of the crystalline bredigite as well as the MNPs powders that is obtained after 10 h of milling with respect to subsequent annealing at 1300°C (i.e. 4 h for bredigite and 3 h of sintering at 1200°C for MNPs sample); this is seen in Fig. 5.10. Also, in fig 5.7, the morphological features of the bredigite nanopowder is shown. The micrograph expresses the nanocrystalline agglomerated bredigite particles (dark black domain) with sphere and round shapes at sizes less than 60 nm.

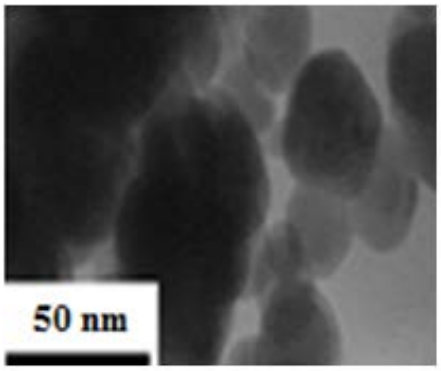

Figure 5.7: TEM images of synthesized bredigite after sintering process at 1300°C for 4 h.

Figure 5.8: Preparation of magnetite powders by sol-gel technique

5.1.3 SEM Analysis

5.1.3.1 Morphology of Bredigite Particles

Fig. 5.9(a-b) shows the morphology of the sample synthesized after 10 h of milling i.e. before and after undergoing sintering for 4 h at 1300°C. From Figure 5.9a, it is seen that the bredigite powder before sintering has a small size and it isn't agglomerated. As can be seen in Fig. 5.9b, the powder milled for 10 h was made up of comparatively distributed uniform particles, which had an average particle size of about 1 μm i.e. after subsequent annealing at 1300°C for 4 h. Moreover, the image also showed that some of smaller particles were welded together during the sintering process, forming larger particles, which were addressed by a high sintering temperature (annealing). Following this, it can be seen that some of the bredigite

particles have been cold welded together; those white particles may be recognized as $CaCO_3$ as indicated by the EDX result in 5.34. Also, a clear deep boundaries with several pores are shown in Figure 5.9.

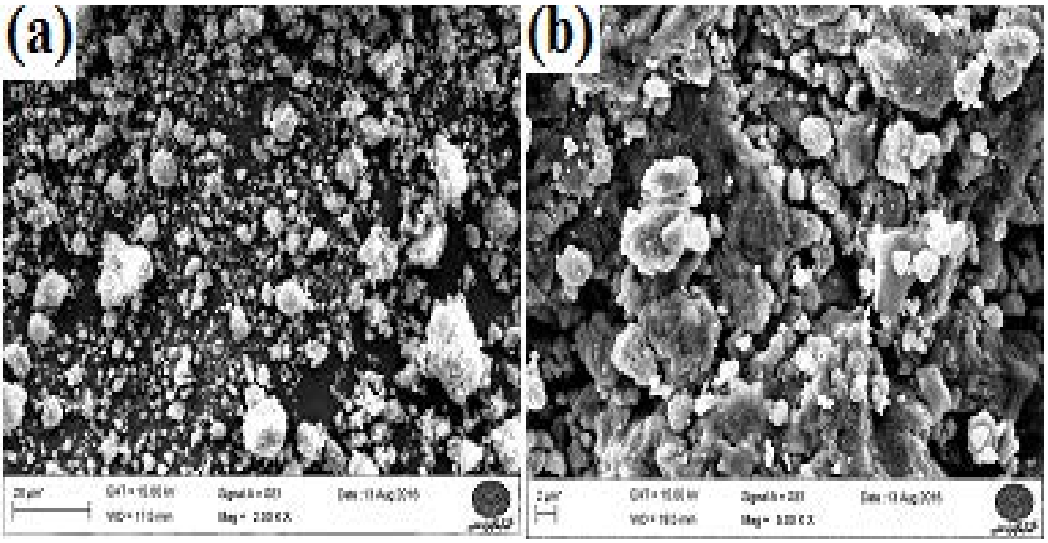

Figure 5.9: SEM images of 10 h milled powders a) before and b) after sintering for 4 h at 1300°C.

As seen in the Fig. 5.9, the particle size obtained from the milling process was within the range of 20–50 (nm); however, a strong adhesion between the particles exists.

5.1.3.2 Ceramography Evaluation of Magnetite Nanoparticles

The magnetite powders were created using the sol-gel technique. This event leads to a higher surface activation of the particles as well as small particle size as seen in Figure 5.10. As the powder is sintered for 3 h at 1200°C, there is a meaningful trend between the agglomeration events of the Fe_3O_4 particles, as shown in Figure 5.10. The particles fuse together and create agglomerated particles that have larger size and irregular shape.

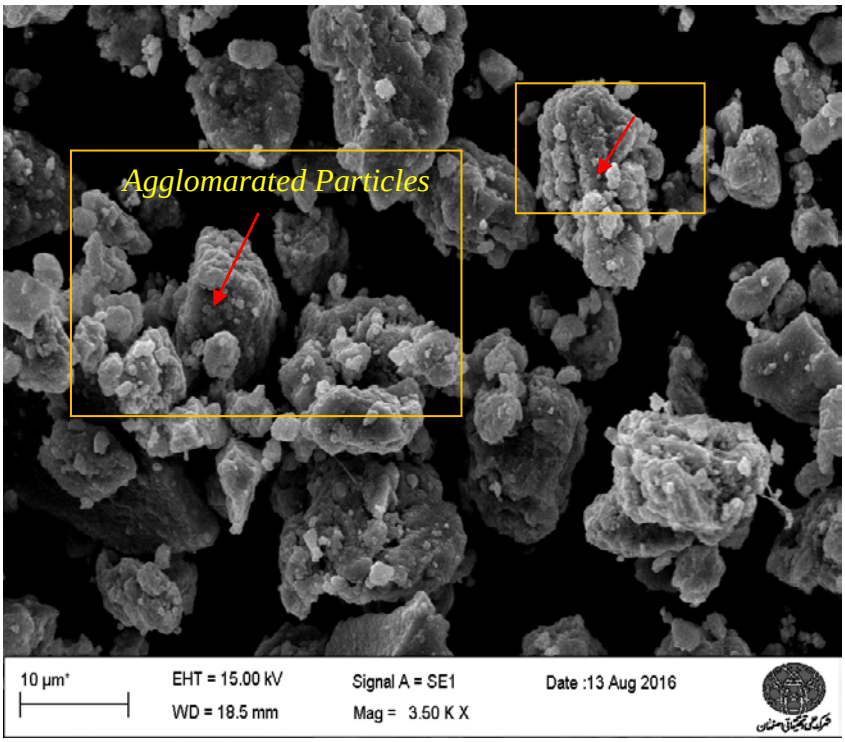

Figure 5.10: Micrograph of magnetite powder synthesized by sol-gel method

5.1.3.3 Morphology of Bredigite-Magnetite Scaffold Nanocomposites

The morphology of the nanocomposite powder is shown in Figure 5.11. The calcinations of the novel bredigite-magnetite scaffold nanocomposite powder was fixed at 650°C for 2 h. Therefore, it can be concluded that the phase of CaO, recognized after the calculations, corresponds to the dissolution of calcium nitrate which thrived within the MNPs gel. In figure 5.11 (a-d), a regular arrangement of MNPs and bredigite particles in the nanocomposite powder was approved. The SEM of nanocomposite showed that additive elements (MNPs) and matrix, have a uniform homogenous dispersion with each other; this is as a result of the similar crystallinity and crystalline size as mentioned in the previous sections. Moreover, the bredigite contains Mg and Si ions within its own structure, and so the main bright particles are usually recognized as the Mg and Si ions based on the EDX results. In conclusion, the range of bioactivity and compressive strength as regards to the initial chemical element and arrangement of the particles in the nanocomposite for the degradation

and chemical stability of the product materials, was explained. Kokubo et al. [198] proposed that the dissolving Si particles with Si-OH, have a significant role to play in the mechanism of the nucleation in the cauliflower and surface of the biomaterial's bio-layer [198]. The sintered Br-MNP nanocomposites showed a proper dense particle due to its pure and fine nanoparticles, which demonstrated nanoscale dimension. A proper nanocomposite should not have any segregation between the nanoparticles. A uniform distribution of the particles means that matrix can tolerate any deterioration or loading, leading to better mechanical properties as shown in Figure 5.11 (c-d). SEM images in Figure 5.11 represent the surface (a) 0 wt.%; (b) 10 wt.%; (c) 20 wt.%; and (d) 30 wt.% Fe_3O_4-bredigite scaffold nanocomposite particles. From Figure 5.11 (a-b), as the MNPs content increases, the nanocomposite containing higher amount of MNPs agglomeration also increases. Despite the combination of the MNPs and Br, which could lead to low sintering density and regular (uniform) phase distribution in the nanocomposite; this is due to presence of a large particle in the matrix.

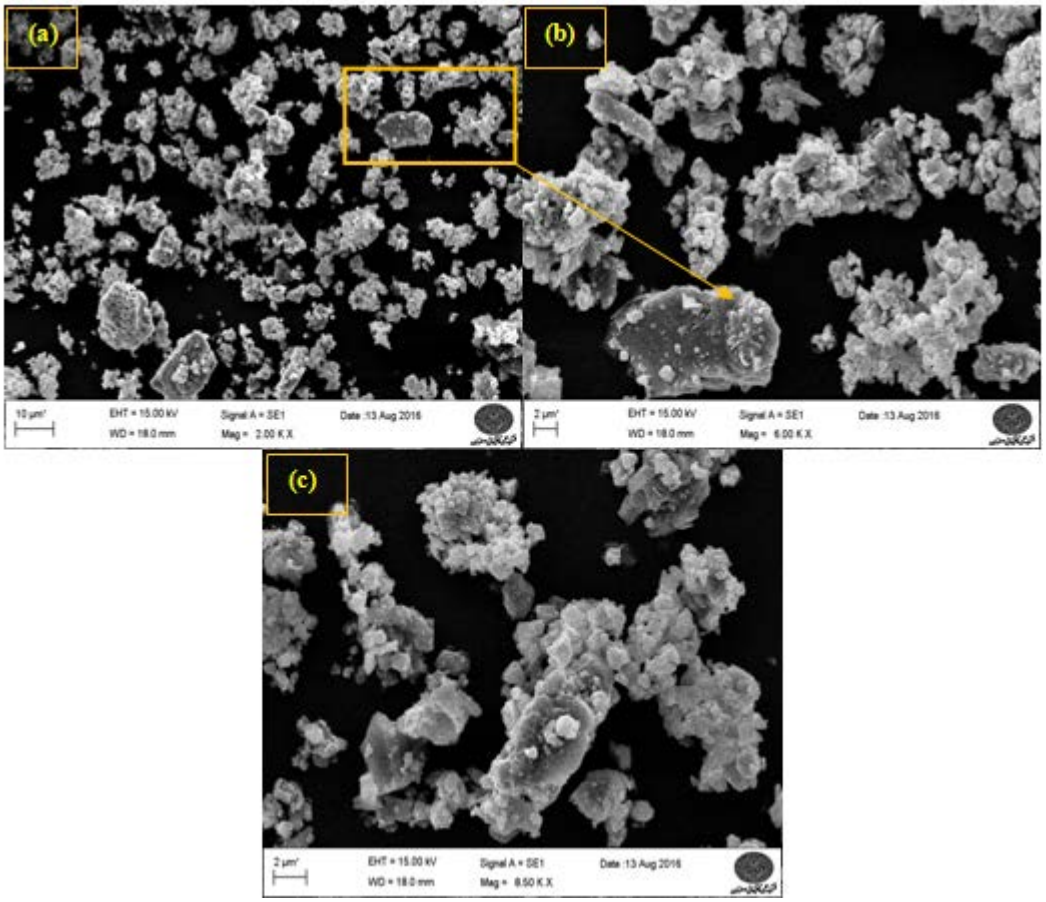

Figure 5.11: SEM images of nanocomposite containing various amount of MNPs.%, a, b) 20 wt.%, and c) 30% wt. after sintering at 650°C for 2 h

5.1.4 FTIR Analysis

5.1.4.1 Functional Groups Evaluation of Bredigite

The FT-IR study was conducted to know the functional groups of bredigite and bredigite-30 wt.% MNPs powder. The FTIR spectrum drawn in the 400–2000 cm^{-1} region had a resolution of 4 cm^{-1}. The FTIR results for bredigite powder (10 h milled, 4 h sintered at 1300°C), was highlighted in fig. 5.12a. In this graph, the band of absorption (475 cm^{-1}) could be ascribed to the occupation of Mg—O band. In addition, some peaks in Si—O bands within the SiO_4 tetrahedron was revealed, leading to a generation of bredigite powder; this is due to the XRD pattern that is represented by the specimen. The following bands corresponds to the bredigite bands; domain with the similar peaks like 770 cm^{-1} for SiO_4 stretching, 620 shows

for SiO_4 bending, and finally, 553 cm^{-1} recognized for Ca—O stretching as shown in Figure 5.12(a). As Figure as illustrated in 5.12(b), the 30 wt.% of MNPs inserted into the bredigite matrix, resulted in two small peaks i.e. about 790 and 1470cm^{-1} for the Fe—O band.

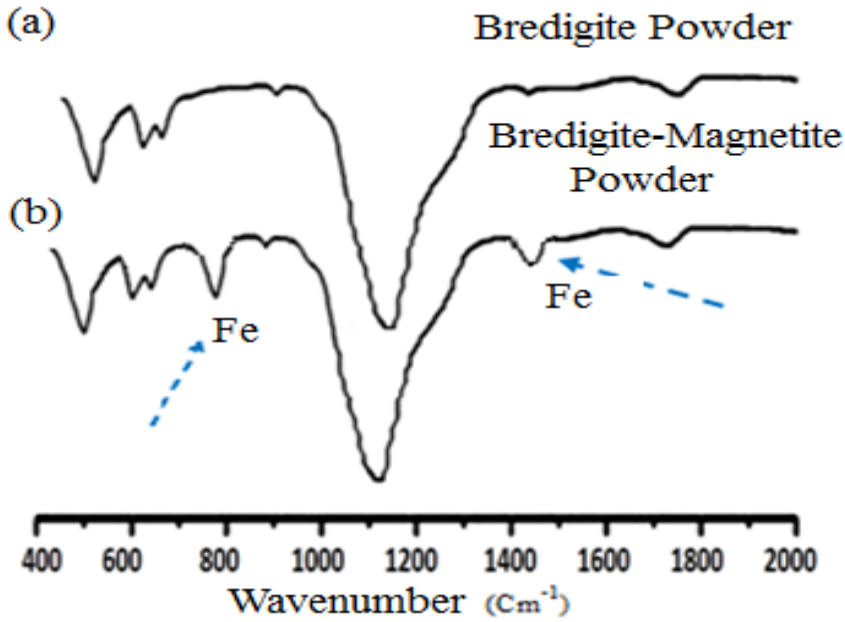

Figure 5.12: FT-IR spectroscopy of (a) Br nanopowder compared with (b) Br-30 wt.% MNPs

Figure 5.12(b) indicates a peak of 776 cm^{-1} as well as a characteristic peak for the Fe—O stretching band. The Fe—O peaks were sharp and happened within the range of 1000–1600 cm^{-1} (i.e. in FTIR spectroscopy). The FTIR represented in Fig. 5.12(b), indicates that the sample containing 30 wt.% MNPs, the functional group of Fe—O, diffused and created a rift in the FTIR.

5.1.4.2 Functional Groups Evaluation of Akermanite

The FTIR result of the milled akermanite powders at 900°C for 6 h is shown in Fig. 5.13. FTIR analysis of akermanite specimen acquired at 900°C, revealed that the O—Ca—O bending modes at 411 cm^{-1} and 473 cm^{-1} for the O—Mg—O bending modes. The Ca=O group has a peak value of 589 cm^{-1}, while the O-Si-O peaks value

occurred within the range of 641 cm^{-1} and 680 cm^{-1}. The peaks at 848 cm^{-1}, 932 cm^{-1} and 981 cm^{-1}, illustrate the importance of the Si—O stretching modes. Symmetric stretching at 1021 cm^{-1} was assigned to a Si—O—Si vibration.

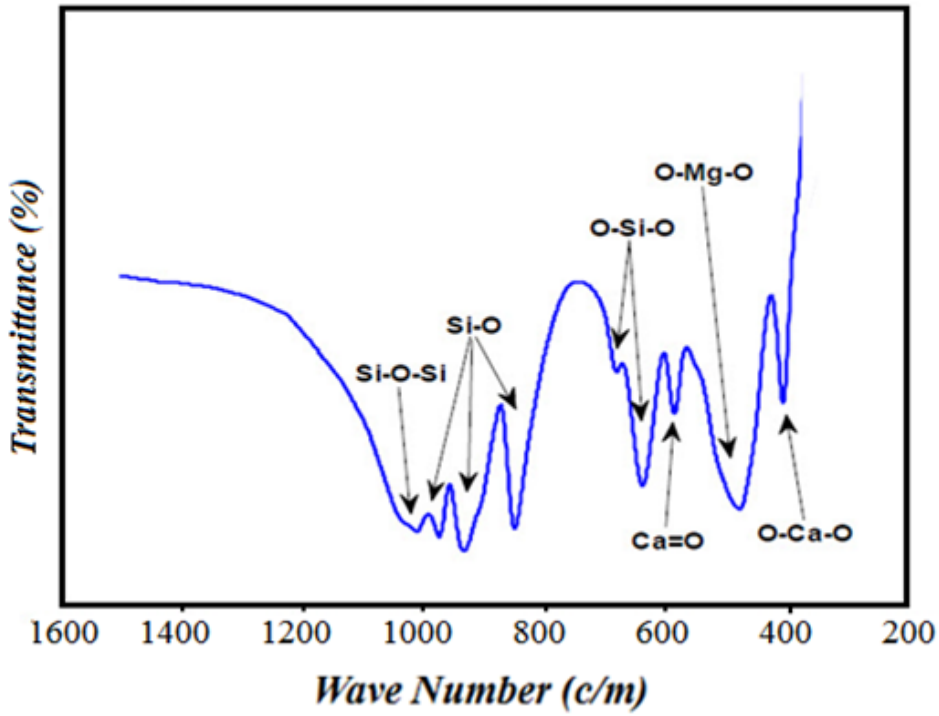

Figure 5.13: FTIR analysis of the milled akermanite.

5.1.5 Thermal Analysis

The DSC and TGA graph analysis of the bredigite powder are presented in Fig. 5.14. Figure 5.14 shows the weight loss of the samples at various temperatures ranging from 500-1000°C. The peaks in the TGA and DSC can be attributed to the desorption of the adsorbed water; meanwhile, more weight loss was observed in the range of 800°C to 900°C. The weight loss is as a result of the loss of water in the lattice structure. The initial endothermic summit occurs at 540°C ; this is associated with the nitrate extraction from magnesium nitrate. While the second endothermic summit was recorded at 650°C, which was related to the elimination of nitrate from calcium nitrate. The exothermic summit peaks at 800°C, which corresponds to the

generation of the bredigite powders. Furthermore, secondary weight loss after the dissolution of the calcium nitrate in the TGA diagram has been observed. However, most of the weight loss were higher than 90% of the precursor powder; this takes place prior to the synthesis of the bredigite powder due to the extraction of nitrate from magnesium nitrate.

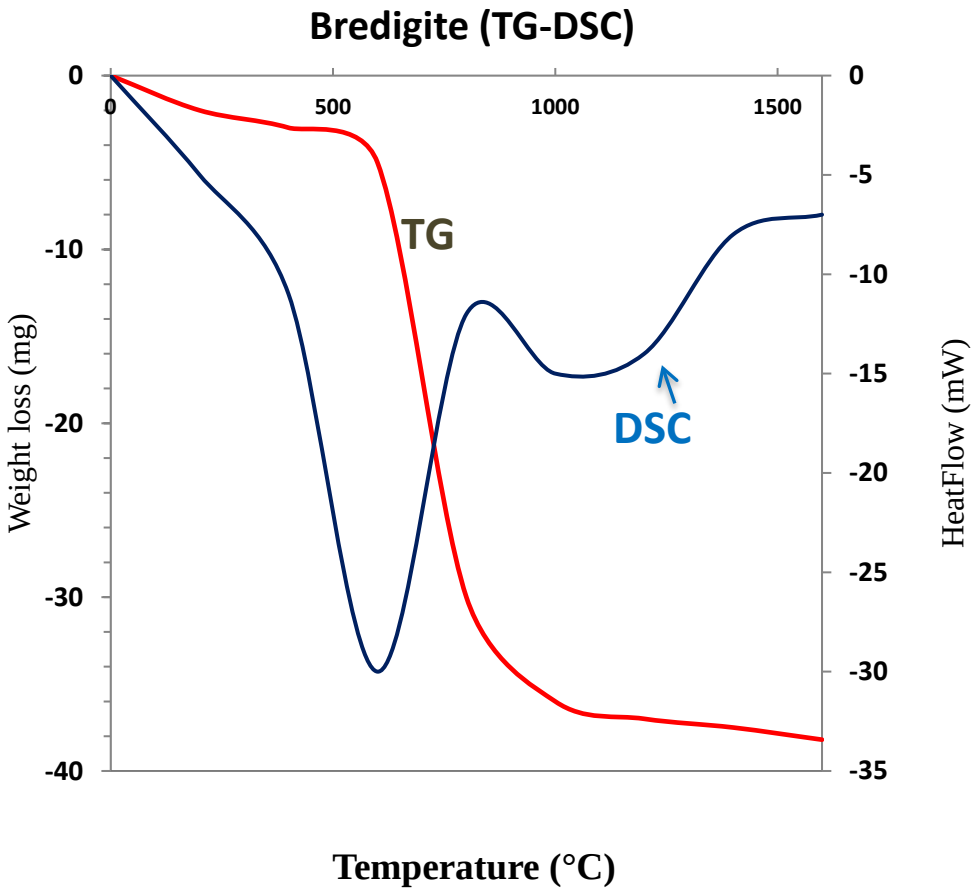

Figure 5.14: DSC and TGA diagrams of the milled bredigite powders

5.2 Mechanical Testing

5.2.1 Fracture Toughness and Bending Strength Evaluation

According to current ongoing research, bredigite-magnetite nanocomposites has a value of bending strength (148 MPa), fracture toughness (2.69 MPa $m^{1/2}$) and Young's modulus (29 GPa) i.e. for a sample containing 30 wt.% MNPs (see Figure

5.15). However, other studies indicate that value of bending strength, fracture toughness and Young's modulus of pure CaPs, is within the range of 115–200 MPa, 0.6–1.0 MPa $m^{1/2}$ and 80–120 GPa, respectively [192, 265]. As a matter of fact, earlier studies have revealed that the diopside powder have proper biological property, superior bending strength and fracture toughness [37, 249]. The modulus of the bredigite has been proven to have a lower value; as a result, an improvement in the bioactivity of the scaffold tissue (for degradation of particles) was depicted in section 5.4.3, where a comparison with the CaPs bioceramics was made. The bending strength and modulus values of the bredigite bioceramics are likened to the human bone cortical as represented in other studies; for instance, the bending strength and modulus were reported to be 50–150 MPa and 7–30 GPa, respectively [265-266]. Furthermore, a CaO—SiO_2-based bond is capable of increasing the toughness and strength of the silicate ceramics like the bredigite and diopside powder. The strong bonding between O—Si—O, causes the bredigite and diopside bioceramics in their macroscopic structure to have higher strength (the SiO_2 amount in diopside and bredigite 4.61 is about 5 wt.%). Figure 5.15 shows that as the MNPs amount increases from 0 to 30 wt.%, the bending strength also doubles proportionally, which is as a result of the presence of amorphous MNPs in the nanocomposites structures.

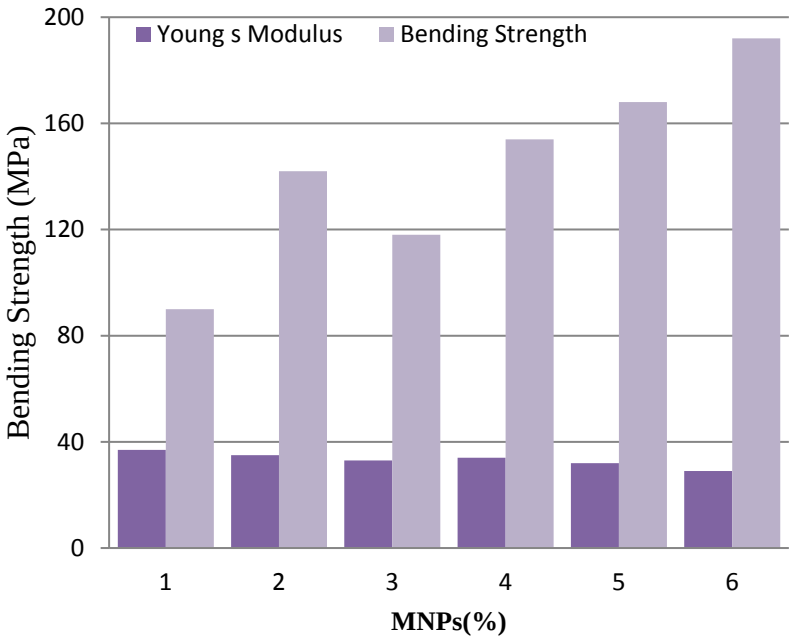

Figure 5.15: Bending strength and Young Modulus in sample containing various amounts of MNPs as additives.

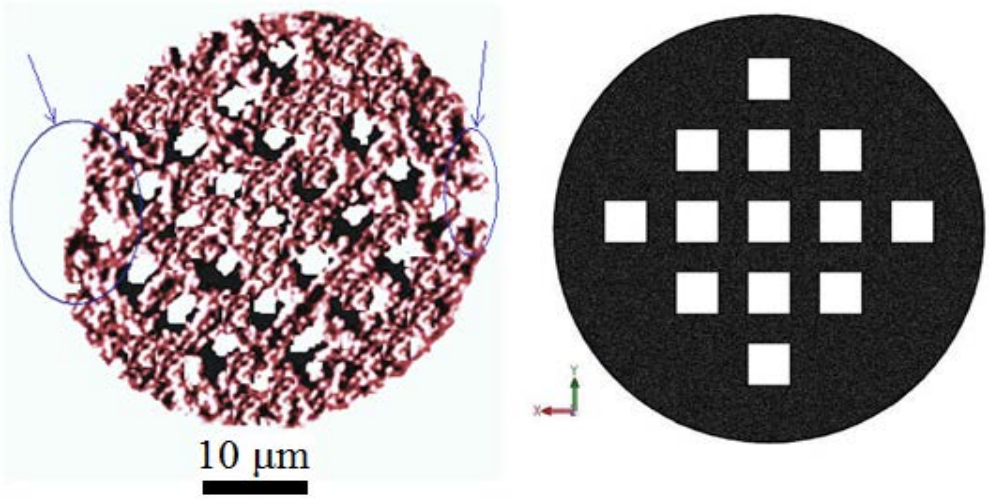

Figure 5.16: Schematic of images for 3DP nanocomposite containing 30 wt.% MNPs

Moreover, the magnification picture of the scaffold 3DP nanocomposite shows egg-shaped elliptical grains having 10 µm as their mean size, which begins necking after a compressive stress from the edge of the specimen is applied. By observation, it can be seen that the grain and boundaries of the specimens started developing as the sintering temperature changed to a higher temperature. However, the porous

microstructures of nanocomposite remained stable geometrically, this is attested by the glassy bonds (Si—O—Si) and high fracture toughness value of the specimen, containing 30 wt.% MNPs. Therefore, the mentioned properties means that silicate bioceramics materials can be used as implantable bioceramics for hard tissue engineering application; this is due their higher strength and density i.e. when compared to pure CaPs ceramics. However, despite the advantages of CaPs, their surface deteriorates and in some cases, distributes/separates. Consequently, bioactive additives can be employed to improve their structures. Additives like ZrO_2 [6-7], Al_2O_3 [267], Fe_3O_4 [303], and TiO_2 [16] are used to improve the CaPs and calcium-silicate bioceramics characteristics; such characteristics include its chemical stability, compressive strength, fracture toughness and bending strength. Furthermore, several works have been done to investigate the effect of the additives on bioceramics; examples of such bioceramics are zirconia, Iron, Silica, Ferrite, iron/silica [268], ZrO_2—Al_2O_3 [269], and PVA [270]. These have various applications like dental implant coatings, bone tissue engineering, bone filler, and artificial biomedical device. From the investigation carried out, the fracture toughness of CaPs ceramics doesn't exceed the value of ~1.0 MPa $m^{1/2}$, while the fracture toughness of human cortical bone was shown to be between 2–12 MPa $m^{1/2}$. Approximately, the fracture toughness declines linearly with respect to the increasing porosity value [37, 38]. It should be noted that fracture toughness is a factor of the grain size modification (normally reduced). However, in some substances, mainly non-cubic ceramics, the fracture toughness approaches its maximum value and then quickly reduces when the grain size decreases. In addition, for those non-cubic ceramic materials, the fracture toughness attains its highest value.

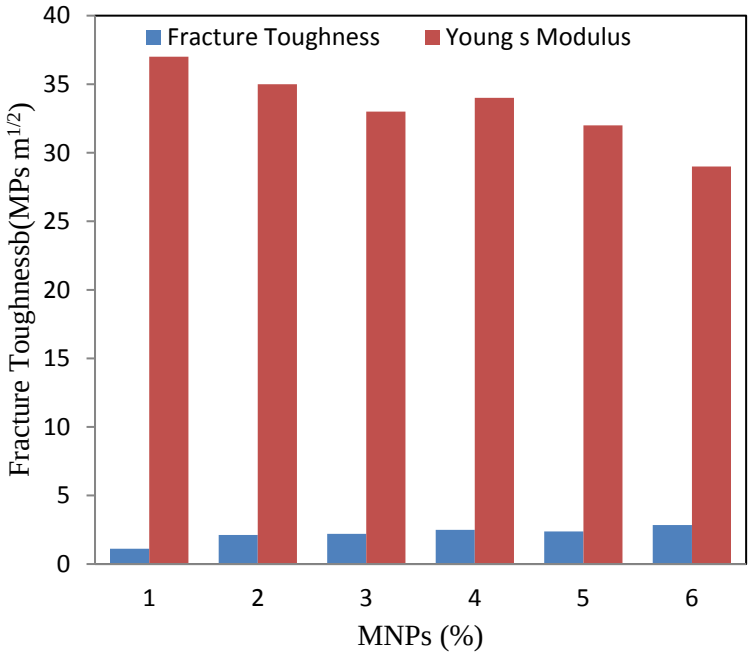

Figure 5.17: Fracture Toughness vs. Young Modulus of the sample containing various amounts of MNPs in nanocomposite.

In this study, the fracture toughness increased proportionally with respect to an increasing MNPs percentage as seen in Figure 5.17. However, it is important to note that crystallite size and structure of crystals play a major role in influencing the fracture toughness, as clearly seen in this thesis (see section 5.2.1.). Halouani et al. [55] studied the fracture toughness of HA sample (with 0.2 and 1.2 μm as its grain sizes) that had been hot-pressed. From their results, two different trends occurred; the fracture toughness increased in proportion to a reducing grain size sample (more than about 0.4 μm); consequently, the reverse was the case for a reducing grain size. Therefore, the highest fracture toughness estimated was 1.20 ± 0.05 MPa $m^{1/2}$ at 0.4 μm grain size. Additionally, in the recent studies, researchers have indicated that the fracture toughness of diopside scaffold, prepared with sol-gel technique, was about 4 ± 0.3 MPa $m^{1/2}$ [37].

Table 5.4: Comparison of the relative density, bending strength, and fracture toughness and Young's modulus of the current work with other work [271]

Powder Name	Compressive Strength (MPa)	Relative Density (%)	Bending Strength (MPa)	Fracture Toughness (MPa $m^{1/2}$)	Sintering (°C)	Young's Modulus (GPa)	Researcher
Bredigite	--	94.2±1.2	156±6	1.57±0.12	1350° C for 8h	43.00±4.53	Wu et al. [271]
Current study	2.4-2.8	--	148±3	2.69 ±0.2	1300° C for 4h	29±3.2	--

Wu et al. [271] research showed that the calcium magnesium silicate have a bending strength, fracture toughness and Young's modulus of about 156 MPa, 1.57 MPa $m^{1/2}$ and 43 GPa, respectively (see Table 5.4). Variations in the density of the structures is the reason behind the major differences in mechanical and chemical stability. Also, in another study, an investigation carried out on akermanite ceramic showed that the fracture toughness and bending strength were significantly weaker, when compared to bredigite as shown in Table 5.4 [37-38, 41]. In addition, it is clearly shown that the bending strength of such bioceramic was close to 350 ± 7 MPa; this is higher than the value that was reported for the HA ceramic (more than 3 times its value) [4-5, 37].

5.2.2 Compression Strength Evaluation

An evaluation of the major problems facing the manufacture of scaffolds for bone tissue application led to a second challenging issue, which is the scaffolds' compressive strength. It should be noted that it is absolutely essential that the ceramic scaffolds have an adequate compressive strength, when compared to the conventional human bone [41]. However, although the scaffolds have many beneficial properties like cell ingrowths and proliferation in their channels, their compression strength is significantly low due to an increase in the pore size of the structures.

In Figure 5.18, the compressive strength of scaffolds nanocomposite containing (0, 10, 20, and 30 wt.%) MNPs were measured within the range of 1.8-3.6 MPa.

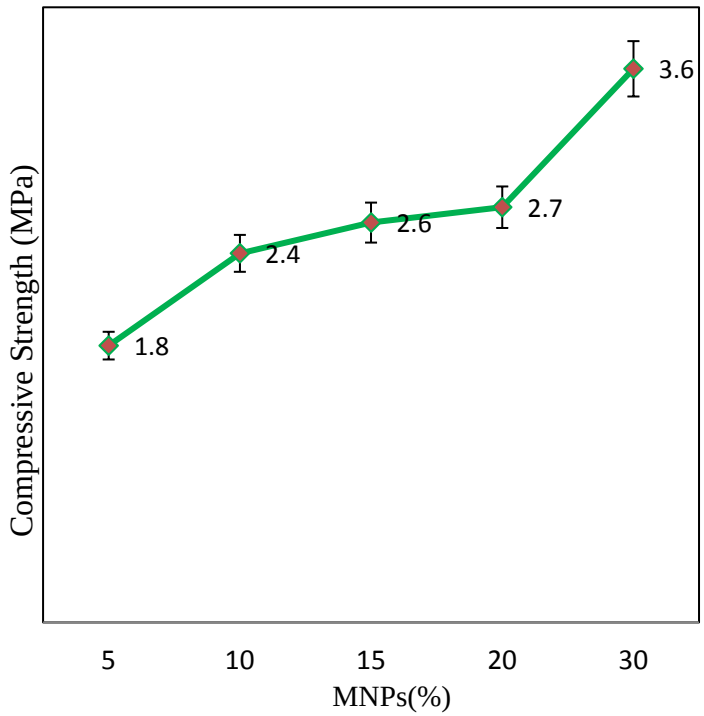

Figure 5.18: Compressive strength of the bredigite scaffold nanocomposite containing various amounts of MNPs bioceramics produced in this study

The compressive strength of the cancellous bone was recorded as 0.28–11.61 MPa as seen in the literatures [41]. From our research, our results yields values similar to that of earlier observation, which describes the hydroxyapatite scaffold compressive strength [196, 272-274]. For example, Roohani et al. [274] produced HA-β-TCP scaffolds with a value of 0.1±0.05 MPa and 91%, for compressive strength and porosity, respectively. These results arises from significant enhancement in sinterability and grain growth reduction, during the process of sintering at a certain time and temperature. The Hall-Petch formula can explain the correlation between compressive strength and size of particle grain in the metals and composites [275]. Based on the Hall–Petch equation, the compressive strength of the scaffolds

increased because the grain size of the nanomaterials reduced [276]. Shiota et al. [277] reported that the compressive strength of HA/β-TCP decreased due to the addition of β-TCP. In this study, we found out that the combination of MNPs with bredigite, increased the compressive strength of the scaffold nanocomposites. Therefore, according to the previous sections (5.2.1) both the fracture toughness and compressive strength of the nanocomposite developed in this research. In another study, Najafinezhad et al. [41] made a comparison of the biological and mechanical properties of three types of silicate bioceramics (i.e. diopside, akermanite and baghdadite). In other words, a comparison of the mechanism of bone apatite formation and the compressive strength of three silicate bioceramics. Based on the data acquired from the compressive strength test and the Najafinezhad et al. result, we found that the bredigite have a higher compressive strength compared to diopside and akermanite, however, when compared to a baghdadite sample, it has lower compressive strength in the bulk form. As shown in Figure 5.19, the maximum compressive strength was obtained by calcium-zirconium-silicate (baghdadite), while the minimum compressive strength was obtained by $Ca_2MgSi_2O_7$ (akermanite) [38, 41, and 278]. According to our investigation, the sample without MNPs recorded a compressive strength of 1.8 MPa, while sample containing 30 wt. % MNPs, recorded a compressive strength of 3.6 MPa. The results confirmed that after 40 (s) of force was loaded on the specimen with high amount of MNPs, the sample was completely destroyed; on the other hand, when the sample was loaded for 15 second, the MNPs failed to collapse. It should be noted that the MNPs, due to their high modulus, have a glassy structure which increases the strength of the bredigite particles in the nanocomposite. The compression strength test showed that all the samples were destroyed, confirming that the linear elastic zone resulted from a collapse of the

plateau, which was presumably dominated by an inelastic fracture (brittle). The results showed that the clusters of small MNPs and the sintering process were mutual; this created larger particles that could be ascribed to heating the synthesized bredigite, resulting in a proper reinforcement.

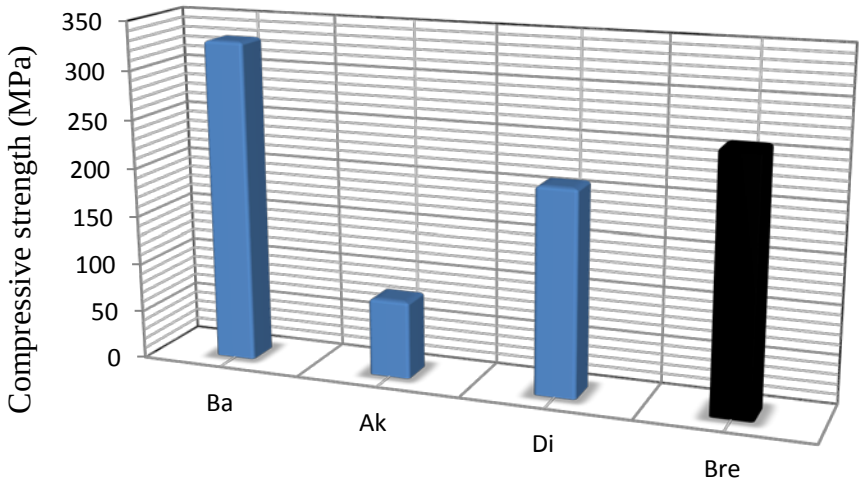

Figure 5.19: Compressive strength comparison of the bulk baghdadite (Ba), diopside (Di), akermanite (Ak), and bredigite (Bre).

The additive materials plays an important role in influencing the microstructure mechanism of the scaffold. It is during the process of reinforcement that the extension of these elements will lead to an improvement in the mechanical properties (e.g. fracture toughness and compressive strength) of silicate bioceramics such as adding HA to bredigite powder [247]. It has been advised that introducing trace elements like Mg, Cu, and Zn into the bioceramics, will help in controlling the calcium molecules in its microstructure. Also, it can restrain the structure, leading to a proper stabilized architecture. Moreover, as an example, the X-O bond (where X = Mg^{2+}, Zn^{2+}) have greater energy than the Ca-O bond. Furthermore, these bonding will help in building a stable structure [41].

5.3 Electrical and Magnetic Behavior Evaluation

5.3.1 Electrical-Relevant Properties Evaluation

The electrical conductivity (EC) of Br-MNPs scaffolds nanocomposite increased dramatically in the sample containing 10 wt.% MNPs. The second law of Nernst's defines a relationship between the voltage and ion flux across the membrane of that cell. Moreover, an electric field can be formed in a polarized tissue, which can influence the voltage and ion flux of the adjacent cells and tissue. It is assumed that any conductive scaffold materials used for bone healing approach in the *in vivo* trials by applying electrical or magnetic inducements, will result in changes in the viability and response of the cell [279-281].

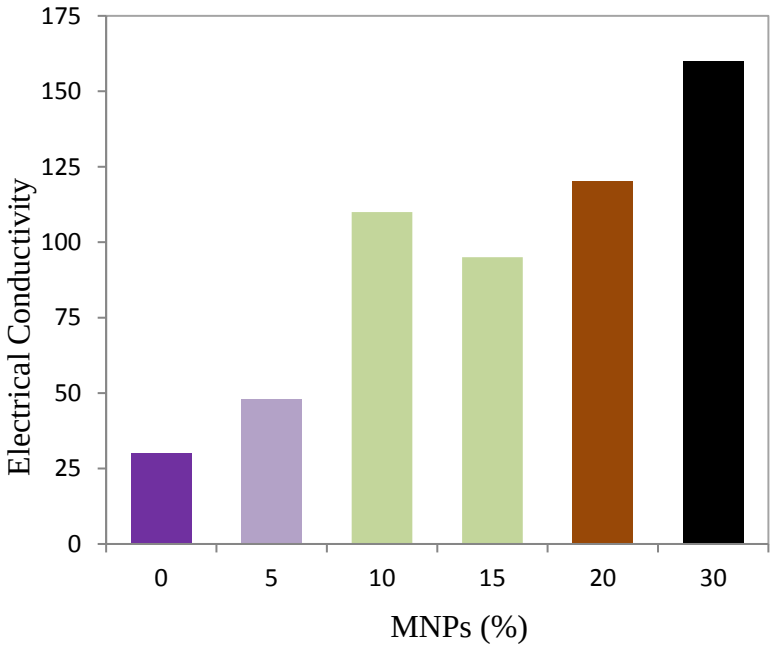

Figure 5.20: The electrical conductivity (EC) of Br-MNPs scaffolds nanocomposite with various amount of magnetite powder.

It is seen in Figure 5.20 that the higher EC (160 µS/m) belongs to the sample with higher percentage of MNPs, while the sample without the MNPs powder have the lowest measured ECs (35 µS/m). This shows that the sample with 30 wt. % MNPs,

can attract more electrical signals than the sample without MNPs. Because of the anion loss, the presence of mixed valence states of Fe^{2+}/Fe^{3+} within the 3D metal ions in magnetite (Fe_3O_4) exists; as a result, this gives rise to a magnetite with proper electrical and magnetic materials features. It is well-known that the combination of materials at the nano-scale, gives rise to improved characteristics such as a larger surface area, better chemical reactivity, sinterability, electrical and magnetic behavior [282]. The SEM images analysis of nanocomposite (see section 5.1.3.3 morphology of nanocomposites (Br-MNPs)) illustrated that an increase in a single region of the Fe_3O_4 nanopowders, leads to change in magnetic moment and consequently, larger particles accumulation. Those agglomerated single domain magnetite, practice dipole-dipole cooperation and they have magnetic internal energy, which may be converted into heat. The heat released helps cultivate an advanced stage for small agglomerates to attach to each other as well as create large agglomerated particles.

5.3.2 Hyperthermia-Relevant Bredigite-Magnetite Scaffold Nanocomposites

The calculated value of the lattice constant (LC) for magnetite was about 8.680 Å. Taking into consideration the Full Width at Half Maximum (FWHM) of the (110) plane of the Fe_3O_4 diffraction pattern at $2\theta = 35.5°$, the range of the crystallite size was measured to be 40-50 (nm) i.e. using Scherer's equation [17] (Fig. 5.21c). This value matches the results of the SEM (see Fig. 5.21a). The magnetization (Ms) value was 90 emu/g, which means it is close to almost half of the value for the bulk 160 emu/g, that is owing to the small size of the powders and moderate crystallinity. The Specific Absorption Rate (SAR) value enhanced to the extent that no hysteresis was observed as discussed in section (1.4.5); therefore, it can be concluded that no super paramagnetic properties will be found. As the MNPs amount increased, the

crystallinity also increased; this lead to a higher 2 Θ angle, causing the porosity to also increase. The magnetic hysteresis loop of Fe_3O_4 powder i.e. after 10 h of milling, is shown in Fig. 5.21d. It can be seen that the hard-magnetic properties of the powder mixture are very low as a result of the lack of the hard-magnetic phase. The hysteresis loop of the 10 h milled powders after undergoing 3 h of sintering at 1200°C, is also visible in Fig. 5.21d. The loop illustrates a soft magnetic natural formation, and low amount of hard magnetic phase (See XRD analysis in the inset of Fig. 5.21b-c). The graph in Fig. 5.21b illustrates the heat that is released by those soaked powders in the ferrofluid (here we used ethanol liquid for hyperthermia evaluation) i.e. within adiabatic conditions (Δt=10 adiabatic time about less than 10 (s)).

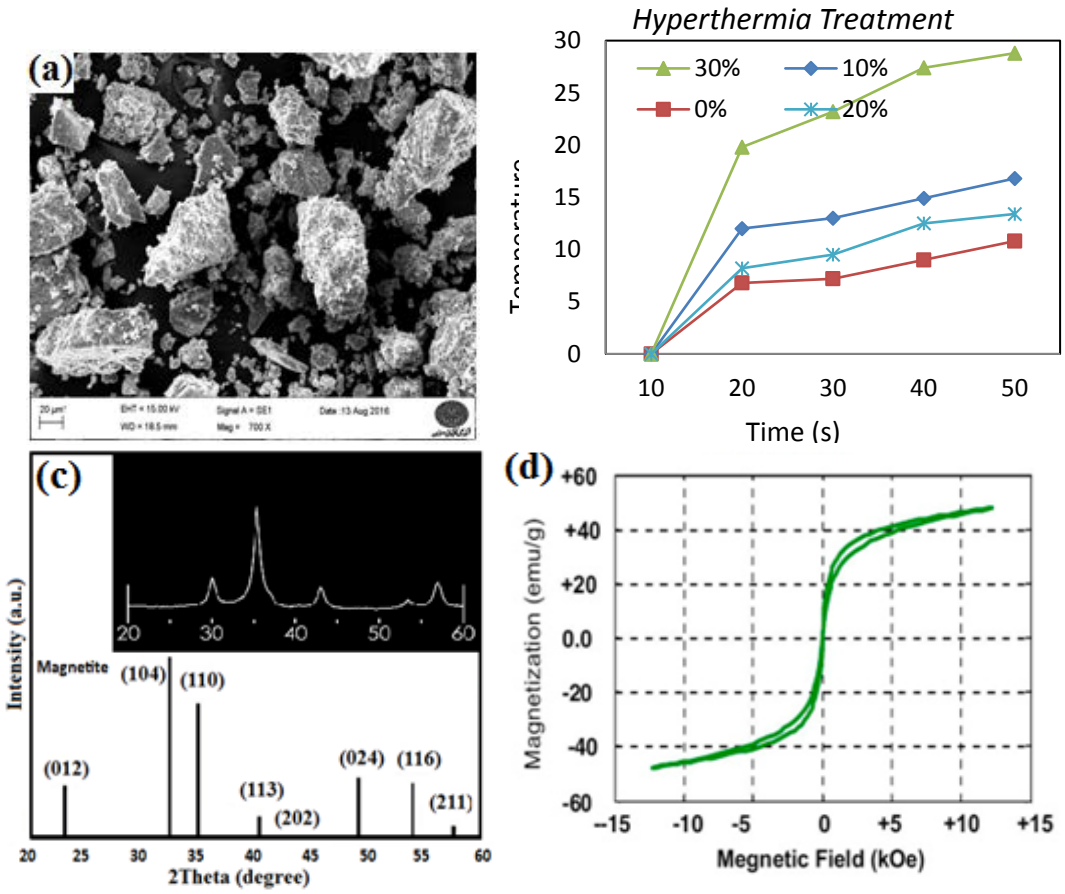

Figure 5.21: (a) SEM image; (b) Hyperthermia evaluation Temperature vs. time (c) XRD pattern; and (d) magnetization of the magnetite in the magnetic field

Higher Ms value gives rise to higher SAR value; this is shown in Figure 5.21b. Moreover, the increase in heat vs. time in the magnetic field was also observed in Fig 5. 21b. The sample with a 30 wt.% MNPs, exhibited a temperature increase of about 25°C within 60 seconds; also, within the same condition, the temperature increased to about 15°C i.e. for the sample containing 10 wt.% MNPs. As highlighted in Figure 5.2, a much higher hyperthermia effect was confirmed within the sample that had the highest amount of Fe_3O_4. An effective hyperthermia treatment contributes to a rise in the perfusion within the tumor tissue; this leads to an increase in the concentration of oxygen at the localized region, resulting in an optimal condition for the higher energy radiation (γ) to thrive, which in effect, damages the cells [303]. The diameters of hydrodynamic for bredigite-magnetite nanocomposite powder with 0, 10, 20, and 30 wt.% MNPs were measured 0.58, 0.41, 0.35, and 0.28 μm, respectively. The outcomes showed that the incorporation of MNPs will slightly affect the nanoparticles size, resulting in an increase in the nanocomposites. However, composite particles can be directly implanted into the bone defects after the tumor bone is extracted. The magnetic behavior of all specimens was gotten by using a vibrating sample magnetometer (VSM); the results were reported in Fig. 5.21d. Furthermore, Bsoul et al. [283] reported a critical value of 460 nm for single a magnetic domain structure. This means that the initial high-energy milling of the precursors, helped the formation of single domain magnetic particles.

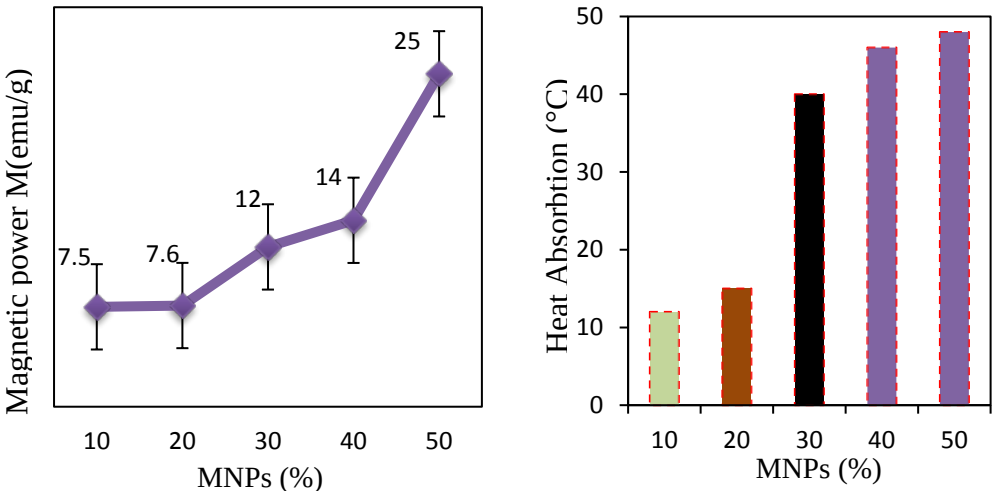

Figure 5.22: (a) Heat Absorption and (b) Magnetic power of scaffold nanocomposite in different amount of MNPs

Figure 5.22a, shows an increase in Ms with a proportional increase in MNPs, when the bredigite powder is added. A maximum value of Ms of 26 emu/g was measured from Br-MNPs 50 wt. %. Moreover, this was obvious in the sample having Br-30 wt. % MNPs surfaces have different magnetic properties, with all being ferromagnetic. Fig. 5.22 (a-b) shows that the sample with a higher amount of MNPs, has a higher heat absorption property. The temperature trends in the composite samples, when applied into an alternating magnetic (AC) field, were depicted in Fig. 5.22b. As the MNPs concentration increased, the temperature also increased in effect. Particularly, for samples with 30 wt.% MNPs, the temperature increased to more than 30°C over a period of 50 seconds. There are some concerns that the bredigite amount has an important effect on hyperthermia, although this focus was on the MNPs amount. Notwithstanding, our study revealed a great hyperthermia reaction, which was more useful than other published research for magnetite and CaPs materials [284]. Ansar et al. [284] manufactured Fe_3O_4-HA composite by using a simple technique. After the formation of Fe_3O_4 nanoparticles by co-precipitation, they applied heat at an initial temperature of 343 K and then, the increased the temperature to about 353 K for 1 h,

in order to analyse the HA powders. Moreover, annealing for 1 day at room temperature was required after the heating process was finalised. Therefore, it is clearly seen that our employed technique was simpler and more economical than theirs.

5.4 Biological Testing

5.4.1 Wettability and Roughness Evaluation

The surface hydrophilicity of the scaffold nanocomposite was investigated by measuring its wettability value when a drop of SBF on a scaffold nanocomposite surface was carried out as discussed in section (3.5.1). In our current work, we used an electron irradiation (low-energy) to obtain a tuneable contact angle for bredigite-magnetite scaffold nanocomposite. The results, as shown in the Figure 5.23, indicate that the sample with 30 wt. % MNPs have a contact angle ranging from 65° to 23°. As seen in the Fig. 5.23, by increasing the time of exposure of the scaffold nanocomposite (30 wt. % MNPs), the contact angle moves slowly towards a lower angle. In addition, Figure 5.24 showed that by adding more MNPs, an increase in the surface roughness of the scaffold nanocomposite occurred; subsequently, an upward trend was also observed (excluding the pure bredigite scaffold).

Figure 5.23: Wettability of scaffold nanocomposite containing various amounts of MNPs

Table 5.5 shows the connection between the roughness values and wettability value of the samples. The outcome of Table 5.5 shows that roughness values of the scaffold has an inverse relationship with the wettability data. For example, in the scaffold nanocomposite containing 30 wt.% MNPs, the roughness and wettability values were measured to be 33.23 (μm) and 23.3°. However, in the sample without MNPs, the values were 30 (μm) and 58.3°. And so, by adding glassy MNPs, a higher roughness value was achieved; In contrast, the wettability of the surface dropped. Additionally, the bredigite-magnetite scaffold nanocomposite was deposited with a bigger particle size on the surface of scaffold, which was related to the nanocomposite agglomeration and cluster particles. Due to the fact that the wettability values are below 90°, the nanocomposite can truly be called hydrophilic nanocomposite.

Table 5.5: Roughness and wettability value of scaffold nanocomposite fabricated by 3D printing method

	Roughness Value		**Wettability Value**	
Nanocomposite (MNPs %)	**Ra (μm)**	**Average (μm)**	**Θ°**	**Average (Θ°)**
0	25.2	30	65	58.3
0	28.3		50	
0	36.5		60	
10	18.5	22.8	55	55
10	24.5		60	
10	25.6		50	
20	29.5	26.7	45	46.6
20	24.1		50	
20	26.5		45	
30	31.4	33.23	30	23.3
30	35.6		20	
30	32.7		20	

The contact angle for a smooth or rough surface can be evaluated the surface between the SBF liquid and high summit of the sample (SBF drop and sample

surface) for intermolecular interactions. The value of the wettability can be defined higher than Θ>90° or less than Θ<90° which assumed as hydrophobic and hydrophilic tendency. Several surface properties like the chemistry of the surface materials, range of porosity, surface adhesion, surface charge and surface roughness may effect on the contact angle values predominately which leads to better wettability and bioactivity for hard tissues implants.

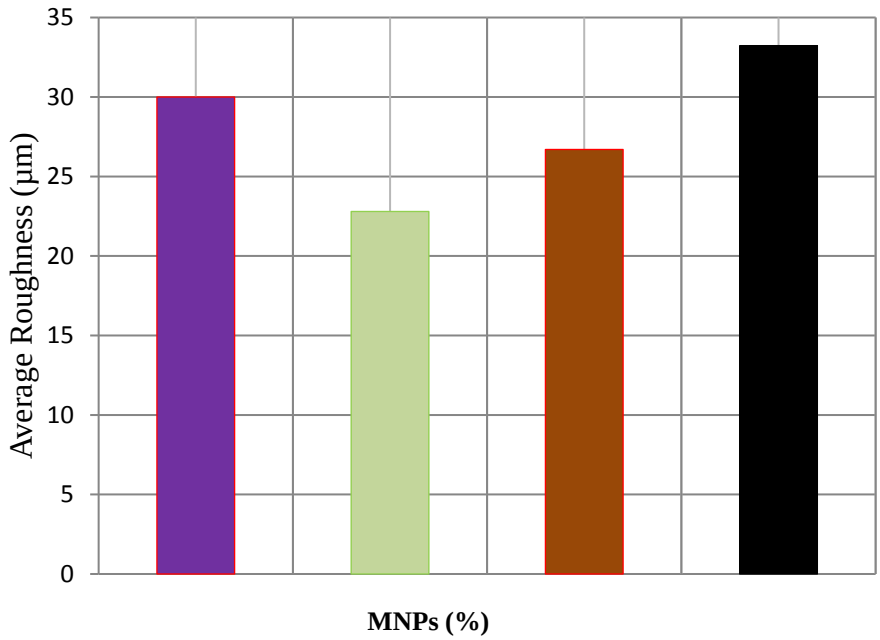

Figure 5.24: The average roughness of scaffold nanocomposite in different amount of MNPs

The results obtained from this work proved that the incorporation of different percentages of MNPs would lead to significant changes on the surface properties of the bredigite ceramic structures; also, it would lead to a decrease in the degradation rate, as represented in the following sections (5.4.3). In fact, it was shown that the addition of MNPs, will bring about an increase in the surface roughness as well as a decrease in the wettability, which would also lead to non-uniform struts.

5.4.2 Porosity Evaluation

As the sintering temperature increases from 1000°C to 1300°C, the total porosity of the particles decreases by 5% and 9%, respectively. The result of the porosity proved that some micro pores were present; this was most likely formed during the particles' sintering process. During the preparation of scaffold nanocomposite, the sintering temperature set at 650°C for 2 h (after 3D printing and after composite fabrication) affected the porosity of the scaffolds nanocomposite, (porosity changes from 75.9% to 58.2% in sample without MNPs and with 30 wt.% MNPs). In addition, the appearance density of the scaffolds nanocomposite increased with respect to an increase in the MNPs content. From Figure 5.25, high number of additives (MNPs) leads to lower value of porosity; moreover, it influences the apatite formation percentages. The maximum porosity value corresponds to the sample with 20%wt.

From Figure 5.26, the grain size and porosity have a mutual trend compared to each other. Moreover, some pure and ultrafine grains nanostructure of the bredigite powder (concluded from XRD result), will help in enhancing the porosity of the scaffolds nanocomposite. Two important parameters like; a) high energy and b) density will be possessed by the powder interfaces.

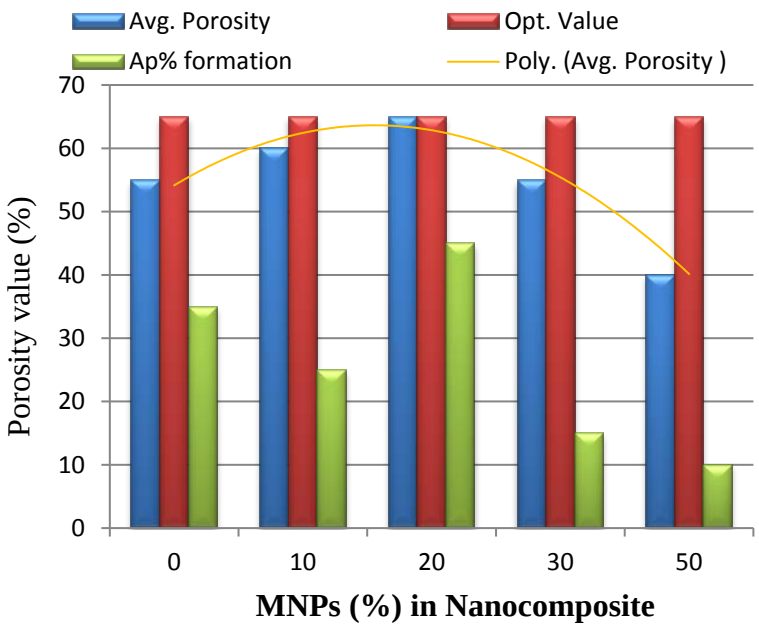

Figure 5.25: Porosity (optimum value and Avg.) and apatite formation of scaffold nanocomposite containing various amounts of MNPs in Br bioceramic

The data derived from the current thesis is in agreement with the outcome of other published papers like hydroxyapatite-bredigite scaffold composite, pure diopside scaffold, and hydroxyapatite-diopside scaffold composite [196, 249, and 286]. According to our results, samples containing 30 wt.% of MNPs in bredigite showed higher density, smaller grain size, more micro-pore and had the highest porosity values. Moreover, the strength decreases almost exponentially with the increasing porosity.

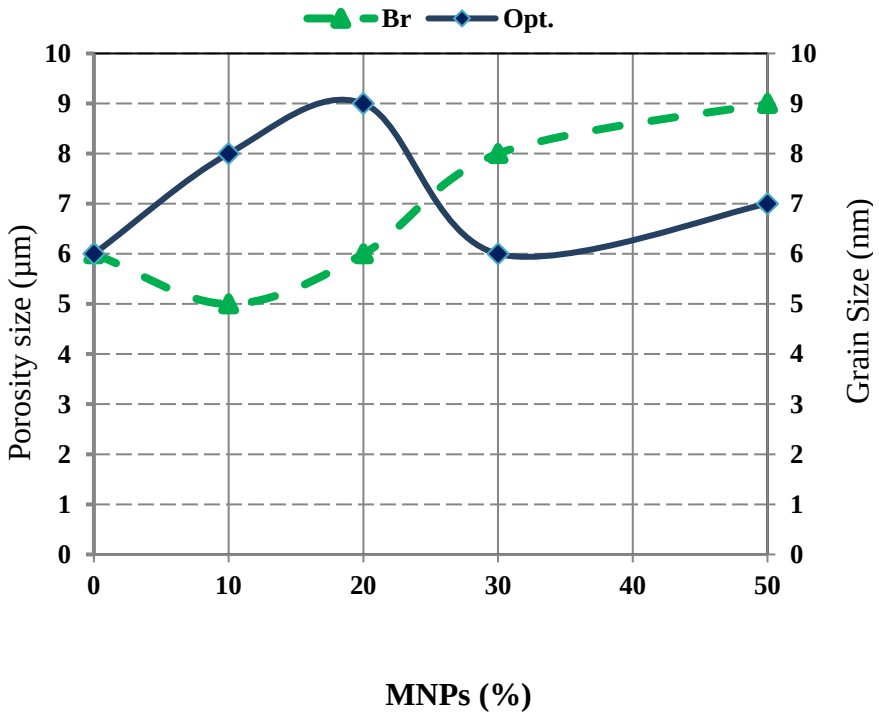

Figure 5.26: The average micropore size vs. the grain size of the scaffold nanocomposite

Figure 5.27 shows the image of the scaffold nanocomposite sample containing 10, 20, and 30 wt.% MNPs with different porosity and porous channel in their structure. As the MNPs amount increased, the nanocomposite structure and the porosity of the materials increased as proven by the SEM in Figure 5.27.

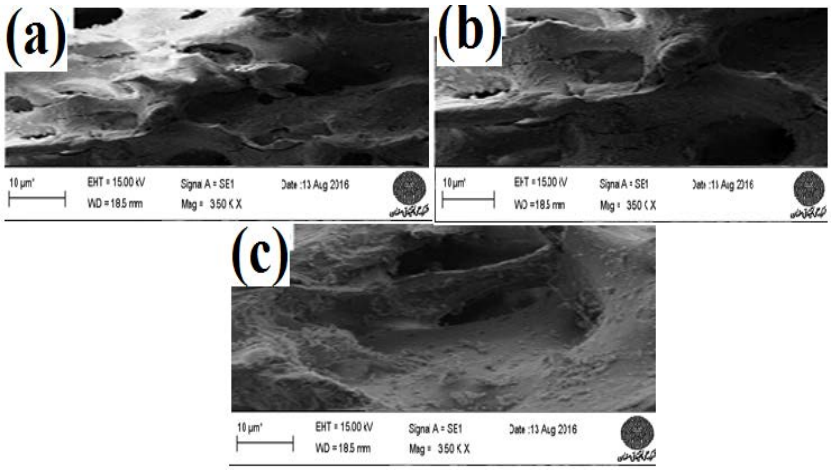

Figure 5.27: SEM images of bredigite-MNPs scaffold nanocomposite with a) 10 wt.% , b) 20 wt.% , and c) 30 wt.% after sintering process for 2 h at 650°C and before soaking in the SBF solution

5.4.3 Biodegradation Rate Evaluation of Scaffold Nanocomposite

Figure 5.28 shows the SEM micrograph of the scaffold nanocomposite containing various amount (0 wt.%, 10 wt.%, 20 wt.%, and 30 wt.%) of MNPs in Br bioceramics, which was submerged in the SBF solution for 4 weeks. The SEM micrographs showed the formation of shiny regions corresponding to the bone-like apatite (cauliflower or shiny agglomerated) on the surface of the scaffold nanocomposite as shown in Figure 5.28 (a-h). As the shiny region increased, the rate of apatite formation also increased. After soaking for 28 days, lath-like formation of apatite appeared on the channel and surface pores of the specimens. The crystalline particles on the surface of scaffold nanocomposite samples were tested with the EDX (Fig. 5.34) and the presence of apatite elements was found with sphere shapes, having sizes less than 20 nm as shown in Figure 5.34. Investigation carried out during subsequent soaking days, showed that the negative charge load on the samples' surface increased. The negative charge load leads to a Ca^{2+} ions in the SBF, which reaches interface and surface very fast. The interchange of Ca ion in solution can cause an increase in the pH dramatically as shown in Figure 5.29 (pH curve). The Ca^{2+} ions present in the SBF liquid is attracted to the layer that exist between the scaffolds surface and SBF liquid. Following this, the Ca^{2+} ions increases on either the calcium-rich or silica-rich film; the diminishing of P ions in the SBF solution is also driven by the Ca^{2+} ions. This leads to a complete precipitation of Ca^{2+} ions on the surfaces of the nanocomposite. This study shows that scaffold nanocomposite, containing bredigite powder possesses properly formed apatite in the SBF solution with the MNPs. Moreover, the contour variations of calcium, magnesium and other available trace element concentrates (e.g. Fe, P, and Na) and the silica-rich biolayer formation, have similar element to that of the CaO–

SiO_2-based bioactive ceramics like $CaSiO_3$ as shown in Figure 5.29. From the data acquired, the apatite mechanism of the scaffold nanocomposite is similar to that of the –SiO_2-based ceramics as shown in other research works like hydroxyapatite-bredigite scaffold and hydroxyapatite-diopside scaffold nanocomposites [196, 286]. In addition, bioactive ceramic tissue can grow strongly in pores and holes. The apatite formation on the pores area increases the chemical and strength stability of the produced scaffold nanocomposite [247, 287-288].

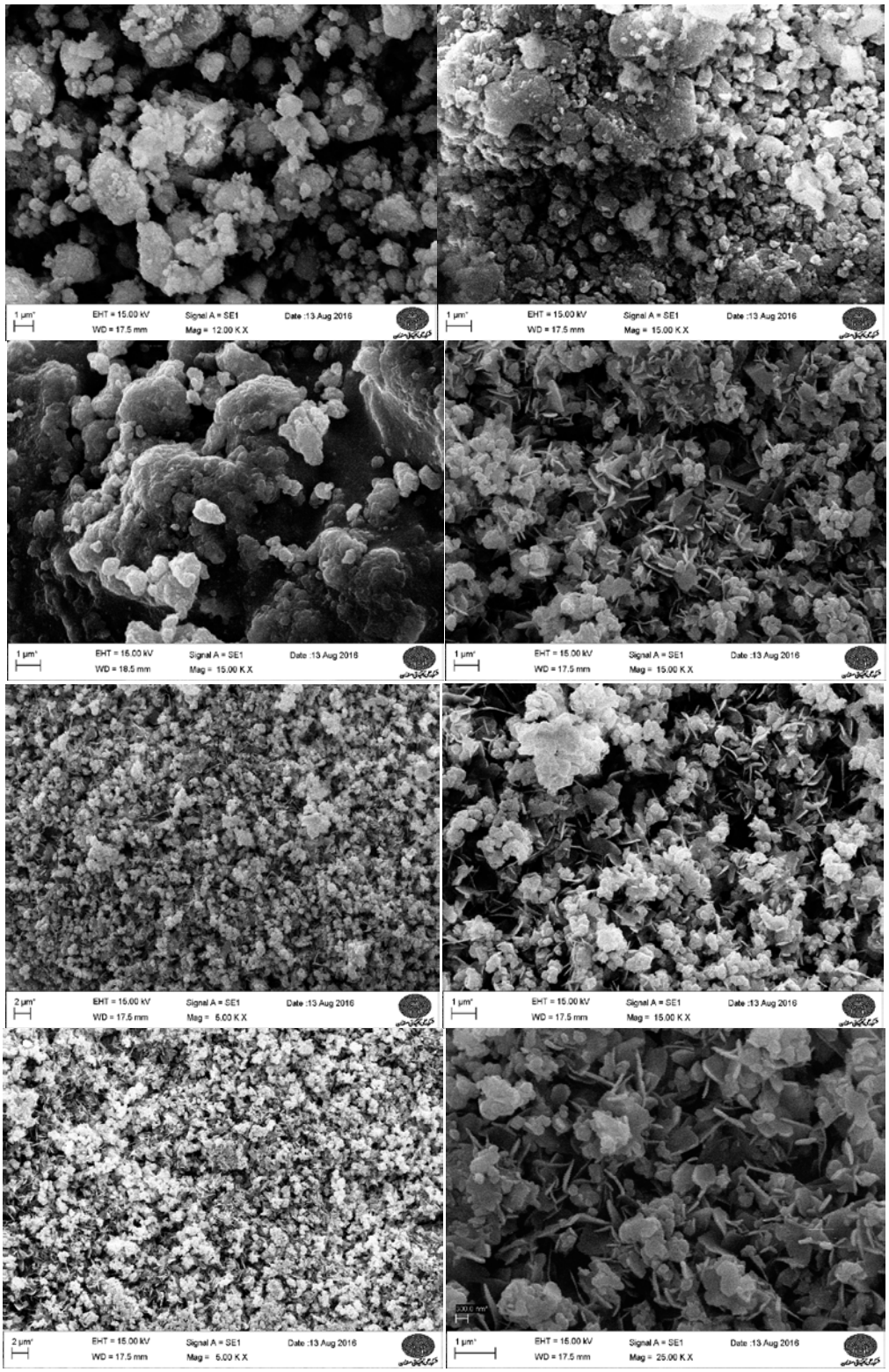

Figure 5.28: Micrograph of scaffolds nanocomposite containing (0, 10, 20, and 30 wt.% MNPs) before (a, c, e, g) and after (b, d, f, h) soaked in SBF for 28 days.

In bredigite-MNPs-30 wt.% scaffold nanocomposite, the plasticizing consequence of MNPs embedment of the glassy particles after sintering of the scaffold nanocomposite is shown in Figure 5.28. In addition, it should be noted that the particles had a well-defined orthogonal hole. From the SEM micrograph, the sample with 10 wt. % MNPs (see Fig 5.28 c-d) have a rocky and irregular surface, whereas the blend with 30 wt.% MNPs (see F ig. 5.28 g-h) have a smooth and flat surface with coarse projections. Fig. 5.29 shows the variations of pH versus time and variation of Mg, Si, P, and Ca concentration versus amount of MNPs. In addition, Figure 5.29 shows the resorbability performance of the synthesized scaffold nanocomposite specimens in the SBF solution. From the Figure, it is obvious that the pH value conditioned the solubility of the bioceramic materials. Meanwhile, the material is absorbed in the SBF; for instance, the magnesium ions first of all switch with the H^+ in the SBF, this leads to a representation of the silanol group ($Si–OH^–$) on the outer layer of the samples. In addition, as the pH value decreases, a negative charge is assigned to the sample surface with the functional group ($Si–OH^–$). Study of the SBF concentration and ionic changes reveals a shift in the Mg and Si concentrations, which leads to an increase in soaking time. In the first week, there is a reduction in the calcium and phosphorus concentrations. Therefore, from our results, the bredigite-magnetite scaffold nanocomposite will have enough bioactivity and chemical reaction in the SBF solution after 4 weeks.

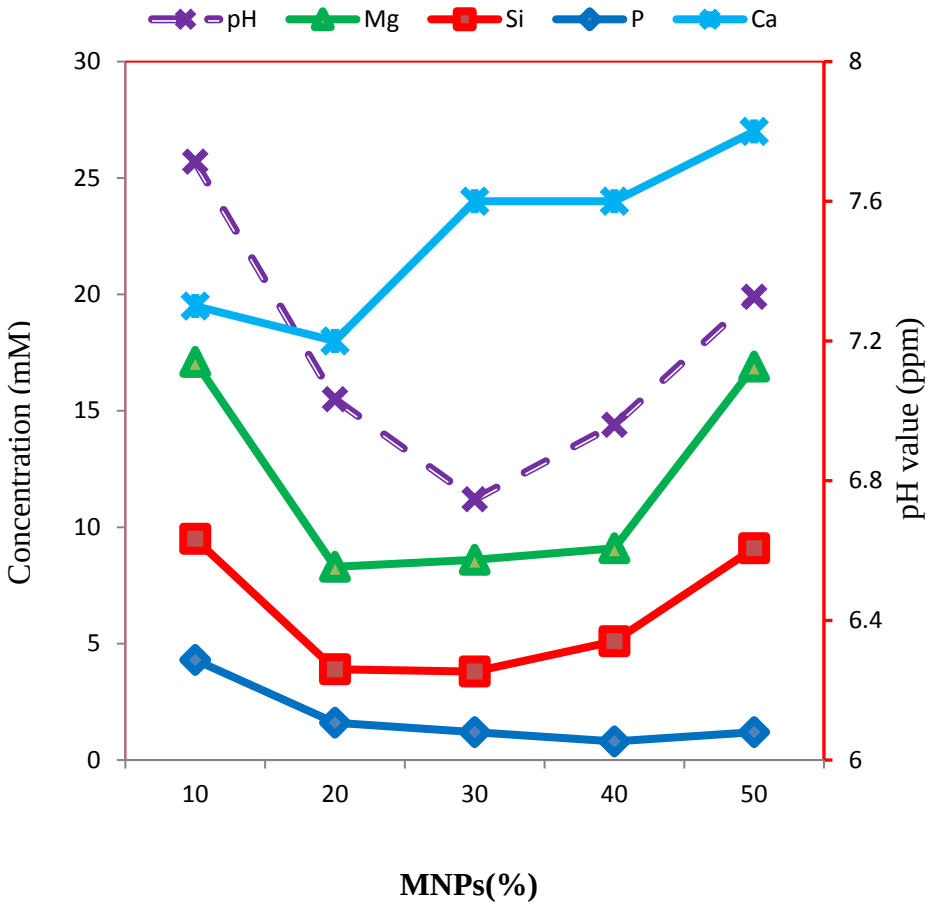

Figure 5.29: The Ion concentration of scaffold nanocomposite containing various MNPs vs. pH, ICP-OES of optimum sample soaked in SBF solution.

Figure 5.29 shows soaking samples in the SBF solution after 28 days; from the graph, the calcium ion content increases from 19 mM (bredigite scaffold) to 23 mM (at 30 wt.% MNPs) and then, stays constant at 24 (at 30 wt.% MNPs) for the following days. The released calcium ions from the bredigite content is generated based on an increase in Ca ion concentration within the SBF solution. These changes could be due to the formation of supersaturated solution around the scaffolds nanocomposite, resulting in a deposition of Ca^{2+} and PO_4^{2-} ions on the surface. Note that the surface of the scaffold nanocomposite was flat before it was soaked; however, after it was soaked for 7 days, the surface became rough and a layer of lath-like with 10-20 (nm) diameter was created with a network-like morphology. Now

after it was soaked for 10 days, the lath-like crystallites became denser and the size of the crystalline particles was about 20-30 nm in width and 50 nm in diameter. The concentrations of ions like Mg and Si in the SBF liquid increased as the time passed by. The pH of the SBF solution decreased suddenly within the first day of soaking and continued to decreased for 14 days. The reason for the decreasing pH was due to the saturation of Ca ion in the SBF solution. FTIR analysis for the soaked sample showed that in the bioceramic samples, phosphate bonds were fully substituted with the O—Ca—O, O—Mg—O, and Zr—O—Si groups [38, 41, and 289]. This event proved that during the initial immersion time, the ions possessed hydrolyzed features. With respect to our findings, the bending vibration modes for phosphate occurred at 478 cm^{-1}, whereas the phosphate stretching vibration bands occurred within the range of 970–1082 cm^{-1} distance. The band at 1420 cm^{-1} is ascribed to the functional group of the carbonates.

Figure 5.30 shows the weight change (loss) of nanocomposite soaked in the PBS solution for 28 days. From the Figure, the scaffolds nanocomposite weight loss increases (samples weight reduced) as the soaking time increases. The main reason for the weight loss was due to the pure grain size which had low bonding with the ions. The second reason was due to the high interface between the samples and SBF solution, which increased the degradation rate of scaffolds nanocomposites. The results revealed that the surface morphology and particles interface had a meaningful effect on the biodegradation rate. Besides, the sample containing 30 wt.% MNPs, was shown to have an apatite-formation property; this lead to a direct relationship with the degradability of the bredigite material. Therefore, by decreasing the

bredigite amount (more MNPs powder) and Si ions, the bone-like apatite and degradation rate of scaffold nanocomposite was enlarged.

As seen in the sample with higher amount of MNPs, there is less change in the weight of the sample than the sample with lower MNPs content. Therefore, MNPs powder helps in the chemical stability of the scaffold nanocomposites as shown by the green curve in Figure 5.30.

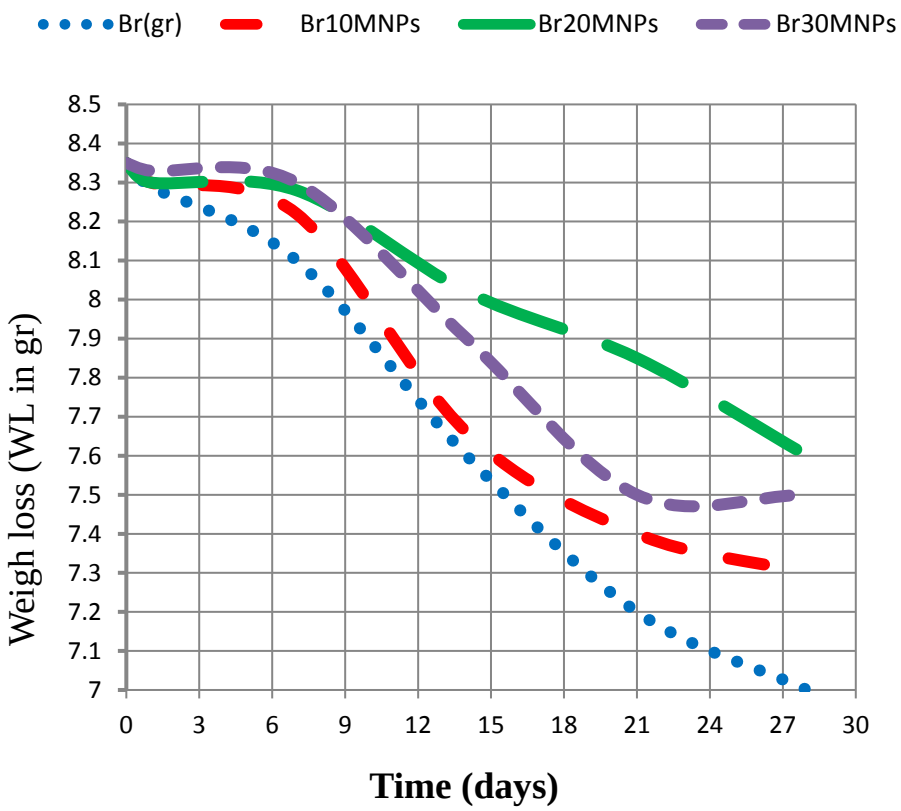

Figure 5.30: The weight loss of scaffold nanocomposite samples containing different amount of MNPs soaked in the PBS solution for 28 days.

Notwithstanding, the Ca/P ratio (assumed for HA=1.67) and other important properties like bioceramics crystallinity, are almost insoluble in any type of physiological solution within a pH range of 7.4 ppm. However, these parameters were crucial in abetting the solubility of bioceramics in an acidic medium, i.e., below

a pH of 6.5 ppm. Moreover, an increase in the MNPs concentration, changed the originally designed squared pores into slightly rounded ones as seen in Figure 5.31 (a-d). Figure 5.31 summarizes the differences found within the struts and pores size, with respect to the amount of MNPs added to the nanocomposite.

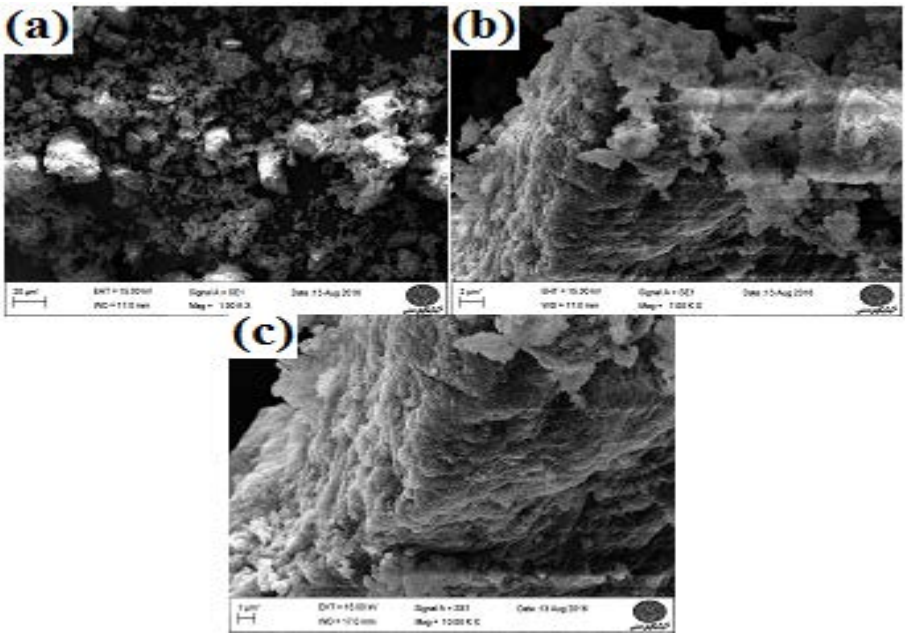

Figure 5.31: Micrograph of sample in the weight loss test of scaffolds nanocomposite containing a) 10, b) 20, and c) 30 wt.% MNPs in bredigite scaffold nanocomposite after soaked in PBS for 28 days.

It is very easy to understand that sample with a higher roughness value have a higher bioactivity rate. From our results, it can be clearly seen that a proper surface roughness would grow the bioactivity of the silicate ceramics surface [38]. After soaking the specimens in the solutions, some particles will break apart, reducing the particles size after three weeks of soaking. Amongst CaPs, HA and TCP, are the most regularly applied phases, since they have osteogenic feature as well as the possibility to make great interaction with the organism's bone tissues. While the solubility of TCP is much greater than HA, the TCP is regarded as a bioresorbable ceramic.

Figure 5.32 shows a high magnification of apatite formation, resulting in the pores size being soft and porous (spongy), with a size of less than 10 nm.

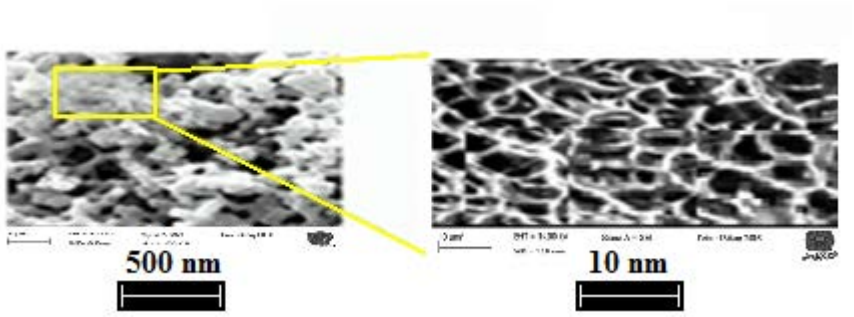

Figure 5.32: high magnification of apatite formation, resulting in the pores size being soft and porous (spongy), with a size of less than 10 nm.

If an incomplete sintering process is performed (i.e. from 550°C for 1 h to 650°C for 2 h), it may have an influence on the formation of apatite due to existing impurity in the materials (see Fig 5.33). Moreover, as the impurity are removed, the bone apatite formation improves. Therefore, the intensity of the bioceramics' purity, has a direct relationship with the bone-like apatite formation in the *in vitro* tests. From our observation, the presence of carbon is clearly noticed; also, other useless elements might be the reason behind the functional groups not being able to precipitate on the scaffold nanocomposite.

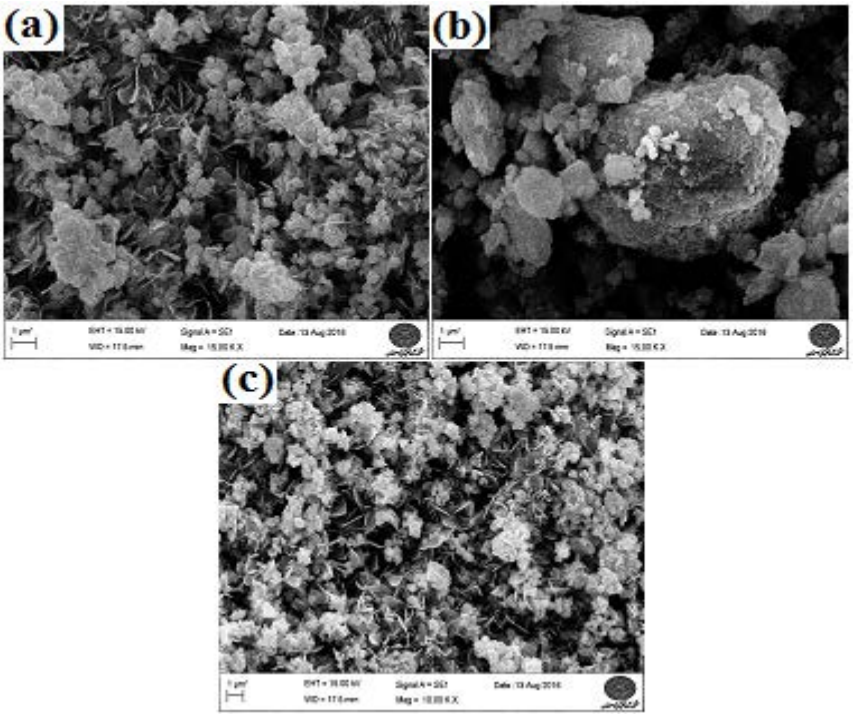

Figure 5.33: SEM micrograph of scaffold nanocomposite a) 10, b) 20, and c) 30wt.% soaked in SBF for 28 days.

The Ca—P ratio of sample was measured by EDX within the range of 3.4-3.8 as shown Figure 5.34. A silica-rich and calcium-rich layer, precipitates on the scaffold nanocomposite, having a thickness of 0.5-1 μm. Also, as scaffolds porosity increases, the thickness of the scaffold nanocomposite sample decreases. As previously discussed, the best scaffold nanocomposite for the bioactivity evaluation, recorded a sample containing 30 wt.% MNPs in the bredigite powder due to high chemical stability. The analysis of scaffold nanocomposite show that the scaffold nanocomposite samples sintered for 2 h at 650°C; this contributed to a higher apatite formation during the soaking time, because the base scaffold surface had a denser and higher chemical stability for apatite to precipitate on them. Higher apatite formation is dependent on the amount of hydroxyl (OH^-) groups present in the scaffold nanocomposite surface, in meeting with the circulatory liquid which performs as a nuclei for apatites formation. It is obvious that the dissolution of the

Ca^{2+} ions, from bredigite content, produces a calcium and silica-rich biolayer, that is assigned to the Si–OH groups on the surface of the scaffold. In addition, the silanol groups in the silica-rich biolayer, have a great influence on the preparation of apatite. Therefore, it should be assumed that the decomposition of calcium ions from the bredigite content, throughout the immersion, causes a reproduction of silica-rich layer with Si—OH groups; however, it hardly brought about apatite nucleation. Therefore, an investigation was launched to find out how the addition of trace elements may control the rate of apatite formation of silicate biomaterials with different energy bond. For example, the M—O bond energy (where M= Mg^{2+}, Zn^{2+}) is larger than the bond energy of Ca—O.

Previous studies have shown that a trace element has a higher impact on the structure's stability (i.e. it influences its mechanical properties) [38]. Consequently, diffusing the trace element into the $CaSiO_3$ bioceramics leads to a formation of multiple proper microstructures with various bond energy amidst its ions [36-38, 290].

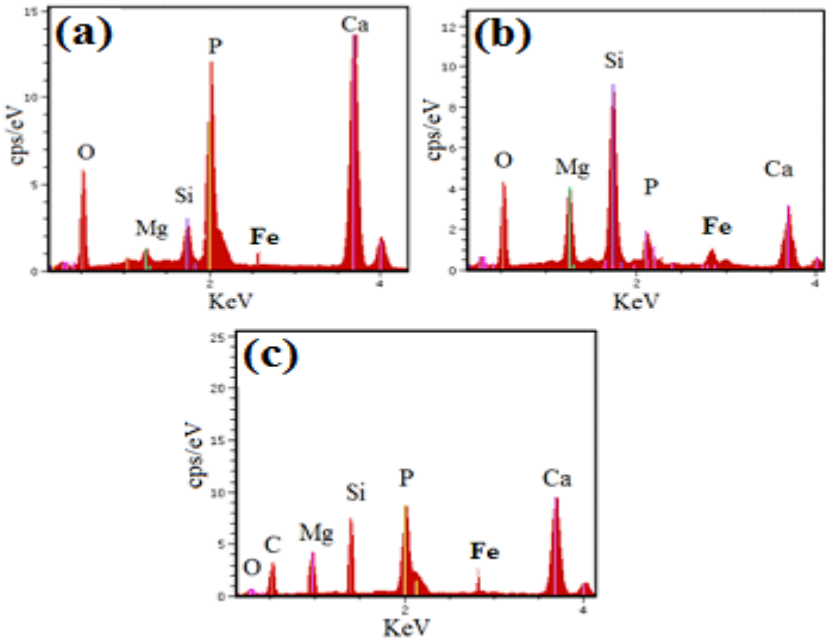

Figure 5.34: The EDX of the soaked bredigite-magnetite scaffold nanocomposite containing a) 10 wt.%, b) 20 wt.%, and c) 30 wt.%, in SBF after 28 days

Silicate bioceramics have a multi-component microstructure and network, which is based on the $Na_2O—SiO_2$ or $CaO—SiO_2$ binary system. The silicate bioceramics releases Na^+ ions into SBF solution via an interchange with the H_3O^+ ions in SBF in order to build Si—OH groups on the scaffold surfaces [198, 291-292]. Following this, the Si-OH groups creates the fastest link with the calcium ions in the SBF in order to make an amorphous calcium silicate on the surface (glassy surface). Then after a while, the calcium silicate couples with phosphate ions in the SBF to create an amorphous CaPs with a low Ca/P atomic ratio. From Figure 5.33, the formed phase in the days that followed transformed into net shape crystal of bone-like apatite, this increases the Ca/P ratio and fuses insignificant ions such as Na^+, Mg^{2+}, and Cl^- i.e. as the amount of MNPs increases (which is present in the SBF solution). With absence of silicon, the phosphate was rebuilt in solution. Also, the amount of Mg reduces as illustrated by the EDX analysis. Silicon (Si^{4+}), known as a critical trace element, affects the formation of bone and calcification. Si has been recommended for the

stimulation of cellular actions, like proliferation and differentiation of osteoblast-like cells, and mineralization of human osteoblasts [37-38]. Si^{4+} is located within the bone and connective tissues in the body [202, 291-292].

From our results, it can be seen that the surface of the specimen, after being soaked, produced several uniform micropores (0.5-10 μm). After the soaking operation, the micropores disappeared due to the deposition of HA crystals on the scaffold surface. Moreover, the porous scaffold improved the rate of bone apatite. On the other hand, these micropores (size ≤10 μm) are required for narrow ingrowths of bones cells and cell-matrix interactions. The results show that a great number of magnetite as well as the magnetization values increased, leading to greater bioactivity and larger coercivity. Furthermore, images accumulated from the EDX analysis showed that a nanocrystalline apatite was produced on the surface of the composite samples; this contained minor components such as Na, Cl, and Mg, and showed, a Ca/P atomic ratio higher than 1.67 (see Figure 5.34). The surface roughness and porosity have been considered as the major driver that increased the bioactivity. In addition, the magnetite powder/phase made from nanocrystalline structure with glass precursors, play an important role in enhancing the properties of the composites.

Chapter 6

CONCLUSION

In the current study, the bredigite bioceramics were prepared by high-energy ball milling, also magnetite nanoparticles were produced by sol-gel technique. The aim of this study is to evaluate the thermal, electrical, mechanical, biological and magnetic behavior of the bredigite-magnetite scaffold nanocomposite for bone tissue engineering application. This is the very first study conducted on the novel bredigite-magnetite scaffold nanocomposite, which involves the application of hyperthermia treatment and evaluation of the artificial tissue's behavior under the temperature change and AC magnetic field. From the results, it is observed that the higher electrical conductivity (160 µS/m) belongs to the sample with higher percentage of magnetite nanoparticles, while the sample without MNPs powder shows the lowest amount of electrical conductivity (35 µS/m). The porosity dependent to the compressive strength and the result obtained from the soaking materials in the SBF solution for bioactivity evaluation influence on the mechanical characteristic. The results showed that the porosity has a close relationship with the roughness of scaffold samples. The surface destruction in the scaffolds with 30 wt.% magnetite observed less than the sample without MNPs, which seems to have a significant role in increasing/decreasing apatite formation in samples. The results indicated that the bredigite and magnetite powder in pure and composite form induce the apatite formation on their surface by soaking in the SBF. The magnetic energy was transferred to the heat by which the tendency to the agglomeration increased. Notwithstanding, the hyperthermia

performance has been related to both magnetite and bredigite powders. The machine parameter like deposition rate has an effective influence on porosity and thickness of the sample layer. Our results indicate that bredigite-magnetite scaffold nanocomposite possess good *in vitro* bioactivity, and biocompatibility, which used as bioactive bone repair materials for cancer therapy application.

6.1 Future Recommendations

For future work, more in vivo or animal test investigations must be carried to examine the applicability of silicate bioceramics and magnetite nanoparticles for the bone implant. Also, cell culture of the scaffold needs to be considered. Although these novel type of multifunctional scaffolds have proper properties for using in the bone disease like malignant, they should apply in the AC field with hyperthermia therapy. Also, Using local drug delivery can develop the treatment as well as hyperthermia treatment. More examinations need to be accomplished to monitor the magnetic behavior and the heating influence on drug delivery and *in vivo* osteogenesis. For instance, Cisplatin (cis-dichlorodiammineplatinum(II), CDDP) as one of the most common anticancer drug can be used as a cytotoxic agent with healing action for different types of cancers like ovarian, sarcoma, breast, bladder and small cell lung cancer.

6.2 Shortcomings and Limitations

Including the economic cost and regulatory of scaffolds, it might be extensive outcomes, as the separation of therapeutic tools happens. Apparently, for the purpose of advancing biological activity within the body such as regeneration of bone, and undesirable activity of bone infections. Performing suitable research can enhance the process for making the 3D product utilizing DOE can have both price and time benefit. Applying DOE is reduce the cost and is time-consuming. Using both

numerical and analytical models can be useful tools to find the suitable parameter of the machine process and materials characteristic due to required characteristic.

REFERENCES

[1] Gómez-Barrena, E., Rosset, P., Lozano, D., Stanovici, J., Ermthaller, C., & Gerbhard, F. (2015). Bone fracture healing: cell therapy in delayed unions and nonunions. *Bone*, 70, 93-101.

[2] Griffin, K. S., Davis, K. M., McKinley, T. O., Anglen, J. O., Chu, T. M. G., Boerckel, J. D., & Kacena, M. A. (2015). Evolution of bone grafting: bone grafts and tissue engineering strategies for vascularized bone regeneration. *Clinical Reviews in Bone and Mineral Metabolis*m, 13(4), 232-244.

[3] Flierl MA, Smith WR, Mauffrey C, Irgit K, Williams AE, Ross E, Peacher G, Hak DJ, Stahel PF. Outcomes and complication rates of different bone grafting modalities in long bone fracture nonunions: a retrospective cohort study in 182 patients. *Journal of orthopaedic surgery and research*. 2013 Sep 9;8(1):33.

[4] Doblaré, M., Garcıa, J. M., & Gómez, M. J. (2004). Modelling bone tissue fracture and healing: a review. *Engineering Fracture Mechanics*, 71(13), 1809-1840.

[5] Pazianas, M., Miller, P., Blumentals, W. A., Bernal, M., & Kothawala, P. (2007). A review of the literature on osteonecrosis of the jaw in patients with osteoporosis treated with oral bisphosphonates: prevalence, risk factors, and clinical characteristics. *Clinical therapeutics*, 29(8), 1548-1558.

[6] Karamian, E., Motamedi, M. R. K., Khandan, A., Soltani, P., & Maghsoudi, S. (2014). An in vitro evaluation of novel NHA/zircon plasma coating on 316L stainless steel dental implant. *Progress in Natural Science: Materials International*, 24(2), 150-156.

[7] Karamian, E., Khandan, A., Kalantar Motamedi, M. R., & Mirmohammadi, H. (2014). Surface characteristics and bioactivity of a novel natural HA/zircon nanocomposite coated on dental implants. *BioMed research international*, 2014.

[8] Khandan, A., Abdellahi, M., Barenji, R. V., Ozada, N., & Karamian, E. (2015). Introducing natural hydroxyapatite-diopside (NHA-Di) nano-bioceramic coating. *Ceramics International*, 41(9), 12355-12363.

[9] Haynes, D. R., Crotti, T. N., & Haywood, M. R. (2000). Corrosion of and changes in biological effects of cobalt chrome alloy and 316L stainless steel prosthetic particles with age. *Journal of Biomedical Materials Research Part A*, 49(2), 167-175.

[10] Biesiekierski, A., Wang, J., Gepreel, M. A. H., & Wen, C. (2012). A new look at biomedical Ti-based shape memory alloys. *Acta biomaterialia*, 8(5), 1661-1669.

[11] Khandan, A., Abdellahi, M., Ozada, N., & Ghayour, H. (2016). Study of the bioactivity, wettability and hardness behaviour of the bovine hydroxyapatite-

diopside bio-nanocomposite coating. *Journal of the Taiwan Institute of Chemical Engineers*, 60, 538-546.

[12] Park, J., & Lakes, R. S. (2007). Biomaterials: an introduction. Springer *Science & Business Media*.

[13] Sionkowska, A. (2011). Current research on the blends of natural and synthetic polymers as new biomaterials. *Progress in Polymer Science*, 36(9), 1254-1276.

[14] Leclerc, E., Furukawa, K. S., Miyata, F., Sakai, Y., Ushida, T., & Fujii, T. (2004). Fabrication of microstructures in photosensitive biodegradable polymers for tissue engineering applications. *Biomaterials*, 25(19), 4683-4690.

[15] Khandan, A., Karamian, E., & Bonakdarchian, M. (2014). Mechanochemical synthesis evaluation of nanocrystalline bone-derived bioceramic powder using for bone tissue engineering. *Dental Hypotheses*, 5(4), 155.

[16] Karamian, E., Abdellahi, M., Khandan, A., & Abdellah, S. (2016). Introducing the fluorine doped natural hydroxyapatite-titania nanobiocomposite ceramic. *Journal of Alloys and Compounds*, 679, 375-383.

[17] Karamian, E., Khandan, A., Eslami, M., Gheisari, H., & Rafiaei, N. (2014). Investigation of HA nanocrystallite size crystallographic characterizations in NHA, BHA and HA pure powders and their influence on biodegradation of

HA. In *Advanced Materials Research* (Vol. 829, pp. 314-318). Trans Tech Publications.

[18] Tarafder, S. (2013). Physicomechanical, In Vitro and In Vivo Performance of 3D Printed Doped Tricalcium Phosphate Scaffolds for Bone Tissue Engineering and Drug Delivery. *Washington State University*.

[19] Hull, D., & Clyne, T. W. (1996). An introduction to composite materials. *Cambridge university press*.

[20] Sampath, S., & Lev, O. (1996). Inert metal-modified, composite ceramic− carbon, amperometric biosensors: renewable, controlled reactive layer. *Analytical Chemistry*, 68(13), 2015-2021.

[21] Boccaccini, A. R., Roelher, J. A., Hench, L. L., Maquet, V., & Jérŏme, R. (2008). A composites approach to tissue engineering. In 26th Annual Conference on Composites, *Advanced Ceramics, Materials, and Structures: B: Ceramic Engineering and Science Proceedings*, Volume 23, Issue 4 (pp. 805-816). John Wiley & Sons, Inc..

[22] Krenkel, W. (Ed.). (2008). Ceramic matrix composites: fiber reinforced ceramics and their applications. *John Wiley & Sons*.

[23] Bansal, N. P. (Ed.). (2006). *Handbook of ceramic composites* (Vol. 200). Springer Science & Business Media.

[24] White, A. A., Best, S. M., & Kinloch, I. A. (2007). Hydroxyapatite–carbon nanotube composites for biomedical applications: a review. *International Journal of Applied Ceramic Technology*, 4(1), 1-13.

[25] Chłopek, J., Czajkowska, B., Szaraniec, B., Frackowiak, E., Szostak, K., & Beguin, F. (2006). In vitro studies of carbon nanotubes biocompatibility. *Carbon*, 44(6), 1106-1111.

[26] Witte, F., Feyerabend, F., Maier, P., Fischer, J., Störmer, M., Blawert, C., ... & Hort, N. (2007). Biodegradable magnesium–hydroxyapatite metal matrix composites. *Biomaterials*, 28(13), 2163-2174.

[27] Chawla, K. K. (2006). Metal matrix composites. *Wiley-VCH Verlag GmbH & Co. KGaA*.

[28] Evans, A., San Marchi, C., & Mortensen, A. (2003). Metal Matrix Composites. In *Metal Matrix Composites in Industry* (pp. 9-38). Springer US.

[29] Monteiro, S. N., Lopes, F. P. D., Ferreira, A. S., & Nascimento, D. C. O. (2009). Natural-fiber polymer-matrix composites: cheaper, tougher, and environmentally friendly. JOM *Journal of the Minerals, Metals and Materials Society*, 61(1), 17-22.

[30] Dang, Z. M., Yuan, J. K., Zha, J. W., Zhou, T., Li, S. T., & Hu, G. H. (2012). Fundamentals, processes and applications of high-permittivity polymer–matrix composites. *Progress in Materials Science*, 57(4), 660-723.

[31] Haque, A., & Ramasetty, A. (2005). Theoretical study of stress transfer in carbon nanotube reinforced polymer matrix composites. *Composite Structures*, 71(1), 68-77.

[32] Bell, A. M., Lassila, L. V., Kangasniemi, I., & Vallittu, P. K. (2005). Bonding of fibre-reinforced composite post to root canal dentin. *Journal of dentistry*, 33(7), 533-539.

[33] Fortunati, E., Armentano, I., Zhou, Q., Iannoni, A., Saino, E., Visai, L., ... & Kenny, J. M. (2012). Multifunctional bionanocomposite films of poly (lactic acid), cellulose nanocrystals and silver nanoparticles. *Carbohydrate polymers*, 87(2), 1596-1605.

[34] Chen, F. M., & Liu, X. (2016). Advancing biomaterials of human origin for tissue engineering. *Progress in polymer science*, 53, 86-168.

[35] Holzapfel, B. M., Reichert, J. C., Schantz, J. T., Gbureck, U., Rackwitz, L., Nöth, U., ... & Hutmacher, D. W. (2013). How smart do biomaterials need to be? A translational science and clinical point of view. *Advanced drug delivery reviews*, 65(4), 581-603.

[36] Vallet-Regí, M., & Ruiz-Hernández, E. (2011). Bioceramics: from bone regeneration to cancer nanomedicine. *Advanced Materials*, 23(44), 5177-5218.

[37] Kazemi, A., Abdellahi, M., Khajeh-Sharafabadi, A., Khandan, A., & Ozada, N. (2017). Study of in vitro bioactivity and mechanical properties of diopside nano-bioceramic synthesized by a facile method using eggshell as raw material. *Materials Science and Engineering: C*, 71, 604-610.

[38] Sharafabadi, A. K., Abdellahi, M., Kazemi, A., Khandan, A., & Ozada, N. (2017). A novel and economical route for synthesizing akermanite (Ca 2 MgSi 2 O 7) nano-bioceramic. *Materials Science and Engineering: C*, 71, 1072-1078.

[39] Yi, D., Wu, C., Ma, B., Ji, H., Zheng, X., & Chang, J. (2014). Bioactive bredigite coating with improved bonding strength, rapid apatite mineralization and excellent cytocompatibility. *Journal of biomaterials applications*, 28(9), 1343-1353.

[40] Khandan, A., Karamian, E., Mehdikhani-Nahrkhalaji, M., Mirmohammadi, H., Farzadi, A., Ozada, N., ... & Zamani, K. (2015). Influence of spark plasma sintering and baghdadite powder on mechanical properties of hydroxyapatite. *Procedia Materials Science*, 11, 183-189.

[41] Najafinezhad, A., Abdellahi, M., Ghayour, H., Soheily, A., Chami, A., & Khandan, A. (2017). A comparative study on the synthesis mechanism, bioactivity and mechanical properties of three silicate bioceramics. *Materials Science and Engineering: C*, 72, 259-267.

[42] Bertoni, E., Bigi, A., Cojazzi, G., Gandolfi, M., Panzavolta, S., & Roveri, N. (1998). Nanocrystals of magnesium and fluoride substituted hydroxyapatite. *Journal of inorganic biochemistry*, 72(1), 29-35.

[43] Okazaki, M. (1995). Crystallographic properties of heterogeneous Mg-containing fluoridated apatites synthesized with a two-step supply system. *Biomaterials*, 16(9), 703-707.

[44] Yamasaki, Y., Yoshida, Y., Okazaki, M., Shimazu, A., Uchida, T., Kubo, T., ... & Matsuura, N. (2002). Synthesis of functionally graded MgCO3 apatite accelerating osteoblast adhesion. *Journal of Biomedical Materials Research Part A*, 62(1), 99-105.

[45] Mayer, I., Schlam, R., & Featherstone, J. D. B. (1997). Magnesium-containing carbonate apatites. *Journal of inorganic biochemistry*, 66(1), 1-6.

[46] Jabbarzare, S., Abdellahi, M., Ghayour, H., Arpanahi, A., & Khandan, A. (2017). A study on the synthesis and magnetic properties of the cerium ferrite ceramic. *Journal of Alloys and Compounds*, 694, 800-807.

[47] Ghayour, H., Abdellahi, M., Bahmanpour, M., & Khandan, A. (2016). Simulation of dielectric behavior in RFeO_ {3} orthoferrite ceramics (R= rare earth metals). *Journal of Computational Electronics*, 15(4), 1275-1283.

[48] Saeedi, M., Abdellahi, M., Rahimi, A., & Khandan, A. (2016). Preparation and characterization of nanocrystalline barium ferrite ceramic. *Functional Materials Letters*, 9(05), 1650068.

[49] Shayan, A., Abdellahi, M., Shahmohammadian, F., Jabbarzare, S., Khandan, A., & Ghayour, H. (2017). Mechanochemically aided sintering process for the synthesis of barium ferrite: Effect of aluminum substitution on microstructure, magnetic properties and microwave absorption. *Journal of Alloys and Compounds*, 708, 538-546.

[50] Chanda, S., Saha, S., Dutta, A., & Sinha, T. P. (2013). Raman spectroscopy and dielectric properties of nanoceramic NdFeO 3. *Materials Research Bulletin*, 48(4), 1688-1693.

[51] Minh, N. Q. (1993). Ceramic fuel cells. Journal of the American Ceramic Society, 76(3), 563-588.

[52] Di Bartolomeo, E., Traversa, E., Baroncini, M., Kotzeva, V., & Kumar, R. V. (2000). Solid state ceramic gas sensors based on interfacing ionic conductors with semiconducting oxides. *Journal of the European Ceramic Society*, 20(16), 2691-2699.

[53] Niu, X., Li, H., & Liu, G. (2005). Preparation, characterization and photocatalytic properties of REFeO 3 (RE= Sm, Eu, Gd). *Journal of Molecular Catalysis A: Chemical*, 232(1), 89-93.

[54] Dorozhkin, S. V. (2010). Bioceramics of calcium orthophosphates. *Biomaterials*, 31(7), 1465-1485.

[55] Halouani, R., Bernache-Assolant, D., Champion, E., & Ababou, A. (1994). Microstructure and related mechanical properties of hot pressed hydroxyapatite ceramics. *Journal of Materials Science: Materials in Medicine*, 5(8), 563-568.

[56] Dorozhkin, S. V. (2008). Calcium orthophosphate cements for biomedical application. *Journal of Materials Science*, 43(9), 3028.

[57] Yin, X., & Stott, M. J. (2006). Surface and adsorption properties of α-tricalcium phosphate. *The Journal of chemical physics*, 124(12), 124701.

[58] Dorozhkin, S. V. (2009). Calcium orthophosphates in nature, biology and medicine. *Materials*, 2(2), 399-498.

[59] Dorozhkin, S. V. (2010). Nanosized and nanocrystalline calcium orthophosphates. *Acta biomaterialia*, 6(3), 715-734.

[60] Dorozhkin, S. V. (2010). Amorphous calcium (ortho) phosphates. Acta *Biomaterialia*, 6(12), 4457-4475.

[61] Dorozhkin, S. V. (2012). Biphasic, triphasic and multiphasic calcium orthophosphates. *Acta biomaterialia*, 8(3), 963-977.

[62] Gittings, J. P., Bowen, C. R., Dent, A. C., Turner, I. G., Baxter, F. R., & Chaudhuri, J. B. (2009). Electrical characterization of hydroxyapatite-based bioceramics. *Acta Biomaterialia*, 5(2), 743-754.

[63] Valdes, J. P., Rodriguez, A. V., & Carrio, J. G. (1995). Dielectric properties and structure of hydroxyapatite ceramics sintered by different conditions. *Journal of materials research*, 10(9), 2174-2177.

[64] Fanovich, M. A., Castro, M. S., & Lopez, J. P. (1999). Analysis of the microstructural evolution in hydroxyapatite ceramics by electrical characterisation. *Ceramics International*, 25(6), 517-522.

[65] Bowen, C. R., Gittings, J., Turner, I. G., Baxter, F., & Chaudhuri, J. B. (2006). Dielectric and piezoelectric properties of hydroxyapatite-Ba Ti O 3 composites. *Applied physics letters*, 89(13), 132906.

[66] Khalil, M. S., Beheri, H. H., & Fattah, W. I. A. (2002). Structural and electrical properties of zirconia/hydroxyapatite porous composites. *Ceramics international*, 28(4), 451-458.

[67] Silva, C. C., Graça, M. P. F., Valente, M. A., & Sombra, A. S. B. (2006). AC and DC conductivity analysis of hydroxyapatite and titanium calcium phosphate formed by dry ball milling. *Journal of non-crystalline solids*, 352(9), 1490-1494.

[68] Nakamura, M., Nagai, A., Ohashi, N., Tanaka, Y., Sekijima, Y., Nakamura, S., & Yamashita, K. (2008). Regulation of osteoblast-like cell behaviors on hydroxyapatite by electrical polarization. *In Key Engineering Materials* (Vol. 361, pp. 1055-1058). Trans Tech Publications.

[69] Lazić, S., Zec, S., Miljević, N., & Milonjić, S. (2001). The effect of temperature on the properties of hydroxyapatite precipitated from calcium hydroxide and phosphoric acid. *Thermochimica Acta*, 374(1), 13-22.

[70] Ooi, C. Y., Hamdi, M., & Ramesh, S. (2007). Properties of hydroxyapatite produced by annealing of bovine bone. *Ceramics international*, 33(7), 1171-1177.

[71] Kehoe, S. (2008). *Calcium phosphates for medical applications*.

[72] Mostafa, N. Y. (2005). Characterization, thermal stability and sintering of hydroxyapatite powders prepared by different routes. *Materials chemistry and physics*, 94(2), 333-341.

[73] Dezfuli, S. N., Leeflang, S., Huan, Z., Chang, J., & Zhou, J. (2017). Fabrication of novel magnesium-matrix composites and their mechanical properties prior to and during in vitro degradation. *Journal of the mechanical behavior of biomedical materials*, 67, 74-86.

[74] Peltola, S. M., Melchels, F. P., Grijpma, D. W., & Kellomäki, M. (2008). A review of rapid prototyping techniques for tissue engineering purposes. *Annals of medicine*, 40(4), 268-280.

[75] Hutmacher, D. W. (2000). Scaffolds in tissue engineering bone and cartilage. *Biomaterials*, 21(24), 2529-2543.

[76] Suh, S. W., Shin, J. Y., Kim, J., Kim, J., Beak, C. H., Kim, D. I., ... & Choo, I. W. (2002). Effect of different particles on cell proliferation in polymer scaffolds using a solvent-casting and particulate leaching technique. *ASAIO journal*, 48(5), 460-464.

[77] Chia, H. N., & Wu, B. M. (2015). Recent advances in 3D printing of biomaterials. *Journal of biological engineering*, 9(1), 4.

[78] Dowler, C. (1989). Automatic model building cuts design time, costs. *Plastics Eng*, 45(4), 43-45.

[79] Pattanayak, D. K., Fukuda, A., Matsushita, T., Takemoto, M., Fujibayashi, S., Sasaki, K., ... & Kokubo, T. (2011). Bioactive Ti metal analogous to human cancellous bone: fabrication by selective laser melting and chemical treatments. *Acta Biomaterialia*, 7(3), 1398-1406.

[80] Shikinami, Y., & Okuno, M. (1999). Bioresorbable devices made of forged composites of hydroxyapatite (HA) particles and poly-L-lactide (PLLA): Part I. Basic characteristics. *Biomaterials*, 20(9), 859-877.

[81] Zein, I., Hutmacher, D. W., Tan, K. C., & Teoh, S. H. (2002). Fused deposition modeling of novel scaffold architectures for tissue engineering applications. *Biomaterials*, 23(4), 1169-1185.

[82] Van Noort, R. (2012). The future of dental devices is digital. *Dental materials*, 28(1), 3-12.

[83] Hutmacher, D. W., Schantz, T., Zein, I., Ng, K. W., Teoh, S. H., & Tan, K. C. (2001). Mechanical properties and cell cultural response of polycaprolactone scaffolds designed and fabricated via fused deposition modeling. *Journal of Biomedical Materials Research Part A*, 55(2), 203-216.

[84] Rai, B., Teoh, S. H., Ho, K. H., Hutmacher, D. W., Cao, T., Chen, F., & Yacob, K. (2004). The effect of rhBMP-2 on canine osteoblasts seeded onto 3D bioactive polycaprolactone scaffolds. *Biomaterials*, 25(24), 5499-5506.

[85] Cima, M. J., Sachs, E., Cima, L. G., Yoo, J., Khanuja, S., Borland, S. W., ... & Giordano, R. A. (1994, September). Computer-derived microstructures by 3D printing: bio-and structural materials. *In Solid Freeform Fabr Symp Proc*: DTIC Document (pp. 181-90).

[86] Griffith, L. G., Wu, B. E. N., Cima, M. J., Powers, M. J., Chaignaud, B., & Vacanti, J. P. (1997). In vitro organogenesis of liver tissue. *Annals of the New York Academy of Sciences*, 831(1), 382-397.

[87] Wu, B. M., Borland, S. W., Giordano, R. A., Cima, L. G., Sachs, E. M., & Cima, M. J. (1996). Solid free-form fabrication of drug delivery devices. *Journal of Controlled Release*, 40(1-2), 77-87.

[88] Shanjani, Y., Croos, D., Amritha, J. N., Pilliar, R. M., Kandel, R. A., & Toyserkani, E. (2010). Solid freeform fabrication and characterization of porous calcium polyphosphate structures for tissue engineering purposes. *Journal of Biomedical Materials Research Part B: Applied Biomaterials*, 93(2), 510-519.

[89] Heydary, H. A., Karamian, E., Poorazizi, E., Heydaripour, J., & Khandan, A. (2015). Electrospun of polymer/bioceramic nanocomposite as a new soft tissue for biomedical applications. *Journal of Asian Ceramic Societies*, 3(4), 417-425.

[90] Heydary, H. A., Karamian, E., Poorazizi, E., Khandan, A., & Heydaripour, J. (2015). A Novel Nano-Fiber of Iranian Gum Tragacanth-Polyvinyl Alcohol/Nanoclay Composite for Wound Healing Applications. *Procedia Materials Science*, 11, 176-182.

[91] Seitz, H., Deisinger, U., Leukers, B., Detsch, R., & Ziegler, G. (2009). Different Calcium Phosphate Granules for 3-D Printing of Bone Tissue Engineering Scaffolds. *Advanced Engineering Materials*, 11(5).

[92] Santos, C. F., Silva, A. P., Lopes, L., Pires, I., & Correia, I. J. (2012). Design and production of sintered β-tricalcium phosphate 3D scaffolds for bone tissue regeneration. *Materials science and engineering: C*, 32(5), 1293-1298.

[93] Tarafder, S., Davies, N. M., Bandyopadhyay, A., & Bose, S. (2013). 3D printed tricalcium phosphate bone tissue engineering scaffolds: effect of SrO and MgO doping on in vivo osteogenesis in a rat distal femoral defect model. *Biomaterials Science*, 1(12), 1250-1259.

[94] Tarafder, S., Dernell, W. S., Bandyopadhyay, A., & Bose, S. (2015). SrO-and MgO-doped microwave sintered 3D printed tricalcium phosphate scaffolds: Mechanical properties and in vivo osteogenesis in a rabbit model. *Journal of Biomedical Materials Research Part B: Applied Biomaterials*, 103(3), 679-690.

[95] Suwanprateeb, J., Sanngam, R., Suvannapruk, W., & Panyathanmaporn, T. (2009). Mechanical and in vitro performance of apatite–wollastonite glass ceramic reinforced hydroxyapatite composite fabricated by 3D-printing. *Journal of Materials Science: Materials in Medicine*, 20(6), 1281.

[96] Inzana, J. A., Olvera, D., Fuller, S. M., Kelly, J. P., Graeve, O. A., Schwarz, E. M., ... & Awad, H. A. (2014). 3D printing of composite calcium phosphate and collagen scaffolds for bone regeneration. *Biomaterials*, 35(13), 4026-4034.

[97] Ge, Z., Wang, L., Heng, B. C., Tian, X. F., Lu, K., Tai Weng Fan, V., ... & Tan, E. (2009). Proliferation and differentiation of human osteoblasts within 3D printed poly-lactic-co-glycolic acid scaffolds. *Journal of biomaterials applications*, 23(6), 533-547.

[98] Klammert, U., Vorndran, E., Reuther, T., Müller, F. A., Zorn, K., & Gbureck, U. (2010). Low temperature fabrication of magnesium phosphate cement scaffolds by 3D powder printing. *Journal of Materials Science: Materials in Medicine*, 21(11), 2947-2953.

[99] Lee, J. Y., Choi, B., Wu, B., & Lee, M. (2013). Customized biomimetic scaffolds created by indirect three-dimensional printing for tissue engineering. *Biofabrication*, 5(4), 045003.

[100] Tartaj, P., Veintemillas-Verdaguer, S., & Serna, C. J. (2003). The preparation of magnetic nanoparticles for applications in biomedicine. *Journal of Physics D: Applied Physics*, 36(13), R182.

[101] Bajpai, I., Balani, K., & Basu, B. (2014). Synergistic effect of static magnetic field and HA-Fe3O4 magnetic composites on viability of S. aureus and E. coli bacteria. *Journal of Biomedical Materials Research Part B: Applied Biomaterials*, 102(3), 524-532.

[102] Hou, C. H., Hou, S. M., Hsueh, Y. S., Lin, J., Wu, H. C., & Lin, F. H. (2009). The in vivo performance of biomagnetic hydroxyapatite nanoparticles in cancer hyperthermia therapy. *Biomaterials*, 30(23), 3956-3960.

[103] Tseng, C. L., Chang, K. C., Yeh, M. C., Yang, K. C., Tang, T. P., & Lin, F. H. (2014). Development of a dual-functional Pt–Fe-HAP magnetic nanoparticles application for chemo-hyperthermia treatment of cancer. *Ceramics International*, 40(4), 5117-5127.

[104] Scherer, F., Anton, M., Schillinger, U., Henke, J., Bergemann, C., Krüger, A., ... & Plank, C. (2002). Magnetofection: enhancing and targeting gene delivery by magnetic force in vitro and in vivo. *Gene therapy*, 9(2), 102.

[105] Nielsen, Ole Steen, M. Horsman, and J. Overgaard. "A future for hyperthermia in cancer treatment?." (2001): 1587-1589.

[106] Gupta, Ajay Kumar, and Mona Gupta. "Synthesis and surface engineering of iron oxide nanoparticles for biomedical applications." *Biomaterials* 26.18 (2005): 3995-4021.

[107] Berry, C. C., & Curtis, A. S. (2003). Functionalisation of magnetic nanoparticles for applications in biomedicine. *Journal of physics D: Applied physics*, 36(13), R198.

[108] Néel, L. (1955). Some theoretical aspects of rock-magnetism. *Advances in physics*, 4(14), 191-243.

[109] Deissler, R. J., Wu, Y., & Martens, M. A. (2014). Dependence of Brownian and Néel relaxation times on magnetic field strength. *Medical physics*, 41(1).

[110] Ahmad, S. N., & Shaheen, S. A. (2009). Optimization of (Gd) 5 Si 4 based materials: A step toward self-controlled hyperthermia applications. Journal of *Applied Physics*, 106(6), 064701.

[111] Thorat, N. D., Bohara, R., Yadav, H. M., Otari, S. V., Pawar, S. H., & Tofail, S. A. M. (2016). Multifunctional Magnetic Nanostructures for Cancer Hyperthermia Therapy.

[112] Song, C. W. (1984). Effect of local hyperthermia on blood flow and microenvironment: a review. *Cancer research*, 44(10 Supplement), 4721s-4730s.

[113] Gani, C., Schroeder, C., Heinrich, V., Spillner, P., Lamprecht, U., Berger, B., & Zips, D. (2016). Long-term local control and survival after preoperative radiochemotherapy in combination with deep regional hyperthermia in locally advanced rectal cancer. *International Journal of Hyperthermia*, 32(2), 187-192.

[114] Hajian, S. R., Fard, A. A. T., Pouladian, M., & Hemmasi, G. R. (2016). Modeling pressure distribution and heat in the body tissue and extract the relationship between them in order to improve treatment planning in HIFU. *arXiv preprint arXiv*:1610.08036.

[115] Bao, Y., Wen, T., Samia, A. C. S., Khandhar, A., & Krishnan, K. M. (2016). Magnetic nanoparticles: material engineering and emerging applications in lithography and biomedicine. *Journal of materials science*, 51(1), 513-553.

[116] Nemati, Z., Alonso, J., Martinez, L. M., Khurshid, H., Garaio, E., Garcia, J. A., ... & Srikanth, H. (2016). Enhanced magnetic hyperthermia in iron oxide nano-octopods: size and anisotropy effects. *The Journal of Physical Chemistry C*, 120(15), 8370-8379.

[117] Crezee, J., van Leeuwen, C. M., Oei, A. L., van Heerden, L. E., Bel, A., Stalpers, L. J. A., ... & Kok, H. P. (2016). Biological modelling of the radiation dose escalation effect of regional hyperthermia in cervical cancer. *Radiation Oncology*, 11(1), 14.

[118] Liu, B., Xu, P., Brown, P. B., Xie, J., Ge, X., Miao, L., ... & Pan, L. (2016). The effect of hyperthermia on liver histology, oxidative stress and disease resistance of the Wuchang bream, Megalobrama amblycephala. Fish & shellfish immunology, 52, 317-324.

[119] Tahara, H., & Jinushi, M. (2016). U.S. Patent No. 9,226,934. *Washington, DC:* U.S. Patent and Trademark Office.

[120] Houthuijzen, J. M., Daenen, L. G., Roodhart, J. M., Voest, E. E., Cirkel, G. A., Shaked, Y., & Voest, E. E. (2016). The role of mesenchymal stem cells and macrophages in treatment-induced anti-cancer drug resistance. *Lipid Signaling in Anti-Cancer Drug Resistance*, 106, 7.

[121] Mohammad, F., & Al-Lohedan, H. A. (2017). Luteinizing hormone-releasing hormone targeted superparamagnetic gold nanoshells for a combination

therapy of hyperthermia and controlled drug delivery. *Materials Science and Engineering: C*, 76, 692-700.

[122] Guardia, P., Di Corato, R., Lartigue, L., Wilhelm, C., Espinosa, A., Garcia-Hernandez, M., ... & Pellegrino, T. (2012). Water-soluble iron oxide nanocubes with high values of specific absorption rate for cancer cell hyperthermia treatment. *ACS nano*, 6(4), 3080-3091.

[123] Hergt, R., Dutz, S., Müller, R., & Zeisberger, M. (2006). Magnetic particle hyperthermia: nanoparticle magnetism and materials development for cancer therapy. *Journal of Physics: Condensed Matter*, 18(38), S2919.

[124] Glöckl, G., Hergt, R., Zeisberger, M., Dutz, S., Nagel, S., & Weitschies, W. (2006). The effect of field parameters, nanoparticle properties and immobilization on the specific heating power in magnetic particle hyperthermia. *Journal of Physics: Condensed Matter*, 18(38), S2935.

[125] Hergt, R., & Dutz, S. (2007). Magnetic particle hyperthermia—biophysical limitations of a visionary tumour therapy. Journal of Magnetism and Magnetic Materials, 311(1), 187-192.

[126] Laurent, S., Dutz, S., Häfeli, U. O., & Mahmoudi, M. (2011). Magnetic fluid hyperthermia: focus on superparamagnetic iron oxide nanoparticles. *Advances in colloid and interface science*, 166(1), 8-23.

[127] Gilchrist, R. K., Medal, R., Shorey, W. D., Hanselman, R. C., Parrott, J. C., & Taylor, C. B. (1957). Selective inductive heating of lymph nodes. *Annals of surgery*, 146(4), 596.

[128] Johnson, R. H., Robinson, M. P., Preece, A. W., Green, J. L., Pothecary, N. M., & Railton, C. J. (1993). Effect of frequency and conductivity on field penetration of electromagnetic hyperthermia applicators. *Physics in medicine and biology*, 38(8), 1023.

[129] Van den Berg, C. A., Bartels, L. W., De Leeuw, A. A., Lagendijk, J. J., & Van de Kamer, J. B. (2004). Experimental validation of hyperthermia SAR treatment planning using MR B1+ imaging. *Physics in medicine and biology*, 49(22), 5029.

[130] Morgul, M. H., Raschzok, N., Schwartlander, R., Vondran, F. W., Michel, R., Stelter, L., ... & Sauer, I. M. (2008). Tracking of primary human hepatocytes with clinical MRI: initial results with Tat-peptide modified superparamagnetic iron oxide particles. *The International journal of artificial organs*, 31(3), 252-257.

[131] Maier-Hauff, K., Rothe, R., Scholz, R., Gneveckow, U., Wust, P., Thiesen, B., ... & Jordan, A. (2007). Intracranial thermotherapy using magnetic nanoparticles combined with an external beam radiotherapy: results of a feasibility study on patients with glioblastoma multiforme. *Journal of neuro-oncology*, 81(1), 53-60.

[132] Wust, P., Gneveckow, U., Wust, P., Gneveckow, U., Johannsen, M., Böhmer, D., ... & Ricke, J. (2006). Magnetic nanoparticles for interstitial thermotherapy–feasibility, tolerance and achieved temperatures. *International Journal of Hyperthermia*, 22(8), 673-685.

[133] Behzadian, F. (2015). Additive Manufacturing of Functionally-Graded Porous Biodegradable Scaffolds using Sacrificial Porogens (*Master's thesis, University of Waterloo*).

[134] Niinomi, M., Nakai, M., & Hieda, J. (2012). Development of new metallic alloys for biomedical applications. *Acta Biomaterialia*, 8(11), 3888-3903.

[135] Niinomi, M. (2008). Mechanical biocompatibilities of titanium alloys for biomedical applications. Journal of the mechanical behavior of biomedical materials, 1(1), 30-42.

[136] Niinomi, M., Hattori, T., Morikawa, K., Kasuga, T., Suzuki, A., Fukui, H., & Niwa, S. (2002). Development of low rigidity β-type titanium alloy for biomedical applications. *Materials Transactions*, 43(12), 2970-2977.

[137] Bao, Q., Chen, C., Wang, D., Ji, Q., & Lei, T. (2005). Pulsed laser deposition and its current research status in preparing hydroxyapatite thin films. *Applied Surface Science*, 252(5), 1538-1544.

[138] Wen, C. E., Yamada, Y., Shimojima, K., Chino, Y., Asahina, T., & Mabuchi, M. (2002). Processing and mechanical properties of autogenous titanium

implant materials. *Journal of Materials Science: Materials in Medicine*, 13(4), 397-401.

[139] Li, Y., Yang, C., Zhao, H., Qu, S., Li, X., & Li, Y. (2014). New developments of Ti-based alloys for biomedical applications. *Materials*, 7(3), 1709-1800.

[140] Hench, L. L., & Wilson, J. (Eds.). (1993). An introduction to bioceramics (Vol. 1). World scientific.

[141] Thomas, M. B., Doremus, R. H., Jarcho, M., & Salsbury, R. L. (1980). Dense hydroxylapatite: fatigue and fracture strength after various treatments, from diametral tests. *Journal of Materials Science*, 15(4), 891-894.

[142] Van Dijk, H. J. A., Hattu, N., & Prijs, K. (1981). Preparation, microstructure and mechanical properties of dense polycrystalline hydroxy apatite. *Journal of materials science*, 16(6), 1592-1598.

[143] Silva, P. L., Santos, J. D., Monteiro, F. J., & Knowles, J. C. (1998). Adhesion and microstructural characterization of plasma-sprayed hydroxyapatite/glass ceramic coatings onto Ti-6A1-4V substrates. *Surface and Coatings Technology*, 102(3), 191-196.

[144] Sun, L., Berndt, C. C., Gross, K. A., & Kucuk, A. (2001). Material fundamentals and clinical performance of plasma-sprayed hydroxyapatite

coatings: a review. *Journal of Biomedical Materials Research Part A*, 58(5), 570-592.

[145] Gross, K. A., & Berndt, C. C. (1998). Thermal processing of hydroxyapatite for coating production. Journal of biomedical materials research, 39(4), 580-587.

[146] Lane, W. A. (1895). Some remarks on the treatment of fractures. *British medical journal*, 1(1790), 861.

[147] Sherman, W. O. (1912). Vanadium steel bone plates and screws. *Surg Gynecol Obstet*, 14(6), 629-634.

[148] Hermawan, H., Ramdan, D., & Djuansjah, J. R. (2011). Metals for biomedical applications. *In Biomedical engineering-from theory to applications*. InTech.

[149] Habibovic, P., Barrere, F., Blitterswijk, C. A., Groot, K., & Layrolle, P. (2002). Biomimetic hydroxyapatite coating on metal implants. *Journal of the American Ceramic Society*, 85(3), 517-522.

[150] Lahann, J., Klee, D., Thelen, H., Bienert, H., Vorwerk, D., & Ho¨ cker, H. (1999). Improvement of haemocompatibility of metallic stents by polymer coating. *Journal of Materials Science: Materials in Medicine*, 10(7), 443-448.

[151] Hermawan, H., & Mantovani, D. (2009). Degradable metallic biomaterials: the concept, current developments and future directions. *Minerva Biotecnologica*, 21(4), 207.

[152] Saini, M., Singh, Y., Arora, P., Arora, V., & Jain, K. (2015). Implant biomaterials: A comprehensive review. World Journal of Clinical Cases: WJCC, 3(1), 52.

[153] Sykaras, N., Iacopino, A. M., Marker, V. A., Triplett, R. G., & Woody, R. D. (2000). Implant materials, designs, and surface topographies: their effect on osseointegration. A literature review. *International Journal of Oral & Maxillofacial Implant*s, 15(5).

[154] Wennerberg, A., & Albrektsson, T. (2010). On implant surfaces: a review of current knowledge and opinions. *International Journal of Oral & Maxillofacial Implants*, 25(1).

[155] Hoffmann, O., Angelov, N., Gallez, F., Jung, R. E., & Weber, F. E. (2008). The zirconia implant-bone interface: a preliminary histologic evaluation in rabbits. *The International journal of oral & maxillofacial implants*, 23(4), 691.

[156] Özkurt, Z., & Kazazoğlu, E. (2011). Zirconia dental implants: a literature review. *Journal of Oral Implantology*, 37(3), 367-376.

[157] Adatia, N. D., Bayne, S. C., Cooper, L. F., & Thompson, J. Y. (2009). Fracture resistance of yttria-stabilized zirconia dental implant abutments. *Journal of Prosthodontics*, 18(1), 17-22.

[158] Jinawath, S., Pongkao, D., Suchanek, W., & Yoshimura, M. (2001). Hydrothermal synthesis of monetite and hydroxyapatite from monocalcium phosphate monohydrate. *International Journal of Inorganic Materials*, 3(7), 997-1001.

[159] Nasri, K., El Feki, H., Sharrock, P., Fiallo, M., & Nzihou, A. (2015). Spray-dried monocalcium phosphate monohydrate for soluble phosphate fertilizer. *Industrial & Engineering Chemistry Research*, 54(33), 8043-8047.

[160] Melchels, F. P. W. (2010). Preparation of advanced porous structures by stereolithography for application in tissue engineering. *University of Twente*.

[161] Radi, M. J. (1989). Calcium oxalate crystals in breast biopsies. An overlooked form of microcalcification associated with benign breast disease. *Archives of pathology & laboratory medicine*, 113(12), 1367-1369.

[162] Ribeiro, S., Ramos, A., Brandao, A., Rebelo, J. R., Guerra, A., Resina, C., ... & Ribeiro, F. (1998). Cardiac valve calcification in haemodialysis patients: role of calcium-phosphate metabolism. Nephrology, dialysis, transplantation: *official publication of the European Dialysis and Transplant Association-European Renal Association*, 13(8), 2037-2040.

[163] Hench, L. L., & Polak, J. M. (2002). *Third-generation biomedical materials. Scienc*e, 295(5557), 1014-1017.

[164] Williams, D. F. (2008). On the mechanisms of biocompatibility. Biomaterials, 29(20), 2941-2953.

[165] Rahaman, M. N., Day, D. E., Bal, B. S., Fu, Q., Jung, S. B., Bonewald, L. F., & Tomsia, A. P. (2011). Bioactive glass in tissue engineering. *Acta biomaterialia*, 7(6), 2355-2373.

[166] Serra, T. (2014). Development of 3D-printed biodegradable composite scaffolds for tissue engineering applications.

[167] Saino, E., Focarete, M. L., Gualandi, C., Emanuele, E., Cornaglia, A. I., Imbriani, M., & Visai, L. (2011). Effect of electrospun fiber diameter and alignment on macrophage activation and secretion of proinflammatory cytokines and chemokines. Biomacromolecules, 12(5), 1900-1911.

[168] Hollister, S. J., & Murphy, W. L. (2011). Scaffold translation: barriers between concept and clinic. *Tissue Engineering Part B: Reviews*, 17(6), 459-474.

[169] Helm, R. F., & Potts, M. (2012). Extracellular matrix (ECM). *In Ecology of Cyanobacteria II* (pp. 461-480). Springer Netherlands.

[170] Schumacher, T. C., Volkmann, E., Yilmaz, R., Wolf, A., Treccani, L., & Rezwan, K. (2014). Mechanical evaluation of calcium-zirconium-silicate (baghdadite) obtained by a direct solid-state synthesis route. *Journal of the mechanical behavior of biomedical materials*, 34, 294-301.

[171] Roohani-Esfahani, S. I., Dunstan, C. R., Davies, B., Pearce, S., Williams, R., & Zreiqat, H. (2012). Repairing a critical-sized bone defect with highly porous modified and unmodified baghdadite scaffolds. *Acta biomaterialia*, 8(11), 4162-4172.

[172] Choudhary, R., Vecstaudza, J., Krishnamurithy, G., Raghavendran, H. R. B., Murali, M. R., Kamarul, T., ... & Locs, J. (2016). In-vitro bioactivity, biocompatibility and dissolution studies of diopside prepared from biowaste by using sol–gel combustion method. *Materials Science and Engineering: C*, 68, 89-100.

[173] Ghorbanian, L., Emadi, R., Razavi, M., Shin, H., & Teimouri, A. (2012). Synthesis and Characterization of Novel Nanodiopsidebioceramic Powder. *Journal of Nanostructures*, 2(3), 357-361.

[174] Iwata, N. Y., Lee, G. H., Tsunakawa, S., Tokuoka, Y., & Kawashima, N. (2004). Preparation of diopside with apatite-forming ability by sol–gel process using metal alkoxide and metal salts. *Colloids and Surfaces B: Biointerfaces*, 33(1), 1-6.

[175] Iwata, N. Y., Lee, G. H., Tokuoka, Y., & Kawashima, N. (2004). Sintering behavior and apatite formation of diopside prepared by coprecipitation process. *colloids and surfaces B: Biointerfaces*, 34(4), 239-245.

[176] Bozadjiev, L., & Doncheva, L. (2006). Methods for diopside synthesis. *Journal of the University of Chemical Technology and Metallurgy*, 41(2), 125-128.

[177] Abdellahi, M., Bahmanpour, H., & Bahmanpour, M. (2014). The best conditions for minimizing the synthesis time of nanocomposites during high energy ball milling: modeling and optimizing. *Ceramics International*, 40(7), 9675-9692.

[178] Abdellahi, M., Zakeri, M., & Bahmanpour, H. (2013). Events and reaction mechanisms during the synthesis of an Al2O3-TiB2 nanocomposite via high energy ball milling. *Frontiers of Chemical Science and Engineering*, 7(2), 123-129.

[179] Abdellahi, M., Bhmanpour, M., & Bahmanpour, M. (2014). Optimization of process parameters to maximize hardness of metal/ceramic nanocomposites produced by high energy ball milling. Ceramics International, 40(10), 16259-16272.

[180] Huang, Y., Jin, X., Zhang, X., Sun, H., Tu, J., Tang, T., ... & Dai, K. (2009). In vitro and in vivo evaluation of akermanite bioceramics for bone regeneration. *Biomaterials*, 30(28), 5041-5048.

[181] Mihailova, I. K., Radev, L., Aleksandrova, V. A., Colova, I. V., Salvado, I. M. M., & Fernandes, M. H. V. (2015). Novel merwinite/akermanite ceramics: in vitro bioactivity. Bulg Chem Commun, 47, 253-260.

[182] Xia, L., Yin, Z., Mao, L., Wang, X., Liu, J., Jiang, X., ... & Fang, B. (2016). Akermanite bioceramics promote osteogenesis, angiogenesis and suppress osteoclastogenesis for osteoporotic bone regeneration. *Scientific reports*, 6, 22005.

[183] Wu, C., & Chang, J. (2006). A novel akermanite bioceramic: preparation and characteristics. Journal of biomaterials applications, 21(2), 119-129.

[184] Hou, X., Yin, G., Chen, X., Liao, X., Yao, Y., & Huang, Z. (2011). Effect of akermanite morphology on precipitation of bone-like apatite. Applied Surface Science, 257(8), 3417-3422.

[185] Wu, C., & Chang, J. (2004). Synthesis and apatite-formation ability of akermanite. Materials Letters, 58(19), 2415-2417.

[186] Wu, C., Zhang, M., Zhai, D., Yu, J., Liu, Y., Zhu, H., & Chang, J. (2013). Containerless processing for preparation of akermanite bioceramic spheres with homogeneous structure, tailored bioactivity and degradation. Journal of Materials Chemistry B, 1(7), 1019-1026.

[187] Choudhary, R., Koppala, S., & Swamiappan, S. (2015). Bioactivity studies of calcium magnesium silicate prepared from eggshell waste by sol–gel combustion synthesis. Journal of Asian Ceramic Societies, 3(2), 173-177.

[188] Sautter, V., Jaoul, O., & Abel, F. (1988). Aluminum diffusion in diopside using the27Al (p, γ) 28Si nuclear reaction: preliminary results. Earth and Planetary Science Letters, 89(1), 109-114.

[189] Goel, A., Tulyaganov, D. U., Pascual, M. J., Shaaban, E. R., Muñoz, F., Lü, Z., & Ferreira, J. M. (2010). Development and performance of diopside based glass-ceramic sealants for solid oxide fuel cells. Journal of Non-Crystalline Solids, 356(20), 1070-1080.

[190] Kulakov, O. B., Doktorov, A. A., D'iakova, S. V., Denisov-Nikol'skiĭ, I., & Grötz, K. A. (2005). Experimental study of osseointegration of zirconium and titanium dental implants. Morfologiia (Saint Petersburg, Russia), 127(1), 52-55.

[191] Kulakov, O. B., Doktorov, A. A., D'iakova, S. V., Denisov-Nikol'skiĭ, I., & Grötz, K. A. (2005). Experimental study of osseointegration of zirconium and titanium dental implants. Morfologiia (Saint Petersburg, Russia), 127(1), 52-55.

[192] Wu, C., & Chang, J. (2007). Synthesis and in vitro bioactivity of bredigite powders. Journal of biomaterials applications, 21(3), 251-263.

[193] Huang, X. H., & Chang, J. (2008). Preparation of nanocrystalline bredigite powders with apatite-forming ability by a simple combustion method. Materials Research Bulletin, 43(6), 1615-1620.

[194] Ohtsuki, C., Kokubo, T., & Yamamuro, T. (1992). Mechanism of apatite formation on CaOSiO2P2O5 glasses in a simulated body fluid. Journal of Non-Crystalline Solids, 143, 84-92.

[195] Mirhadi, S. M., Tavangarian, F., & Emadi, R. (2012). Synthesis, characterization and formation mechanism of single-phase nanostructure bredigite powder. Materials Science and Engineering: C, 32(2), 133-139.

[196] Eilbagi, M., Emadi, R., Raeissi, K., Kharaziha, M., & Valiani, A. (2016). Mechanical and cytotoxicity evaluation of nanostructured hydroxyapatite-bredigite scaffolds for bone regeneration. Materials Science and Engineering: C, 68, 603-612.

[197] Wu, C., & Chang, J. (2013). A review of bioactive silicate ceramics. Biomedical materials, 8(3), 032001.

[198] Kokubo, T., Kim, H. M., & Kawashita, M. (2003). Novel bioactive materials with different mechanical properties. *Biomaterials*, *24*(13), 2161-2175.

[199] Kitsugi, T., Nakamura, T., Yamamura, T., Kokubu, T., Shibuya, T., & Takagi, M. (1987). SEM-EPMA observation of three types of apatite-containing glass-ceramics implanted in bone: The variance of a

Ca-P-rich layer. *Journal of Biomedical Materials Research Part A*, *21*(10), 1255-1271.

[200] Amjad, Z. (Ed.). (2013). *Calcium phosphates in biological and industrial systems*. Springer Science & Business Media.

[201] Li, P., Ohtsuki, C., Kokubo, T., Nakanishi, K., Soga, N., Nakamura, T., & Yamamuro, T. (1992). Apatite formation induced by silica gel in a simulated body fluid. *Journal of the American Ceramic Society*, *75*(8), 2094-2097.

[202] Neuman, W. F., & Neuman, M. W. (1958). The chemical dynamics of bone mineral. *The chemical dynamics of bone mineral.*

[203] Gamble, J. L. (1954). *Chemical anatomy, physiology and pathology of extracellular fluid: a lecture syllabus*. Harvard University Press.

[204] Fu, Q., Saiz, E., Rahaman, M. N., & Tomsia, A. P. (2013). Toward strong and tough glass and ceramic scaffolds for bone repair. *Advanced Functional Materials*, *23*(44), 5461-5476.

[205] Hench, L. L. (1991). Bioceramics: from concept to clinic. *Journal of the american ceramic society*, *74*(7), 1487-1510.

[206] Dorozhkin, S. V. (2013). Calcium orthophosphate-based bioceramics. *Materials*, *6*(9), 3840-3942.

[207] Trombetta, R., Inzana, J. A., Schwarz, E. M., Kates, S. L., & Awad, H. A. (2017). 3D printing of calcium phosphate ceramics for bone tissue engineering and drug delivery. *Annals of biomedical engineering*, *45*(1), 23-44.

[208] Tuan, H. S., & Hutmacher, D. W. (2005). Application of micro CT and computation modeling in bone tissue engineering. *Computer-Aided Design*, *37*(11), 1151-1161.

[209] Gittings, J. P., Bowen, C. R., Dent, A. C., Turner, I. G., Baxter, F. R., & Chaudhuri, J. B. (2009). Electrical characterization of hydroxyapatite-based bioceramics. *Acta Biomaterialia*, *5*(2), 743-754.

[210] Hoepfner, T. P., & Case, E. D. (2002). The porosity dependence of the dielectric constant for sintered hydroxyapatite. *Journal of Biomedical Materials Research Part A*, *60*(4), 643-650.

[211] Zakharov, N. A., & Orlovskii, V. P. (2001). Dielectric characteristics of biocompatible Ca 10 (PO 4) 6 (OH) 2 ceramics. *Technical Physics Letters*, *27*(8), 629-631.

[212] Lazić, S., Zec, S., Miljević, N., & Milonjić, S. (2001). The effect of temperature on the properties of hydroxyapatite precipitated from calcium hydroxide and phosphoric acid. *Thermochimica Acta*, *374*(1), 13-22.

[213] Suchanek, W., & Yoshimura, M. (1998). Processing and properties of hydroxyapatite-based biomaterials for use as hard tissue replacement implants. *Journal of Materials Research*, *13*(1), 94-117.

[214] Ishihara, S., Matsumoto, T., Onoki, T., Sohmura, T., & Nakahira, A. (2009). New concept bioceramics composed of octacalcium phosphate (OCP) and dicarboxylic acid-intercalated OCP via hydrothermal hot-pressing. *Materials Science and Engineering: C*, *29*(6), 1885-1888.

[215] LeGeros, R. Z., & LeGeros, J. P. (1993). Dense hydroxyapatite. *Advanced series in ceramics*, *1*, 139-180.

[216] Petcharoen, K., & Sirivat, A. (2012). Synthesis and characterization of magnetite nanoparticles via the chemical co-precipitation method. *Materials Science and Engineering: B*, *177*(5), 421-427.

[217] Lu, A. H., Salabas, E. E., & Schüth, F. (2007). Magnetic nanoparticles: synthesis, protection, functionalization, and application. *Angewandte Chemie International Edition*, *46*(8), 1222-1244.

[218] Wang, Y. M., Cao, X., Liu, G. H., Hong, R. Y., Chen, Y. M., Chen, X. F., ... & Wei, D. G. (2011). Synthesis of Fe 3 O 4 magnetic fluid used for magnetic resonance imaging and hyperthermia. *Journal of Magnetism and Magnetic Materials*, *323*(23), 2953-2959.

[219] Murakami, S., Hosono, T., Jeyadevan, B., Kamitakahara, M., & Ioku, K. (2008). Hydrothermal synthesis of magnetite/hydroxyapatite composite material for hyperthermia therapy for bone cancer. *Journal of the Ceramic Society of Japan*, *116*(1357), 950-954.

[220] Jiang, L., & Gao, L. (2003). Carbon Nanotubes− Magnetite Nanocomposites from Solvothermal Processes: Formation, Characterization, and Enhanced Electrical Properties. *Chemistry of materials*, *15*(14), 2848-2853.

[221] Ajeesh, M., Francis, B. F., Annie, J., & Varma, P. H. (2010). Nano iron oxide–hydroxyapatite composite ceramics with enhanced radiopacity. *Journal of Materials Science: Materials in Medicine*, *21*(5), 1427-1434.

[222] Ai, L., Zhang, C., & Chen, Z. (2011). Removal of methylene blue from aqueous solution by a solvothermal-synthesized graphene/magnetite composite. *Journal of hazardous materials*, *192*(3), 1515-1524.

[223] Wang, J. Z., Zhong, C., Wexler, D., Idris, N. H., Wang, Z. X., Chen, L. Q., & Liu, H. K. (2011). Graphene-Encapsulated Fe3O4 Nanoparticles with 3D Laminated Structure as Superior Anode in Lithium Ion Batteries. *Chemistry-A European Journal*, *17*(2), 661-667.

[224] Liang, J., Xu, Y., Sui, D., Zhang, L., Huang, Y., Ma, Y., ... & Chen, Y. (2010). Flexible, magnetic, and electrically conductive graphene/Fe3O4 paper and its application for magnetic-controlled switches. *The Journal of Physical Chemistry C*, *114*(41), 17465-17471.

[225] He, H., & Gao, C. (2010). Supraparamagnetic, conductive, and processable multifunctional graphene nanosheets coated with high-density Fe3O4 nanoparticles. *ACS applied materials & interfaces*, *2*(11), 3201-3210.

[226] Zhou, K., Zhu, Y., Yang, X., & Li, C. (2010). One-pot preparation of graphene/Fe 3 O 4 composites by a solvothermal reaction. *New Journal of Chemistry*, *34*(12), 2950-2955.

[227] Hu, F. X., Neoh, K. G., & Kang, E. T. (2006). Synthesis and in vitro anti-cancer evaluation of tamoxifen-loaded magnetite/PLLA composite nanoparticles. *Biomaterials*, *27*(33), 5725-5733.

[228] Asmatulu, R., Zalich, M. A., Claus, R. O., & Riffle, J. S. (2005). Synthesis, characterization and targeting of biodegradable magnetic nanocomposite particles by external magnetic fields. *Journal of Magnetism and Magnetic Materials*, *292*, 108-119.

[229] Kim, S. S., Utsunomiya, H., Koski, J. A., Wu, B. M., Cima, M. J., Sohn, J., ... & Vacanti, J. P. (1998). Survival and function of hepatocytes on a novel three-dimensional synthetic biodegradable polymer scaffold with an intrinsic network of channels. *Annals of surgery*, *228*(1), 8.

[230] Wu, B. M., Borland, S. W., Giordano, R. A., Cima, L. G., Sachs, E. M., & Cima, M. J. (1996). Solid free-form fabrication of drug delivery devices. *Journal of Controlled Release*, *40*(1-2), 77-87.

[231] Lam, C. X. F., Mo, X. M., Teoh, S. H., & Hutmacher, D. W. (2002). Scaffold development using 3D printing with a starch-based polymer. *Materials Science and Engineering: C*, *20*(1), 49-56.

[232] Yen, H. J., Tseng, C. S., Hsu, S. H., & Tsai, C. L. (2009). Evaluation of chondrocyte growth in the highly porous scaffolds made by fused deposition manufacturing (FDM) filled with type II collagen. *Biomedical microdevices*, *11*(3), 615-624.

[233] Lee, M., Dunn, J. C., & Wu, B. M. (2005). Scaffold fabrication by indirect three-dimensional printing. *Biomaterials*, *26*(20), 4281-4289.

[234] Melchels, F. P., Domingos, M. A., Klein, T. J., Malda, J., Bartolo, P. J., & Hutmacher, D. W. (2012). Additive manufacturing of tissues and organs. *Progress in Polymer Science*, *37*(8), 1079-1104.

[235] Guillemot, F., Souquet, A., Catros, S., Guillotin, B., Lopez, J., Faucon, M., ... & Chabassier, P. (2010). High-throughput laser printing of cells and biomaterials for tissue engineering. *Acta biomaterialia*, *6*(7), 2494-2500.

[236] Arcaute, K., Mann, B. K., & Wicker, R. B. (2006). Stereolithography of three-dimensional bioactive poly (ethylene glycol) constructs with encapsulated cells. *Annals of biomedical engineering*, *34*(9), 1429-1441.

[237] Cohen, D. L., Malone, E., Lipson, H. O. D., & Bonassar, L. J. (2006). Direct freeform fabrication of seeded hydrogels in arbitrary geometries. *Tissue engineering*, *12*(5), 1325-1335.

[238] Keriquel, V., Guillemot, F., Arnault, I., Guillotin, B., Miraux, S., Amédée, J., ... & Catros, S. (2010). In vivo bioprinting for computer-and robotic-assisted medical intervention: preliminary study in mice. *Biofabrication*, *2*(1), 014101.

[239] Chan, D. C., Kirpotin, D. B., & Bunn, P. A. (1993). Synthesis and evaluation of colloidal magnetic iron oxides for the site-specific radiofrequency-induced hyperthermia of cancer. *Journal of Magnetism and Magnetic Materials*, *122*(1-3), 374-378.

[240] Jordan, A., Wust, P., Fähling, H., John, W., Hinz, A., & Felix, R. (2009). Inductive heating of ferrimagnetic particles and magnetic fluids: physical evaluation of their potential for hyperthermia. *International Journal of Hyperthermia*, *25*(7), 499-511.

[241] Jordan, A., Scholz, R., Wust, P., Schirra, H., Schiestel, T., Schmidt, H., & Felix, R. (1999). Endocytosis of dextran and silan-coated magnetite nanoparticles and the effect of intracellular hyperthermia on human mammary carcinoma cells in vitro. *Journal of Magnetism and Magnetic Materials*, *194*(1), 185-196.

[242] Moroz, P., Jones, S. K., & Gray, B. N. (2002). Magnetically mediated hyperthermia: current status and future directions. *International Journal of Hyperthermia*, *18*(4), 267-284.

[243] Hergt, R., Dutz, S., Müller, R., & Zeisberger, M. (2006). Magnetic particle hyperthermia: nanoparticle magnetism and materials development for cancer therapy. *Journal of Physics: Condensed Matter*, *18*(38), S2919.

[244] Shadjou, N., & Hasanzadeh, M. (2015). Silica-based mesoporous nanobiomaterials as promoter of bone regeneration process. *Journal of Biomedical Materials Research Part A*, *103*(11), 3703-3716.

[245] Abdellahi, M., & Bahmanpour, M. (2015). Rapid synthesis of nanopowders in high energy ball milling; optimization of milling parameters. *Ceramics International*, *41*(1), 1631-1639.

[246] Zhang, Y., & Zhang, M. (2001). Synthesis and characterization of macroporous chitosan/calcium phosphate composite scaffolds for tissue engineering. *Journal of Biomedical Materials Research Part A*, *55*(3), 304-312.

[247] Kouhi, M., Shamanian, M., Fathi, M., Samadikuchaksaraei, A., & Mehdipour, A. (2016). Synthesis, characterization, in vitro bioactivity and biocompatibility evaluation of hydroxyapatite/bredigite (Ca7MgSi4O16) composite nanoparticles. *JOM*, *68*(4), 1061-1070.

[248] Guazzato, M., Albakry, M., Ringer, S. P., & Swain, M. V. (2004). Strength, fracture toughness and microstructure of a selection of all-ceramic materials. Part I. Pressable and alumina glass-infiltrated ceramics. *Dental Materials*, *20*(5), 441-448.

[249] Abdellahi, M., Najafinezhad, A., Ghayour, H., Saber-Samandari, S., & Khandan, A. (2017). Preparing diopside nanoparticle scaffolds via space holder method: Simulation of the compressive strength and porosity. *Journal of the Mechanical Behavior of Biomedical Materials*, *72*, 171-181.

[250] Carey, L. E., Xu, H. H., Simon, C. G., Takagi, S., & Chow, L. C. (2005). Premixed rapid-setting calcium phosphate composites for bone repair. *Biomaterials*, *26*(24), 5002-5014.

[251] An, J., Wolke, J. G., Jansen, J. A., & Leeuwenburgh, S. C. (2016). Influence of polymeric additives on the cohesion and mechanical properties of calcium phosphate cements. *Journal of Materials Science: Materials in Medicine*, *27*(3), 58.

[252] Shahini, A., Yazdimamaghani, M., Walker, K. J., Eastman, M. A., Hatami-Marbini, H., Smith, B. J., ... & Tayebi, L. (2014). 3D conductive nanocomposite scaffold for bone tissue engineering. *International journal of nanomedicine*, *9*, 167.

[253] Paital, S. R., & Dahotre, N. B. (2009). Wettability and kinetics of hydroxyapatite precipitation on a laser-textured Ca–P bioceramic coating. *Acta biomaterialia*, *5*(7), 2763-2772.

[254] De Aza, P. N., Guitian, F., & De Aza, S. (1997). Bioeutectic: a new ceramic material for human bone replacement. *Biomaterials*, *18*(19), 1285-1291.

[255] Balivada, S., Rachakatla, R. S., Wang, H., Samarakoon, T. N., Dani, R. K., Pyle, M., ... & Tamura, M. (2010). A/C magnetic hyperthermia of melanoma mediated by iron (0)/iron oxide core/shell magnetic nanoparticles: a mouse study. *BMC cancer*, *10*(1), 119.

[256] Ebrahimi-Kahrizsangi, R., Abdellahi, M., & Bahmanpour, M. (2015). Ignition time of nanopowders during milling: a novel simulation. *Powder Technology*, *272*, 224-234.

[257] Ferreira, C. (2001, September). Gene expression programming in problem solving. In *6th Online world conference on soft computing in industrial applications (invited tutorial)*.

[258] Abdellahi, M., Bahmanpour, M., & Bahmanpour, M. (2014). The use of artificial bee colony algorithm to speed up the nanopowders synthesis during high energy ball milling. *Powder Technology*, *264*, 61-70.

[259] Ayan, K., & Kılıç, U. (2012). Artificial bee colony algorithm solution for optimal reactive power flow. *Applied soft computing*, *12*(5), 1477-1482.

[260] Roy, R. K. (2001). *Design of experiments using the Taguchi approach: 16 steps to product and process improvement*. John Wiley & Sons.

[261] Koza, J. R. (1992). *Genetic programming: on the programming of computers by means of natural selection* (Vol. 1). MIT press.

[262] Ghayour, H., Abdellahi, M., & Bahmanpour, M. (2015). Artificial intelligence and ceramic tools: experimental study, modeling and optimizing. *Ceramics International*, *41*(10), 13470-13479.

[263] Ghomi, H., Emadi, R., & Javanmard, S. H. (2016). Fabrication and characterization of nanostructure diopside scaffolds using the space holder method: effect of different space holders and compaction pressures. *Materials & Design*, *91*, 193-200.

[264] Ghomi, H., Emadi, R., & Javanmard, S. H. (2016). Preparation of nanostructure bioactive diopside scaffolds for bone tissue engineering by two near net shape manufacturing techniques. *Materials Letters*, *167*, 157-160.

[265] Razavi, M., Fathi, M., Savabi, O., Vashaee, D., & Tayebi, L. (2014). Improvement of biodegradability, bioactivity, mechanical integrity and cytocompatibility behavior of biodegradable Mg based orthopedic implants using nanostructured bredigite ($Ca_7MgSi_4O_{16}$) bioceramic coated via ASD/EPD technique. *Annals of biomedical engineering*, *42*(12), 2537-2550.

[266] Razavi, M., Fathi, M., Savabi, O., Razavi, S. M., Beni, B. H., Vashaee, D., & Tayebi, L. (2013). Surface modification of magnesium alloy implants by nanostructured bredigite coating. *Materials Letters*, *113*, 174-178.

[267] Ma, N., Fan, X., Quan, X., & Zhang, Y. (2009). Ag–TiO 2/HAP/Al 2 O 3 bioceramic composite membrane: fabrication, characterization and bactericidal activity. *Journal of Membrane Science*, *336*(1), 109-117.

[268] Sreenivasulua, S., & chennakeshava Reddyb, A. (2014, December). THERMO-MECHANICAL PROPERTIES OF SILICONNITRATE CERAMIC COMPOSITES FOR FUSED DEPOSITION MODELING. In *International Conference on Advanced Materials and manufacturing Technologies (AMMT)*.

[269] Kong, Y. M., Kim, S., Kim, H. E., & Lee, I. S. (1999). Reinforcement of hydroxyapatite bioceramic by addition of ZrO2 coated with Al2O3. *Journal of the American Ceramic Society*, *82*(11), 2963-2968.

[270] Nayar, S., & Sinha, A. (2004). Systematic evolution of a porous hydroxyapatite–poly (vinylalcohol)–gelatin composite. *Colloids and surfaces B: Biointerfaces*, *35*(1), 29-32.

[271] Wu, C., Chang, J., Wang, J., Ni, S., & Zhai, W. (2005). Preparation and characteristics of a calcium magnesium silicate (bredigite) bioactive ceramic. *Biomaterials*, *26*(16), 2925-2931.

[272] Lee, E. J., Koh, Y. H., Yoon, B. H., Kim, H. E., & Kim, H. W. (2007). Highly porous hydroxyapatite bioceramics with interconnected pore channels using camphene-based freeze casting. *Materials letters*, *61*(11), 2270-2273.

[273] Ghomi, H., Fathi, M. H., & Edris, H. (2012). Effect of the composition of hydroxyapatite/bioactive glass nanocomposite foams on their bioactivity and mechanical properties. *Materials Research Bulletin*, *47*(11), 3523-3532.

[274] Roohani-Esfahani, S. I., Nouri-Khorasani, S., Lu, Z., Appleyard, R., & Zreiqat, H. (2010). The influence hydroxyapatite nanoparticle shape and size on the properties of biphasic calcium phosphate scaffolds coated with hydroxyapatite–PCL composites. *Biomaterials*, *31*(21), 5498-5509.

[275] Nieh, T. G., & Wadsworth, J. (1991). Hall-Petch relation in nanocrystalline solids. *Scripta Metallurgica et Materialia*, *25*(4), 955-958.

[276] Aminzare, M., Eskandari, A., Baroonian, M. H., Berenov, A., Hesabi, Z. R., Taheri, M., & Sadrnezhaad, S. K. (2013). Hydroxyapatite nanocomposites: Synthesis, sintering and mechanical properties. *Ceramics International*, *39*(3), 2197-2206.

[277] Shiota, T., Shibata, M., Yasuda, K., & Matsuo, Y. (2008). Influence of β-tricalcium phosphate dispersion on mechanical properties of hydroxyapatite ceramics. *Journal of the Ceramic Society of Japan*, *116*(1357), 1002-1005.

[278] Wu, C., Ramaswamy, Y., & Zreiqat, H. (2010). Porous diopside (CaMgSi 2 O 6) scaffold: a promising bioactive material for bone tissue engineering. *Acta biomaterialia*, *6*(6), 2237-2245.

[279] Buck, R. P. (1984). Kinetics of bulk and interfacial ionic motion: microscopic bases and limits for the nernst—planck equation applied to membrane systems. *Journal of membrane science*, *17*(1), 1-62.

[280] Levin, M. (2009, July). Bioelectric mechanisms in regeneration: unique aspects and future perspectives. In *Seminars in cell & developmental biology* (Vol. 20, No. 5, pp. 543-556). Academic Press.

[281] Levin, M. (2003). Bioelectromagnetics in morphogenesis. *Bioelectromagnetics*, *24*(5), 295-315.

[282] Kutnjak, Z., Petzelt, J., & Blinc, R. (2006). The giant electromechanical response in ferroelectric relaxors as a critical phenomenon. *Nature*, *441*(7096), 956-959.

[283] Bsoul, I., & Mahmood, S. H. (2010). Magnetic and structural properties of BaFe 12− x Ga x O 19 nanoparticles. *Journal of Alloys and Compounds*, *489*(1), 110-114.

[284] Ansar, E. B., Ajeesh, M., Yokogawa, Y., Wunderlich, W., & Varma, H. (2012). Synthesis and characterization of iron oxide embedded

hydroxyapatite bioceramics. *Journal of the American Ceramic Society*, *95*(9), 2695-2699.

[285] Diba, M., Goudouri, O. M., Tapia, F., & Boccaccini, A. R. (2014). Magnesium-containing bioactive polycrystalline silicate-based ceramics and glass-ceramics for biomedical applications. *Current opinion in solid state and materials science*, *18*(3), 147-167.

[286] Zhang, M., Liu, C., Sun, J., & Zhang, X. (2011). Hydroxyapatite/diopside ceramic composites and their behaviour in simulated body fluid. *Ceramics International*, *37*(6), 2025-2029.

[287] Kouhi, M., Prabhakaran, M. P., Shamanian, M., Fathi, M., Morshed, M., & Ramakrishna, S. (2015). Electrospun PHBV nanofibers containing HA and bredigite nanoparticles: Fabrication, characterization and evaluation of mechanical properties and bioactivity. *Composites Science and Technology*, *121*, 115-122.

[288] Ghomi, H., Jaberzadeh, M., & Fathi, M. H. (2011). Novel fabrication of forsterite scaffold with improved mechanical properties. *Journal of alloys and compounds*, *509*(5), L63-L68.

[289] Sasikumar, S., & Vijayaraghavan, R. (2006). Low temperature synthesis of nanocrystalline hydroxyapatite from egg shells by combustion method. *Trends Biomater Artif Organs*, *19*(2), 70-73.

[290] Wu, C., Chang, J., Zhai, W., Ni, S., & Wang, J. (2006). Porous akermanite scaffolds for bone tissue engineering: preparation, characterization, and in vitro studies. *Journal of Biomedical Materials Research Part B: Applied Biomaterials*, *78*(1), 47-55.

[291] Takadama, H., Kim, H. M., Kokubo, T., & Nakamura, T. (2001). Mechanism of biomineralization of apatite on a sodium silicate glass: TEM− EDX study in vitro. *Chemistry of materials*, *13*(3), 1108-1113.

[292] Takadama, H., Kim, H. M., Kokubo, T., & Nakamura, T. (2002). X-ray Photoelectron Spectroscopy Study on the Process of Apatite Formation on a Sodium Silicate Glass in Simulated Body Fluid. *Journal of the American Ceramic Society*, *85*(8), 1933-1936.

[293] Chantikul, P. G. R. B. R., Anstis, G. R., Lawn, B. R., & Marshall, D. B. (1981). A critical evaluation of indentation techniques for measuring fracture toughness: II, strength method. Journal of the American Ceramic Society, 64(9), 539-543.

[294] Amaral, M., Lopes, M. A., Santos, J. D., & Silva, R. F. (2002). Wettability and surface charge of Si 3 N 4–bioglass composites in contact with simulated physiological liquids. Biomaterials, 23(20), 4123-4129.

[295] Cerruti, M. (2012). Surface characterization of silicate bioceramics. Phil. Trans. R. Soc. A, 370(1963), 1281-1312.

[296] Inzana, J. A., Olvera, D., Fuller, S. M., Kelly, J. P., Graeve, O. A., Schwarz, E. M., ... & Awad, H. A. (2014). 3D printing of composite calcium phosphate and collagen scaffolds for bone regeneration. Biomaterials, 35(13), 4026-4034.

[297] Farzin, A., Fathi, M., & Emadi, R. (2017). Multifunctional magnetic nanostructured hardystonite scaffold for hyperthermia, drug delivery and tissue engineering applications. Materials Science and Engineering: C, 70, 21-31.

[298] Wu, C., Fan, W., Zhu, Y., Gelinsky, M., Chang, J., Cuniberti, G., ... & Xiao, Y. (2011). Multifunctional magnetic mesoporous bioactive glass scaffolds with a hierarchical pore structure. *Acta biomaterialia*, 7(10), 3563-3572.

[299] Meng, J., Zhang, Y., Qi, X., Kong, H., Wang, C., Xu, Z., ... & Xu, H. (2010). Paramagnetic nanofibrous composite films enhance the osteogenic responses of pre-osteoblast cells. *Nanoscale*, 2(12), 2565-2569.

[300] Da Li, G., Lin, Y., Pan, T. H., Chen, G. S., & Yin, Q. D. (2010). Synthesis and characterization of magnetic bioactive glass-ceramics containing Mg ferrite for hyperthermia. *Materials Science and Engineering: C*, 30(1), 148-153.

[301] Ebisawa, Y., SUGIMOTO, Y., HAYASHI, T., KOKUBO, T., OHURA, K., & YAMAMURO, T. (1991). Crystallization of (FeO, Fe2O3)-CaO-SiO2

glasses and magnetic properties of their crystallized products. *Journal of the Ceramic Society of Japan*, 99(1145), 7-13.

[302] Luderer, A. A., Borrelli, N. F., Panzarino, J. N., Mansfield, G. R., Hess, D. M., Brown, J. L., ... & Hahn, E. W. (1983). Glass-ceramic-mediated, magnetic-field-induced localized hyperthermia: response of a murine mammary carcinoma. *Radiation Research*, 94(1), 190-198.

[303] Khandan, A., Ozada, N. (2017), Bredigite-Magnetite ($Ca_7MgSi_4O_{16}$-Fe_3O_4) nanoparticles: A study on their magnetic properties. *Journal of Alloys and Compounds*. 726, 729-736.

[304] Khandan, A., Jazayeri, H., Fahamy, M. D. Razavi,. M. Hydrogels: Types, Structure, Properties and Applications. (2017), *Frontiers in Biomaterials*, Chapter: 4, Publisher: Bentham Science, Editors: Mehdi Razavi, pp.143-169.

[305] Karamian, E., Nasehi, A., Saber-Samandari, S., & Khandan, A. (2017). Fabrication of hydroxyapatite-baghdadite nanocomposite scaffolds coated by PCL/Bioglass with polyurethane polymeric sponge technique. *Nanomedicine Journal*, 4(3), 177-183.

[306] Abdellahi, M., Jabbarzare, S., Ghayour, H., & Khandan, A. Thermal and X-ray analyses of aluminum–titanium nanocomposite powder. Journal of Thermal Analysis and Calorimetry, 1-11.

[307] Razavi, M., Khandan, A., Safety, regulatory issues, long-term biotoxicity, and the processing environment. Nanobiomaterials Science, Development and Evaluation. 261-279.